New Insights into the Oxidative Dehydrogenation of Propane and Ethane on Supported Vanadium Oxide Catalysts

vorgelegt von
Diplom-Ingenieur
Arne Dinse
aus Heidelberg

Von der Fakultät II –Mathematik und Naturwissenschaften-
der Technischen Universität Berlin
zur Erlangung des akademischen Grades

Doktor der Ingenieurwissenschaften
Dr. Ing.

genehmigte Dissertation

Promotionsausschuss:

Vorsitzender: Prof. Dr. rer. nat. Martin Lerch
Berichter: Prof. Dr. rer. nat. Reinhard Schomäcker
Berichter: Prof. Dr. rer. nat. Christian Hess (TU Darmstadt)

Tag der wissenschaftlichen Aussprache: 19.2.2009

Berlin 2009

D 83

Acknowledgement

This study has been performed in the time of November 2005 to February 2009 at the Technical University Berlin. I consider this time as one of the most important parts of my life and I'm happy that I have decided to choose this project back in 2005. I want to thank the German Research Foundation for funding this project which was part of the "Sonderforschungsbereich" 546.

Without the support and help of many people I could have never accomplished this work. Foremost I would like to thank Prof. Dr. Reinhard Schomäcker for his ongoing theoretical and practical support. Most of the presented data were gathered in his laboratory, which is the result of his dedication and commitment. I am also grateful to Prof. Dr. Christian Hess for his suggestions and many fruitful discussions. He participated in three publications, which could be published as a result of this study.

Part of this work has been accomplished at the University of California, Berkeley. This, again, would have not been possible without the help of Prof. Dr. Reinhard Schomäcker. During this time I was especially supported by Prof. Dr. Alexis T. Bell and Prof. Dr. Enrique Iglesia. This period gave me the opportunity to broaden my scientific and personal horizon. I found many still lasting friendships.

I would also like to acknowledge many other people who have supported me during this period. They are:

Benjamin Frank	Christa Löhr	Jonas Dimroth
Detlef Grimm	Dr. Evgenii Kondratenko	Torsten Otremba
Dr. Daniela Habel	Michael Knuth	Sonja Jost
Rita Herbert	Rolf Kunert	Axel Schiele
Ariana Finkel	Prof. Dr. Robert Schlögl	Michael Zboray
Martin Übelhör	Sabine Wrabetz	William Vining
Moritz Niemeyer	Michele Gore	Andrew Behn
Philipp Quentmeier	Crystal Collins	Nicholas Stephanopolous
Fabian Geppert	Moritz Kauth	Joseph Zakzeski

An interesting part of this study was a project in collaboration with my dad Prof. Dr. Klaus-Peter Dinse and Andrzej Ozarowski, performed in the National High Field Laboratory in Tallahassee, Florida. I'm very greatful for this experience. Mostly, however, I want to thank my family, especially my parents without whom I could have never reached this point in my life.

„Die Größte Sehenswürdigkeit, die es gibt, ist die Welt
– sieh sie dir an.“

Kurt Tucholsky

Abstract

The oxidative dehydrogenation of propane (ODP) and ethane (ODE) was investigated using different supported vanadium oxide catalysts in order to get a better insight into the reaction mechanism. Initial results revealed a strong influence of the support material (CeO_2, TiO_2, Al_2O_3, ZrO_2 and SiO_2) on selectivities, activation energies and turn over frequencies of ODP.

Because of their different catalytic behaviour, TiO_2, γ-Al_2O_3 and SiO_2 (SBA-15) supported catalysts were subject to a subsequent study by High-Frequency Electron Paramagnetic Resonance (HF-EPR) in order to determine the paramagnetic V^{4+} and V^{3+} states, before and after being exposed to ODP reaction conditions. While the SBA-15 support exhibits reduced vanadium sites as the only electron sink during the catalytic reaction, Al_2O_3 apparently localizes further electron density as oxoradicals in the support surface. If TiO_2 is used as a support, Ti^{3+} as well as surface trapped $O_2^{(-)}$ species are generated, indicating a more complex involvement of the support material in the reaction. The increase in catalytic activity in the order of SBA-15 < Al_2O_3 < TiO_2 was attributed to different reduction mechanisms depending on the support material. No V^{3+} was detected in any of the samples, indicating that such centres are either short lived or non-existent during ODP.

Because the SBA-15 supported catalyst showed no influence of the support material on the catalytic reaction it was used for a kinetic study of ODP in a fixed bed reactor. Because of fast reoxidation processes it could be shown that the applied microkinetic model simplifies to a first order rate law. In this study kinetic parameters are provided and it is indicated that the weaker allylic C-H bond of propene is involved in the rate determining step of the consecutive propene combustion.

Finally, Al_2O_3 supported vanadium oxide was investigated to understand the effects of lattice oxygen and vanadium oxidation state on the product selectivity. Both fully oxidized catalysts, and samples partially reduced by H_2 were exposed to ODE without the presence of gas phase oxygen. The ethene selectivity increases upon pre-reduction in H_2, which could be explained by a lower ratio of V^{4+} to V^{3+} cations attained as compared to a pre-reduction in C_2H_6. As a consequence, the lower Lewis acidity of the catalyst inhibits the adsorption of the nucleophilic ethylene double bond and therefore its consecutive combustion.

Zusammenfassung

Die vorliegende Arbeit gewährt einen tiefer gehenden Einblick in die oxidative Dehydrierung von Propan (ODP) und Ethan (ODE) an unterschiedlich geträgerten Vanadiumoxid-Katalysatoren. Zunächst wurde ein starker Einfluss des Trägermaterials (CeO_2, TiO_2, Al_2O_3, ZrO_2 and SiO_2) auf Selektivität, Aktivierungsenergie und Aktivität der ODP festgestellt.

Aufgrund ihres unterschiedlichen katalytischen Verhaltens wurden TiO_2, γ-Al_2O_3 and SiO_2 (SBA-15) geträgerte Katalysatoren, bevor und nachdem diese für die ODP verwendet wurden, mit Hilfe von Hochfrequenz-Elektronspinresonanz (HF-ESR) untersucht, um die paramagnetischen V^{4+} und V^{3+} Zustände nachzuweisen. Während der SBA-15 Träger reduzierte Vanadiumzentren als einzige Elektronensenke aufweist, wurden bei Al_2O_3 auch Elektronen als Oxoradikale an der Trägeroberfläche lokalisiert. Im Fall von TiO_2 wurden sowohl Ti^{3+} als auch oberflächenlokalisierte $O_2^{(-)}$-Radikale nachgewiesen. Die Zunahme der katalytischen Aktivität in der Reihenfolge SBA-15 < Al_2O_3 < TiO_2 kann damit verschiedenen Reduktionsmechanismen zugeschrieben werden. V^{3+}-Zentren konnten in keiner der Proben nachgewiesen werden, was darauf hindeutet dass diese Spezies entweder sehr kurzlebig oder nicht an der Reaktion beteiligt ist.

Der SBA-15-geträgerte Katalysator wurde aufgrund des geringen Einflusses des Trägers auf die Reaktion für eine weitergehende kinetische Studie der ODP in einem Festbettreaktor ausgewählt. Das angewandte mikrokinetische Modell vereinfacht sich aufgrund der schnellen Reoxidation des Katalysators zu einem Geschwindigkeitsgesetz erster Ordnung. Die ermittelten kinetischen Parameter deuten eine Beteiligung der allylischen C-H-Bindung des Propens im geschwindigkeitsbestimmenden Schritt der Propenverbrennung an.

Abschließend wurde der Effekt von „Gittersauerstoff“ und Oxidationszustand des Vanadiums auf die Produktselektivität an einem Al_2O_3 geträgerten Katalysator untersucht. Sowohl an einem voll oxidierten als auch partiell mit H_2 reduziertem Katalysator wurde die ODE ohne Zugabe von Gasphasensauerstoff untersucht. Dabei nahm die Produktselektivität bei Vorreduktion in H_2 zu. Dies kann mit einem, im Gegensatz zu einer Reduktion in C_2H_6, geringeren Verhältnis von V^{+4} zu V^{+3} erklärt werden. Die dann geringere Lewis-Acidität des Katalysators verhindert dann die Adsorption der nucleophilen Ethen-Doppelbindung und damit dessen Verbrennung.

Table of Contents

List of Tables

List of Figures

Symbols and Abbreviations

K_i	-	equilibrium constant of reaction i
k_i	s^{-1} $(m^3\ mol^{-1})^{m-1}$	kinetic rate constant of reaction i (with reaction order m)
θ_i	-	degree of adsorption of component i
r_i	mol m^{-3} s^{-1}	rate of reaction i
n	-	reaction order
O*	-	lattice oxygen
*	-	oxygen vacancy
c_i	mol m^{-3}	concentration of component i
ΔH	J mol^{-1}	adsorption enthalpy
E_A	J mol^{-1}	activation energy
r_{eff}	mol m^3 s^{-1}	effective reaction rate
η	-	effectiveness factor
ψ'	-	Weisz modulus
L	m	characteristic length
m	-	reaction order
ρ_{cat}	g mol^{-1}	catalyst density
D_{eff}	m^2 s^{-1}	effective diffusivity
φ	-	differential selectivity
S	-	integral selectivity
z	m	position inside reactor
X	-	conversion
Y	-	yield
TOF	s^{-1}	turn over frequency
$\dot{n}_i$	mol s^{-1}	molecular flow of compound i

m_{cat}	-	catalyst mass
M	g mol^{-1}	molecular weight
w	%	mass percentage
R	J mol^{-1} K^{-1}	ideal gas constant
T	K	temperature
s_c	m^2	molecular cross section
a	m^{-1}	specific surface area
n	-	integral number
λ	m	wavelength
d	m	distance between the layers and
θ	°	diffraction angle
ν	s^{-1}	frequency
B	T	magnetic field
μ_B	J T^{-1}	Bor magneton
ODP		Oxidative Dehydrogenation of Propane
ODE		Oxidative Dehydrogenation of Ethane
ODH		Oxidative Dehydrogenation
SBA-15		Santa Barbara – 15
Eqn.		Equation
PFTR		Plug Flow Tubular Reactor
CSTR		Continuous Stirred Tank Reactor
TPR		Temperature Programmed Reduction
HF-EPR		High Frequency - Electron Paramagnetic Resonance
HF-ESR		Hochfrequenz - Elektronenspinresonanz
XRD		X-Ray Diffraction
ICP		Inductively Coupled Plasma

1 Introduction

1.1 Motivation

The production of lower alkenes is of special interest, because they are important raw materials for the chemical industry. At present such compounds are produced via steam cracking of naphtha and natural gas leading mostly to ethylene, whereas propylene is obtained as a by-product of this reaction. Energy intensive thermal cracking of propane to produce propylene is additionally performed to account for the increasing demand of propylene for the production of engineering polymers.[1] Increasing energy and oil prices, therefore, led to increased research activities on alternative production routes. One of them can be found in the oxidative dehydrogenation reaction of lower alkanes to alkenes. The oxidative pathway is exothermic, thermodynamically not restricted, the applied reaction temperature is comparably low and coke deposition, leading to catalyst deactivation, is minimized in the oxidizing atmosphere. However, the key factors for the control of the catalytic performance, i.e. catalytic activity and product selectivity of this reaction are still not fully understood. Supported vanadia catalysts offer a high catalytic activity, but the similarity of reactants and products leads to a poor selectivity which makes the overall product yield too low for commercial application.[2] For the optimization of process conditions it is mandatory to have a profound insight into the reaction mechanism.

In addition to its commercial implementation, which due to a missing scientific breakthrough still seems to be out of sight, the oxidative dehydrogenation of propane (ODP) on supported vanadia catalysts also is an important test reaction for the fundamental understanding of heterogeneous catalysis on a molecular basis. Knowledge about this reaction type might also be applied to other fields of catalysis.

The goal of the present investigation, therefore, was to elucidate more clearly the mechanistics of the oxidative dehydrogenation of propane (ODP) and ethane (ODE) by means of a structure-reactivity relationship. This was done by shedding light onto the interplay of the reaction participants, which are catalyst, consisting of support material and active component as well as reactants, the lower alkane and oxygen. Based on the resulting insights, it was of special interest to determine product selectivity controlling factors.

1.2 Current State of Research

Vanadia dispersed on metal oxides are known to be active for the oxidative dehydrogenation (ODH) of light alkanes to olefins.[3-16] Analytical investigations indicate that monomeric and/or associated vanadium species are present at the surface of the support materials studied,[8,17] especially depending on the vanadium loading on the respective support material as simplified in Figure 1-1. The investigated support materials are mostly Al_2O_3, TiO_2 and SiO_2.[8] In the case of SiO_2 (SBA-15)-supported vanadium oxide catalysts a strong influence of water on the vanadia dispersion was found. The hydrated state resembles a water containing vanadia gel ($V_2O_5 \cdot H_2O$), which, upon dehydration, undergoes a structural change, leading to a substantial increase in vanadia dispersion.[18,19]

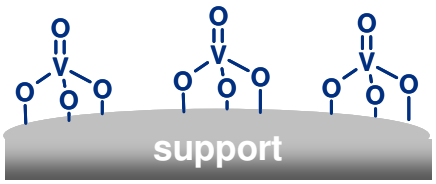

Raman (UV-Vis) (< 1 V nm^{-2})

Wu et al.[20]

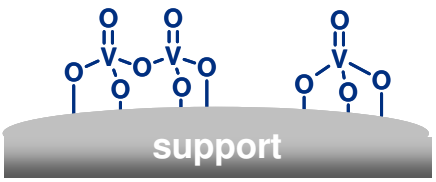

NO/CO molecule probing (< 2 V nm^{-2})

Venkov et al.[17]

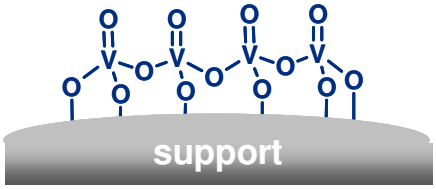

UV-Vis/Raman (2-8 V nm^{-2})

Tian et al.[21]

Raman/XRD (> 8 V nm^{-2})

Weckhuysen et al.[8]

Figure 1-1. Suggested structures of supported vanadium oxide catalysts including the respective analytical method and the range of vanadium surface density.

The generally accepted reaction network of ODH of light alkanes is depicted in Figure 1-2.[22] It describes how the alkane reacts to carbon oxides and the respective alkene, which can subsequently also combust to carbon oxides. Kinetic studies,[13,23,24] however, indicate that the direct oxidation of the alkane to carbon oxides occurs only to a small extent.

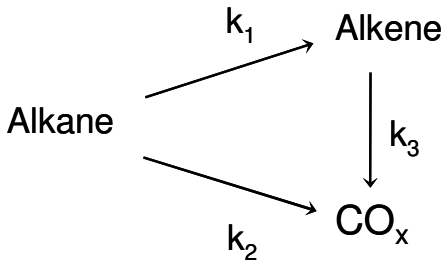

Figure 1-2. Reaction network of ODH.

For the dehydrogenation of propane (ODP) to propene, theoretical DFT calculations were performed by Rozanska et al.[16] for silica supported vanadium oxide catalysts represented by a cubic silsesquioxane $H_8Si_8O_{12}$, in which one Si-H group was replaced by a vanadyl group. Gilardoni et al.[15] presented a study for the (010) surface of a V_4O_{14} cluster. The proposed reaction mechanisms are depicted in Figure 1-3.

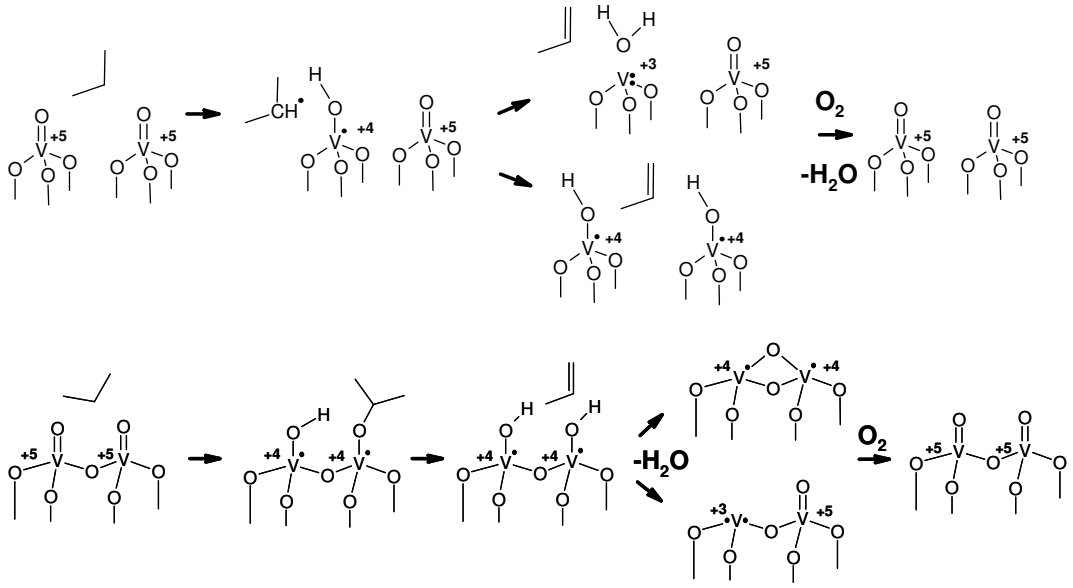

Figure 1-3. Reaction mechanisms of ODP as proposed by Rozanska et al.[16] for monomeric vanadium surface species (top) and Gilardoni et al.[15] for associated vanadium surface species (bottom), respectively.

The illustrated reaction mechanisms indicate that vanadium may change between its oxidation states V^{3+}, V^{4+}, V^{5+}. Based on the lower activation barriers, a one electron reduction (V^{5+} to V^{4+}) was found to be more likely than a two electron reduction (V^{5+} to V^{3+}). The suggested mechanisms are also consistent with isotopic tracer experiments performed by Chen et al.[25,26] All studies conclude that abstraction of the secondary

hydrogen atom is the rate determining step, followed by a second hydrogen transfer leading to the formation of propene and two hydroxyl groups, which subsequently recombine to form water. The authors also conclude that the vanadyl oxygen, which is often denoted as "lattice oxygen", is the main active site. For the consecutive oxidation of propene, it was shown that also a C-H bond cleavage is the rate determining step and carbon oxide species form under further participation of lattice oxygen.[22] According to isotopic tracer experiments for ethane oxidative dehydrogenation (ODE) a similar reaction mechanism is assumed.[7]

Furthermore Chen et al.[27] suggested that the catalytic activity is primarily influenced by the catalyst's reducibility, which is a measure for the ability to delocalize electrons during a catalytic turn over. The increase in reducibility with increasing vanadium loading may be explained by the formation of active polyvanadate species on the support surface which facilitate electron delocalization and lead to an increase in the initial rate of alkane combustion, alkene formation and carbon oxide formation, r_1, r_2, and r_3, respectively. Since a change in reducibility affects the rate constants to different extents as expressed by the ratio of k_3 to k_1,[24] it could also explain a change in the selectivity towards propene. The formation of three-dimensional V_2O_5 structures at very high vanadium loadings leads to a decrease in alkene formation rates because active sites become increasingly unavailable for catalysis.[24]

1.3 Fundamentals

In heterogeneous catalysis substrates and catalysts exist in different phases. Typical reactions are the reduction of nitric oxide under oxidation of carbon monoxide on supported Platinum, Rhodium and/or Palladium catalysts as it is found in the exhaust lines of automobiles (three-way-catalyst) or ODH of lower alkanes on supported vanadium oxide catalysts. The mechanisms of such reactions involve diffusion of the substrate to the active site, adsorption, subsequent reaction, desorption of the product and finally its diffusion from the active site into the product stream. The catalyst itself takes part in the reaction without, however, being altered.

1.3.1 General Kinetics

The kinetic description of heterogeneously catalyzed reactions can be based on different reaction models, namely Langmuir-Hinshelwood or Eley-Rideal. In addition microkinetic approaches, such as the Mars-van-Krevelen (MvK) type mechanism can be used. The bimolecular Langmuir-Hinshelwood model describes the reaction of substrates adsorbed on a catalyst surface, which is expressed in eqns. (1.4) - (1.6).

$$A_{gas} + B_{gas} \overset{K_{ads}}{\rightleftharpoons} A_{ads} + B_{ads} \tag{1.4}$$

$$A_{ads} + B_{ads} \xrightarrow{k_1} C_{ads} \tag{1.5}$$

$$C_{ads} \overset{K_{des}}{\rightleftharpoons} C_{gas} \tag{1.6}$$

In the case of both, a fast substrate adsorption and product desorption, the rate equation can be described as done in eqn. (1.7)

$$r_{AB} = k_1 \Theta_A \Theta_B \tag{1.7}$$

in which r_i is the reaction rate, k_i, the rate constant and θ_i the degree of adsorption which is defined as the ratio of adsorbed molecules n_{ads} to available adsorption places n_0 and usually based on the adsorption model of Langmuir. In this model it is assumed that all adsorption sides are equivalent, each site can only hold one molecule and there are no interactions between adsorbed molecules on adjacent sites. The bimolecular Eley-Rideal type reaction model describes a reaction in which one reactant is adsorbed while the other one reacts out of the gas phase (eqns. (1.8) - (1.10)).

$$A_{gas} \overset{K_{ads}}{\rightleftharpoons} A_{ads} \tag{1.8}$$

$$A_{ads} + B_{gas} \xrightarrow{k_1} C_{ads} \tag{1.9}$$

$$C_{ads} \overset{K_{des}}{\rightleftharpoons} C_{gas} \tag{1.10}$$

In the case of both, fast substrate adsorption and product desorption, the reaction rate is expressed in eqn. (1.11).

$$r_{AB} = k_1 \Theta_A c_B \tag{1.11}$$

If the degree of adsorption is expressed as a function of the respective equilibrium constants, the rate equations discussed above can often be expressed in the generalized form of eqn. (1.12), which is also known as the Hougen-Watson formalism.

$$r_{AB} = \frac{(kinetic\ term)(potential\ term)}{(adsorption\ term)^n} \tag{1.12}$$

In this case, the rate law is a function of a kinetic, potential and adsorption term. The kinetic term describes the rate determining step. The potential term is a measure for the force of the thermodynamic equilibrium and the adsorption term stands for the inhibition of the reaction by coverage of active sites with reactants or products. The power of n describes the number of adsorbed species involved in the rate determining reaction step.

1.3.2 Microkinetics

The processes taking place at a catalyst surface are generally more complex than the kinetic models described above. A given rate law, however, is only of microkinetic nature and, therefore, of mechanistic relevance, if it is a function of elementary reaction steps. An elementary reaction is defined as a process which cannot be subdivided into further elementary steps and a chemical bond has to be cleaved or formed. The development of a microkinetic rate law is described in the following for a substrate reacting with a catalytic active species, often "lattice" oxygen O*, abundant on the catalyst surface. Reactions proceeding via such mechanism are, for example, the CO oxidation on RuO_2 and ODH of lower alcohols and alkanes on supported vanadium oxide catalysts. The reaction scheme is illustrated in eqns. (1-13) - (1-15) and also known as a MvK type reaction mechanism.

$$A_{gas} \overset{K_{ads}}{\rightleftharpoons} A_{ads} \tag{1.13}$$

$$A_{ads} + O* \xrightarrow{k_1} AO** \tag{1.14}$$

$$2* + O_{2,gas} \xrightarrow{k_{reox}} 2O* \tag{1.15}$$

Initially, the substrate A adsorbs on the active site. The subsequent rate determining reaction step leads to the product AO* under formation of oxygen vacancies *, which

are subsequently reoxidized by gas phase oxygen. The respective rate law is expressed by eqn. (1.16).

$$r_{AO*} = k_1 \Theta_A c_{O*} \tag{1.16}$$

The rate depends on the amount of adsorbed substrate and on the concentration of available "lattice" oxygen. For the further development of the MvK rate law, the elementary reaction steps and their dependencies on the reaction conditions, mainly partial pressures of the reactants, have to be known. In the exemplarily case of ODP, based on isotopic tracer experiments by Chen et al.,[22] they are shown in Table 1-1.

Table 1-1. Reaction equations and requirements describing the mechanism of ODP.

Equation	Reaction	Equation
(1-17)	$C_3H_8 + O* \overset{K_1}{\rightleftharpoons} C_3H_8O*$	$K_1 = \frac{c_{C_3H_8O*}}{p_{C_3H_8} c_{O*}}$
(1-18)	$C_3H_8O* + O* \xrightarrow{k_2} C_3H_7O* + OH*$	$r_2 = k_2 c_{C_3H_8O*} c_{O*}$
(1-19)	$C_3H_7O* \xrightarrow{k_3} C_3H_6 + OH*$	$r_3 = k_3 c_{C_3H_7O*}$
(1-20)	$OH* + OH* \overset{K_4}{\rightleftharpoons} H_2O + O** + *$	$K_4 = \frac{c_{OH*}^2}{c_{H_2O} c_{O*} c_*}$
(1-21)	$O_2 + * + * \xrightarrow{k_5} O* + O*$	$r_5 = 2k_5 p_{O_2} c_*^2$

Initially, propane adsorbs on abundant surface "lattice" oxygen atoms to form the activated complex C_3H_8O*. This is followed by hydrogen abstraction of adsorbed propane involving a neighbouring oxygen atom and desorption of propene. The subsequent formation of water under recombination of two neighbouring hydroxyl groups produces reduced vanadium centers depicted as *. Finally, the catalyst is reoxidized with gas phase oxygen. The thermodynamically controlled adsorption of propane on the active site was assumed to be reversible. The only other reversible step was found to be the recombination of two hydroxyl groups to form water. This is based on the fact, that water reveals an inhibiting effect on the overall reaction rate which was not possible if this step would be irreversible. Their study also showed that hydrogen abstraction of the secondary carbon atom in propane is the irreversible, rate determining

step in ODP. The reoxidation of the catalyst was found to be irreversible referring to the results of oxygen isotope scrambling effects.

The rate law of the rate determining step as depicted in eqn. (1-16) leads to the problem that not only the concentration of adsorbed propane, but also of actual "lattice" oxygen remains inaccessible. It is mandatory that the rate law is expressed only as a function of compounds that can be detected experimentally. Using eqn (1-17), eqn (1-21) can be rewritten as eqn. (1-22).

$$r_2 = k_2 K_1 p_{C_3H_8} c_{O*}^2 \tag{1-22}$$

To calculate the unknown concentration of active sites c_{O*}, one has to solve the material balance of the abundant active site. The concentration of all available lattice oxygen atoms is given in eqn (1-23).

$$c_{O*}^{total} = c_{O*} + c_{OH*} \tag{1-23}$$

The unknown concentration of hydroxyl groups can be derived by rearranging eqn (1-20), leading to eqn. (1-24).

$$c_{OH*}^2 = K_4 c_{H_2O} c_{O*} c_* \tag{1-24}$$

At steady state, the concentration of lattice oxygen vacancies c_* is unknown but constant. Hydrogen abstraction being the rate determining step and the irreversible catalyst reoxidation lead to an equal formation and consumption rate of c_*. Hence, eqn. (1-18) is equal to eqn. (1-21), giving eqn. (1-25).

$$c_* = \sqrt{\frac{k_2 K_1 p_{C_3H_8} c_{O*}^2}{2 k_5 p_{O_2}}} \tag{1-25}$$

Inserting eqn. (1-24) and eqn. (1-25), one can write eqn. (1-23) as eqn. (1-26), describing the total number of active sites.

$$c_{O*}^{total} = c_{O*} + c_{O*} \sqrt{K_4 p_{H_2O} \sqrt{\frac{k_2 K_1 p_{C_3H_8}}{2 k_5 p_{O_2}}}} \tag{1-26}$$

Solving eqn. (1-26) for c_{O*} and inclusion in eqn. (1-22) leads to the MvK rate law for ODP, expressed in eqn. (1-27).

$$r_{C_3H_6} = \frac{\left(c_{O*}^{total}\right)^2 k_2 K_1 c_{C_3H_8}}{\left(1 + \frac{\left(K_4 c_{H_2O}\right)^{0.5} \left(k_2 K_1 c_{C_3H_8}\right)^{0.25}}{\left(2k_5 c_{O_2}\right)^{0.25}}\right)^2} \qquad (1\text{-}27)$$

Since the concentration of all active sites involved in the reaction is constant at steady state, it is usually expressed as the rate constant. The rate law includes kinetic and thermodynamic constants. For a discussion of the temperature dependence, the energy profile of adsorption and dehydrogenation of an alkane molecule on the catalyst surface is illustrated in Figure 1-4.

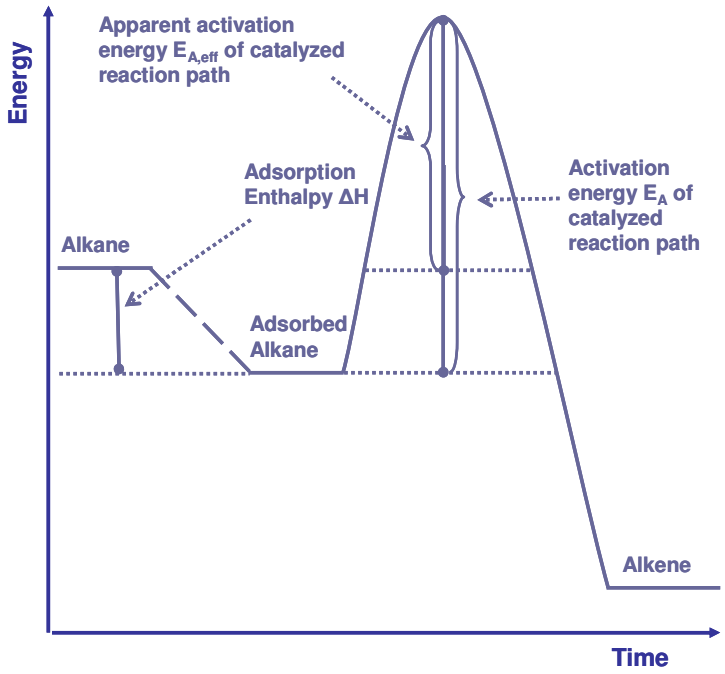

Figure 1-4. Potential energy diagram for alkane ODH.

A catalytic turn over includes the exothermic adsorption (negative ΔH) of the lower alkane and the actual dehydrogenation step with a positive activation energy E_a. With increasing temperature the degree of adsorption is, therefore, decreasing, while the rate constant k_i is increasing.

1.3.3 Mass Transport

Before microkinetic evaluation, the aspect of mass transport limitations has to be considered in order to avoid errors in the interpretation of experimental results. Inside of a porous catalyst particle the reaction rate is often limited by diffusion processes. This leads to a concentration gradient of the substrate between catalyst surface and inside of the particle, thus affecting the local reaction rate. The ratio of the rate influenced by diffusion r_{eff} and the non-influenced rate r_i is also known as the effectiveness factor (eqn. (1-28)).

$$\eta = \frac{r_{eff}}{r_i} \tag{1-28}$$

As η approaches the value 1, no diffusional limitations are present while at lower values the reaction is more or less influenced by mass transport. For an empirical estimation of mass transport phenomena, the effectiveness factor can be plotted as a function of the Weisz modulus Ψ' as shown in Figure 1-5.

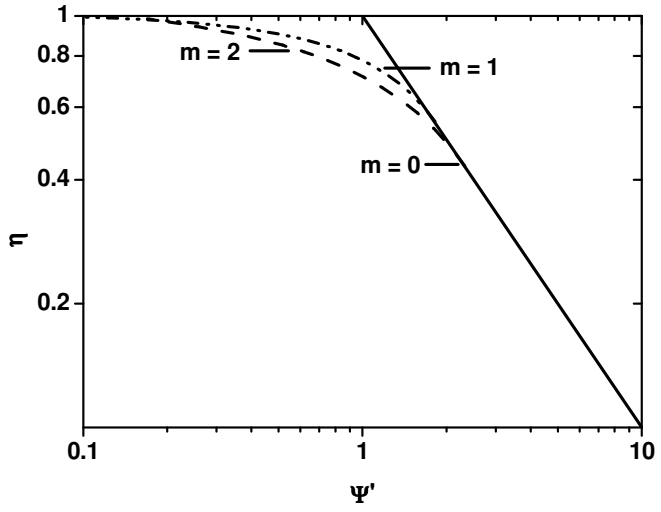

Figure 1-5. Effectiveness factor η as a function of the Weisz modulus ψ' for different reaction orders m.

The Weisz modulus describes the ratio of reaction rate to reactant diffusion rate as shown in eqn. (1-29).

$$\Psi' = L^2 \frac{m+1}{2} \frac{r_{eff}\,\rho_{cat}}{D_{eff,C_3H_8}\,c_{C_3H_8}} \qquad (1\text{-}29)$$

L is the characteristic length of catalyst particle, m the reaction order of the limiting reactant, r_{eff} the measured effective reaction rate, ρ the catalyst density, D_{eff} the effective diffusivity and c_{C3H8} the reactant concentration (here propane). With decreasing values of Ψ' and therefore smaller particles, lower effective reaction rates and/or high diffusion rates, the value of η increases, thus reflecting a decrease in the influence of pore diffusion.

1.3.4 Determination of Activity and Selectivity

Generally, a chemical reaction network is the sum of different simultaneous and/or consecutive reactions, for each of which a rate law can be formulated as it was done above for the propane dehydrogenation step. In the case of ODP the overall network, however, consists of the dehydrogenation, parallel combustion of propane and consecutive combustion of propene to carbon oxides as described in Figure 1-2. The interplay of the mentioned reaction rates leads to a certain product selectivity. The differential selectivity towards the desired product propene at every position in the reactor is defined by eqn. (1-30), which describes the interplay of product forming (propane dehydrogenation) as well as substrate (propane dehydrogenation, propane combustion) and product (propene combustion) consuming reactions.

$$\varphi_{C_3H_6,i} = \frac{r_{C_3H_6,ODH} - r_{C_3H_6,comb}}{-r_{C_3H_8,ODH} - r_{C_3H_8,comb.}} \qquad (1\text{-}30)$$

As can be seen, the product selectivity depends on the rates of all reaction steps, whereas each rate is a function of the respective rate constant (see above). The rate constant itself can be influenced by various factors, since it is a function of temperature, activation energy and pre-exponential factor. Such factors could be, for example, the nature of catalytic active species, e.g. the topology of lattice oxygen atoms. Furthermore the electronic properties of the catalyst surface can influence the activated complex by interaction with the electrons of the substrate molecule.

The integral selectivity, analytically measured at the reactor outlet is the integral of the differential selectivities at different locations z between reactor inlet and outlet, as expressed in eqn. (1-31).

$$S_{C_3H_6} = \int_{i=inlet}^{outlet} \varphi_{C_3H_6} dz = \frac{c_{C_3H_6}}{c_{0,C_3H_8} - c_{C_3H_8}} \tag{1-31}$$

The differential and integral selectivities differ if a plug flow tubular reactor (PFTR, Figure 1-6) is used at high reactant conversions as opposed to the application of a continuous stirred tank reactor (CSTR, Figure 1-6). In the latter, reactants and products are ideally mixed by stirring features, resulting in a gradient free distribution of reactants inside the reactor. In a PFTR, compound concentrations and reaction rates are a function of the position inside the reactor. At low conversions the PFTR can also be used as a gradientless reactor, because in such case the concentration of the reaction participants is roughly the same at any point of the reactor.

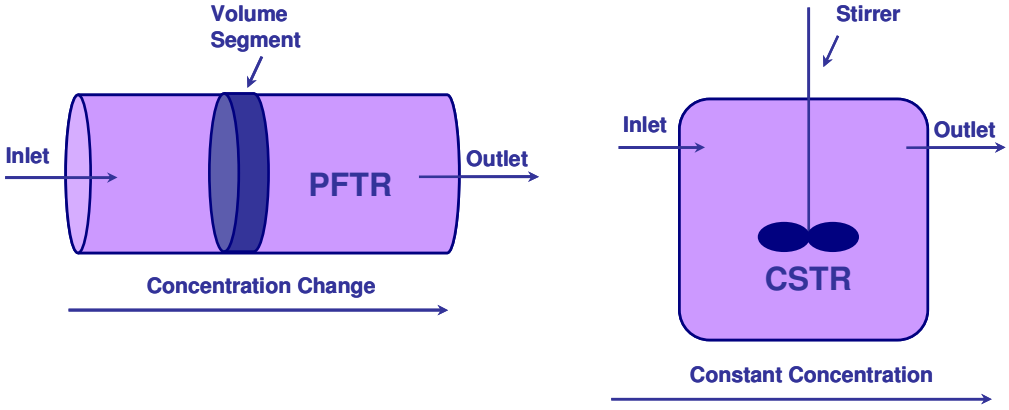

Figure 1-6. Scheme of PFTR and CSTR reactor types**.**

The integral selectivity and the substrate conversion (1-32), reflecting the catalytic activity, lead to the overall product yield Y_i, defined in eqn. (1-33).

$$X_{C_3H_8} = 1 - \frac{c_{C_3H_8}}{c_{C_3H_8,0}} \tag{1-32}$$

$$Y_{C_3H_6} = X_{C_3H_8} S_{C_3H_6} \tag{1-33}$$

The catalytic activity is often also expressed as number of converted substrate molecules per catalytic site, the so called turn over frequency (TOF), which is given in eqn. (1-34).

$$TOF = \frac{\dot{n}_{C_3H_8,0} \cdot X_{C_3H_8} \cdot M_{O*}}{m_{cat} \cdot w_{O*}} \tag{1.34}$$

where $\dot{n}_{i,0}$ is denoted as the substrate inlet flow, X_i the conversion, M_i the molar mass of the active site, m_{cat} the catalyst weight and w_i the active site content by mass.

The product yield is of fundamental meaning for a commercial implementation of a chemical process, since the separation of undesired side products leads to a strong increase in installation and production costs. Commonly, the product selectivity should be higher than 90 % at a reasonable conversion (> 10 %) in order to achieve cost efficiency. One crucial question is, therefore, by which factors the product selectivity is determined. Hence, it is essential to have a profound insight into the structure-reactivity relationship, reflected by reaction mechanism and catalyst structure. Initially, this can be achieved by kinetic parameter determination for each reaction step. Subsequently a molecular model has to be developed. The various vanadium oxidation states involved in a catalytic turn over, for example, could be of decisive relevance and different coordinated lattice oxygen atoms could favour different reaction routes. The present study attempts to find answers to these questions by performing a series of experiments described in the following sections.

2 Experimental

2.1 Catalyst Preparation

For this study three different methods for catalyst preparation were used in order to account for different reaction conditions and catalyst characterization procedures, being applied prior to this study.

For the investigation of the support effect on ODP and the study of reduced active sites a saturation wetness impregnation was used because of its ability to produce highly dispersed vanadia surface species at low catalyst loadings (< 2 V nm^{-2}). The chosen support materials were alumina (Alfa Aesar), ceria (Alfa Aesar), titania (Sachtleben Chemie), zirconia (Alfa Aesar) and silica (BASF). Except for CeO_2 these were received as porous pellets. Prior to the impregnation, pellets were crushed and sieved to a particle size fraction of 0.1 to 0.3 mm. The CeO_2 powder was first pressed to tablets at a pressure of 100 bar for 5 min and then crushed and sieved. The impregnation procedure consisted of the following steps: First a saturated solution of vanadyl acetylacetonate (Sigma-Aldrich, > 97%) in toluene was heated under reflux. For each catalyst sample, about 2 g of the support was added to 250 ml of the solution and boiled

under reflux for about 1 h. The impregnated particles were thoroughly washed with fresh toluene to remove unbound vanadyl species, then dried at 353 K, and finally calcined in air at 773 K for 3 h. The calcined catalysts were sieved again. Please note that special care was taken to prepare all catalysts in the same way, using identical precursor concentrations, boiling and calcination times for each batch. In the following impregnated and subsequently calcinated support materials are denoted as V-CeO_2, V-TiO_2, V-Al_2O_3, V-ZrO_2 as well as V-SiO_2 and pure support materials as CeO_2, TiO_2, Al_2O_3, ZrO_2 and SiO_2. The resulting catalyst particles are depicted in Figure 2-1.

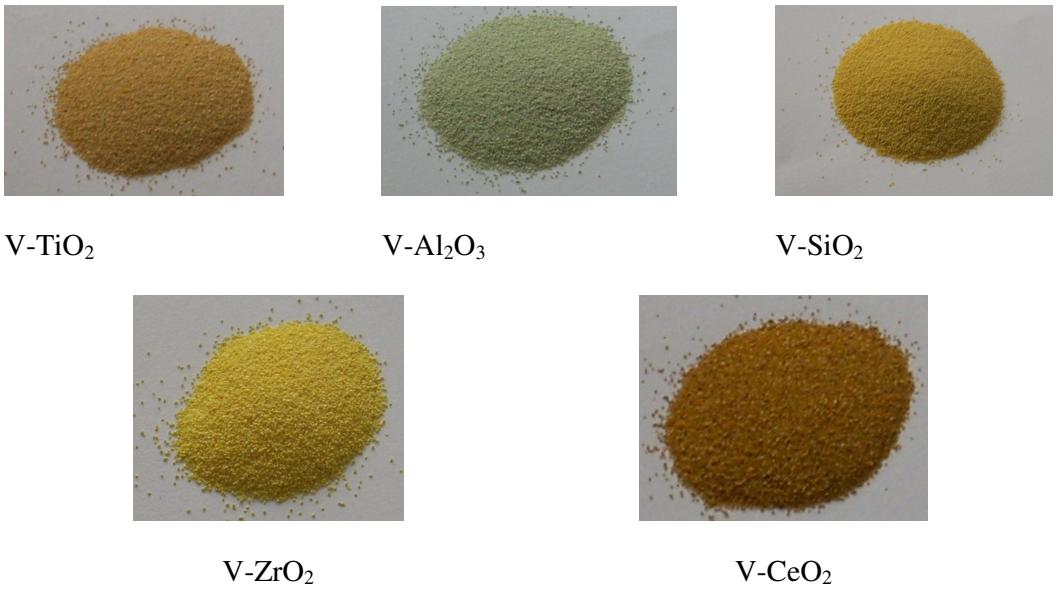

Figure 2-1. Different supported catalysts used for the study of support effects on ODP.

For the investigation of the kinetics of ODP and the study of reduced active sites, a silica (SBA-15) supported vanadium catalyst (V-SBA-15) was used in addition. In this case a grafting/ion-exchange method was invoked,[28] because samples prepared by this method had been characterized in detail before.[17,19] The silica SBA-15 supported vanadia catalysts were prepared by a grafting/ion-exchange procedure consisting of (1) surface functionalization of SBA-15 using 3-aminopropyltrimethoxysilane (APTMS) and subsequent HCl treatment leading to the formation of the corresponding ammonium salt (functionalized SBA-15), (2) ion exchange of decavanadate and (3) a final calcination step at 550°C. For the catalytic material used here (V-SBA-15) 73 mg of ammonium decavanadate were added to a suspension of 1 g of functionalized SBA-15

in water. The calcinated catalyst consisted of bright yellow particles as shown in Figure 2-2.

Figure 2-2. V-SBA-15 catalyst used for the kinetic simulation study of ODP.

The investigation concerning the role of lattice oxygen in ODE was done at the University of California, Berkeley. For this non-steady state study higher vanadium loadings were needed in order to obtain measurable signal intensities during the product analysis with a mass spectrometer. In this range of vanadium loadings (~ 7 V nm^{-2}) an incipient wetness impregnation was found to be best for reproducible catalyst samples. The support material (γ-alumina, Degussa AG, 119 m^2 g^{-1}) was impregnated with vanadyl isopropoxide (Sigma-Aldrich, 99%) in 2-propanol (Sigma-Aldrich, 99.9%). Impregnation was performed in a glovebag purged with N_2 (Paraxair, 99.99%) to prevent hydrolysis of the alkoxide precursor. After impregnation, the sample was dried overnight at ambient temperature. The sample was transferred to and sealed in a quartz reactor. The catalyst (400 mg) was treated at 393 K for 1 h followed by 1 h at 573 K in He (Praxair, 99.999%) flowing at 1.67 cm^3 s^{-1}. The flow of He was then replaced by an equivalent flow of dry air and treatment of the catalyst was continued at 573 K for 1 h, after which the temperature was raised to 773 K and held at this level for 2 h. The resulting catalyst, shown in Figure 2-3**,** is further denoted as V-Al_2O_3-H.

Figure 2-3. V-Al_2O_3-H used for the investigation of the role of lattice oxygen in ODE.

2.2 Physico-Chemical Characterization

2.2.1 Nitrogen Physisorption

Nitrogen physisorption is used for the determination of specific surface areas. At a given temperature, the adsorbed gas volume is a function of the gas pressure. At the point of monolayer adsorption the isotherme changes into a plateau. With the given cross section s_c of the adsorbed gas (s_c = 0.162 nm^2 for nitrogen), the volume of gas needed for a molecular monolayer a_m leads to the specific surface area S of the investigated compound expressed in eqn. (2.1)

$$S = a_m N_A s_c \tag{2.1}$$

The empirical adsorption isotherm of Brunauer, Emmett and Teller (BET) shown in eqn. (2.2) extends the monolayer adsorption to multilayer adsorption in the range of relative pressures p/p_0 of 0.05 to 0.35:

$$\frac{\frac{p}{p_0}}{a(1-\frac{p}{p_0})} = \frac{1}{a_m c} + \frac{c-1}{a_m c}\frac{p}{p_0} \tag{2.2}$$

in which c is the BET constant. The method is based on the following assumptions: (i) The gas molecules physically adsorb on a solid in infinite layers and (ii) there are no interactions between the layers.

Catalyst and support surface area were determined by nitrogen adsorption at liquid nitrogen temperature (77 K), using a Micromeritics 2375 BET device equipped with a Vacprep 061 degasser. Samples were degassed for 1 h at 300 °C and 0.15 mbar before experiments to ensure a clean and dry surface. Surface areas were calculated using the BET method.

2.2.2 X-ray Diffraction

The diffraction of X-rays on condensed matter is used to structurally characterize crystals and quasi-crystals. Diffraction occurs if the distance between adjacent layers of atoms is in the range of the wavelength of the incoming X-ray, as it is the case in crystallites. The incoming X-rays induce excitation of the abundant electrons, which subsequently emit X-rays. Depending on the arrangement and distance of the lattice

atoms the constructive or destructive interferences of these waves lead to certain patterns, which can be resolved in a diffractogram. The interference depends on the angle of the incoming light and leads to the Bragg equation (eqn. 2.3), which is the mathematical description of the interference phenomenon.

$$n\lambda = 2d\sin(\Theta) \tag{2.3}$$

with n an integral number, λ the wavelength of the incoming light, d the distance between the layers and θ the angle between incoming and scattered light. The right side of eqn. (2.3) describes the retardation between two, at different layers diffracted, light beams while the left side is an integer multiple of the wavelength. If the retardation is an integer of the wavelength, constructive interference occurs, which leads to a signal in the diffractogram. In this study, XRD led to information about the phase of the respective support material, but also about crystalline V_2O_5 which might be found at the catalyst surface.

Experiments were carried out using a Theta-Theta-diffractometer D 5005 (Siemens) with Cu-K_α radiation (λ = 0,1542 nm) at 40 kV and 30 mA covering a scanning angle from 10 to 90°. Data analysis was done with Bruker Diffrac-Plus.

2.2.3 Raman Spectroscopy

Raman spectroscopy was used as an additional method for characterization, because XRD is limited in its sensitivity towards detection of crystalline surface vanadium species. It is based on inelastic scattering of light with molecules in various states of aggregation. During an experiment a monochromatic light source, e.g. laser light, is radiated onto the sample, which leads to light scattering. Besides scattered intensities of the incoming wavelength (Rayleigh scattering), additional frequencies can be observed in the light detector. The change in frequencies originates from interactions of the light wave with rotational and vibrational states of the respective molecule. This so called "Raman effect" occurs if energy is transferred from the light beam onto the matter (Stokes effect) or vice versa (anti-Stokes effect). Since the wavelength of the scattered light depends on its energy, the scattered light is shifted to certain wavelength resulting in a spectrum which depends on the characteristics of the investigated molecule.

Raman experiments were performed using a fiber probe, which was inserted into an *in situ* Raman cell. The powder samples were placed "as is" in a stainless steel

sample holder with a 0.6 mm deep rectangular well covering an area of (12×8) mm^2. Prior to experiments the samples were dehydrated by treatment in 20% O_2/He (50 ml min^{-1}) at 300 °C for 60 min and subsequently cooled to room temperature. Raman spectra were recorded using 514 nm laser excitation (5 mW) at 5 cm^{-1} spectral resolution (Kaiser Optical). Sampling times were typically 30 min. For the investigation of the catalysts structural stability, samples were also studied after the reaction. Prior to the Raman experiments these samples were treated in air at 450°C to reduce the absorbance of Raman light through carbon surface species. Some of the samples still had a greyish color after the treatment. However, to avoid structural changes of the catalyst the temperature was not further increased.

2.2.4 Temperature-Programmed Reduction (TPR)

TPR is used for the investigation of the reducibility of a given catalyst. During the experiment the catalyst is exposed to a constant flow of the probe molecule, which is usually hydrogen (H_2). The concentration of this probe gas is followed by mass spectrometry, while the temperature in the reaction chamber is slowly increased. At a certain temperature, the so called onset, the catalytic active site starts to react with the reducing agent and lowers its concentration in the gas phase, while usually the concentration of produced water increases concurrently. The onset temperature gives information about the reducibility of the catalyst and can therefore be used as a measure for its activity. The amount of hydrogen, expressed in the area of the reduction peak, may be used for the quantification of active sites. However, one has to be sure that hydrogen is only activating the investigated site. In some cases, a hydrogen spill-over effect may take place, which artificially increases the amount of activated hydrogen, since it is incorporated into the catalyst. The number of reduction peaks, furthermore, indicates the number of different active sites, in case their reactivity is considerably different. In case of a similar reducibility, the reduction peaks may merge into a single peak.

In case of catalyst characterization of different supported vanadium oxide catalysts (V-Al_2O_3, V-TiO_2, V-SiO_2, V-CeO_2 and V-ZrO_2), TPR experiment samples of about 200 mg each were used. Experiments were performed in a 5 Vol% H_2/Ar stream, with a heating rate of 20 °C min^{-1} and 50 cm^3 min^{-1} flow rate. Hydrogen consumption was recorded by an InProcessInstruments mass spectrometer. Ahead of experiments,

samples were treated in an O_2/Ne flow (20 Vol% O_2) at 773 K for 0.5 h and cooled down to 323 K. Samples were then purged with Ne for 15 min. The hydrogen flow was started subsequently.

For the study of the role of lattice oxygen in ODE involving the quantitative reduction of V-Al_2O_3-H, TPR was carried out with 400 mg of catalyst using a 1.5 % H_2/Ar mixture flowing at 1 cm^3s^{-1} and a heating rate of 0.33 Ks^{-1}. Hydrogen consumption was recorded by an MKS Mini-Lab quadrupole mass spectrometer. Prior to each experiment, the catalyst was treated in a 10% O_2/He flow at 773 K for 45 min and cooled down to 323 K. After purging in He for 15 min, the flow of hydrogen was initiated. Following reduction, oxygen was pulsed over the catalyst, each pulse corresponding to an amount of 1.8 µmol O_2, in order to calculate the number of reduced sites. This method was found to give a reproducible measure of the extent of catalyst reduction, since the amount of hydrogen consumed during the TPR does not correspond to the total number of active sites being reduced.[29]

2.2.5 Calorimetric Measurements

Calorimetry is used for the measurement of heat transfer related to certain endothermic or exothermic physical, chemical or biological processes. It is, for example, used to determine the specific heat capacity of a sample and the adsorption enthalpies of gases on solids. Calorimetric measurements can be conducted in adiabatic or isothermal mode. In the case of adiabatic mode, the temperature difference between a given sample and the calorimeter is compensated by in- or decreasing the temperature, whereas isothermal measurements are conducted under a constant temperature.

For calorimetric measurements, a Calvet calorimeter (MS70 SETARAM) had been combined with a house-designed high vacuum system, which enables the dosage of probe molecules within a range of 0.02 µmol. The pressure-controlled dosing systems allows for the detection of adsorbed amounts of molecules (adsorption isotherm) as well as differential heat of adsorption and gives the possibility to elucidate the distribution of the adsorption sites along the range of adsorption heats.[30] The samples were pre-treated and activated under mild conditions to minimize thermal and mechanical stress. All samples were pressed under low pressures (125 MPa; V-SBA-15 nearly stable up to 376 MPa, decrease of surface area (10 %) of SBA-15 beyond 296 MPa) and cut into small pellets, which were sieved to a diameter of 0.4 to 0.6 mm due

to ultra high vacuum (UHV) conditions.[31,32] The activation was conducted separately in the calorimetric cell connected to a turbomolecular pump (Balzers). The activation was performed for 17 h at 373 K. The final pressure in the degassed cell was 10^{-6} mbar. The cell was cooled down to 313 K, placed inside the calorimeter and connected to the micro calorimetric gas-adsorption system, subsequently. Propane 3.5 (Messer Griesheim) was dosed stepwise. Pressures (mbar), adsorption temperatures (°C) and the heat signals (V) were recorded.

2.2.6 High Frequency Electron Paramagnetic Resonance (EPR)

EPR spectroscopy is used to measure the absorption of electromagnetic radiation in samples with paramagnetic sites in a magnetic field. Thus it is suitable for the investigation of substances containing permanent paramagnetic moments. In a magnetic field, otherwise degenerated m_S spin sublevels are split, also known as the "Zeeman effect". If resonance conditions are met, net absorption from a microwave field can be detected. The splitting of energy levels depends on the local environment and symmetry at the paramagnetic site. The resulting spectra, therefore, are fingerprints of the local properties of the paramagnetic center. The experiment is usually carried out by slowly changing the magnetic field while irradiating the sample with an electromagnetic field of constant frequency. The resulting absorption is conventionally expressed as a function of the swept external field. For comparison of spectra, taken at different microwave frequencies it is more appropriate to plot the data as function of the g value, which is defined in eqn. (2.4)

$$g = \frac{\nu}{\mu_B B} \tag{2.4}$$

in which ν is the frequency of the incoming microwave, B the magnetic field intensity and μ_B the Bohr magneton.

The high-frequency EPR measurements were performed at the National High Magnetic Field Laboratory (NHMFL), Tallahassee.[33] The setup used operates in transmission mode and employs oversized cylindrical waveguides. The microwaves were generated by a phase-locked Virginia Diodes source generating frequency of 13 ± 1 GHz and producing its harmonics, of which the 4^{th}, 8^{th}, 16^{th}, 24^{th} and 32^{nd} were available. A frequency range of ca. 48 – 448 GHz can be covered. Microwave power

incident on the waveguide was adjusted to approximately 5 mW. Microwave power incident on the sample probably was in the order of 1 mW. No resonator was used. Microwave detection was performed with a low-noise, fast-response InSb hot-electron bolometer (QMC Ltd.), operated at liquid helium temperature. A field modulation in the range of 10–50 kHz was used to obtain “first-derivative-type” EPR spectra. Microwave frequencies in the range of 200 to 400 GHz were chosen for our experiments to allow for optimal spectral dispersion and frequency resolution. A superconducting magnet (Oxford Instruments), capable of reaching a field of 14.9 T was employed, thus covering the important ”g = 2“ region of spectra, characteristic for doublet radicals.

2.3 Reactor Setup

Catalytic measurements were performed in a 6-channel screening-apparatus at ambient pressure with U-shaped fixed-bed quartz reactors (6 mm internal diameter) connected in parallel. The reactant mixture passed a static mixer and was pre-heated up to 423 K prior to entering the reactors. The reactors, containing the diluted catalyst between two layers of quartz particles, were heated in a temperature controlled fluidized sand bed. The reaction temperature was measured in a separate quartz tube placed in the respective position of the sand bed. For the measurement of the temperature profile in the catalyst bed during the reaction, a special reactor was designed, containing an axially movable thermocouple located in a quartz capillary in the center. The reactor setup is shown in Figure 2-4. The flow scheme is illustrated in Figure 2-5.

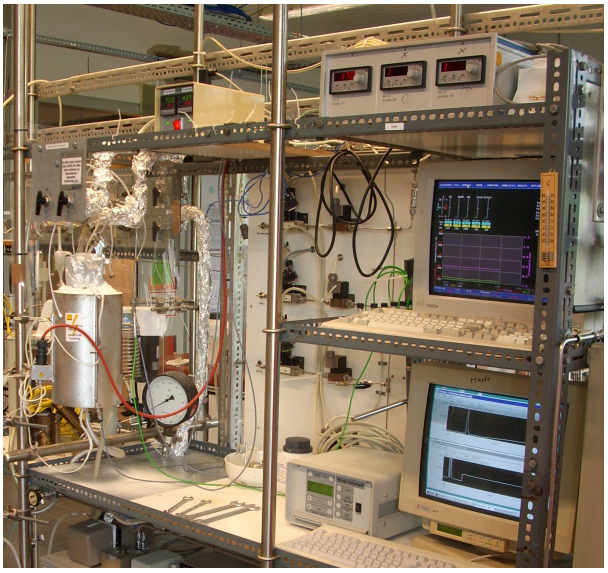

Figure 2-4. Reactor setup used for the investigation of ODP.

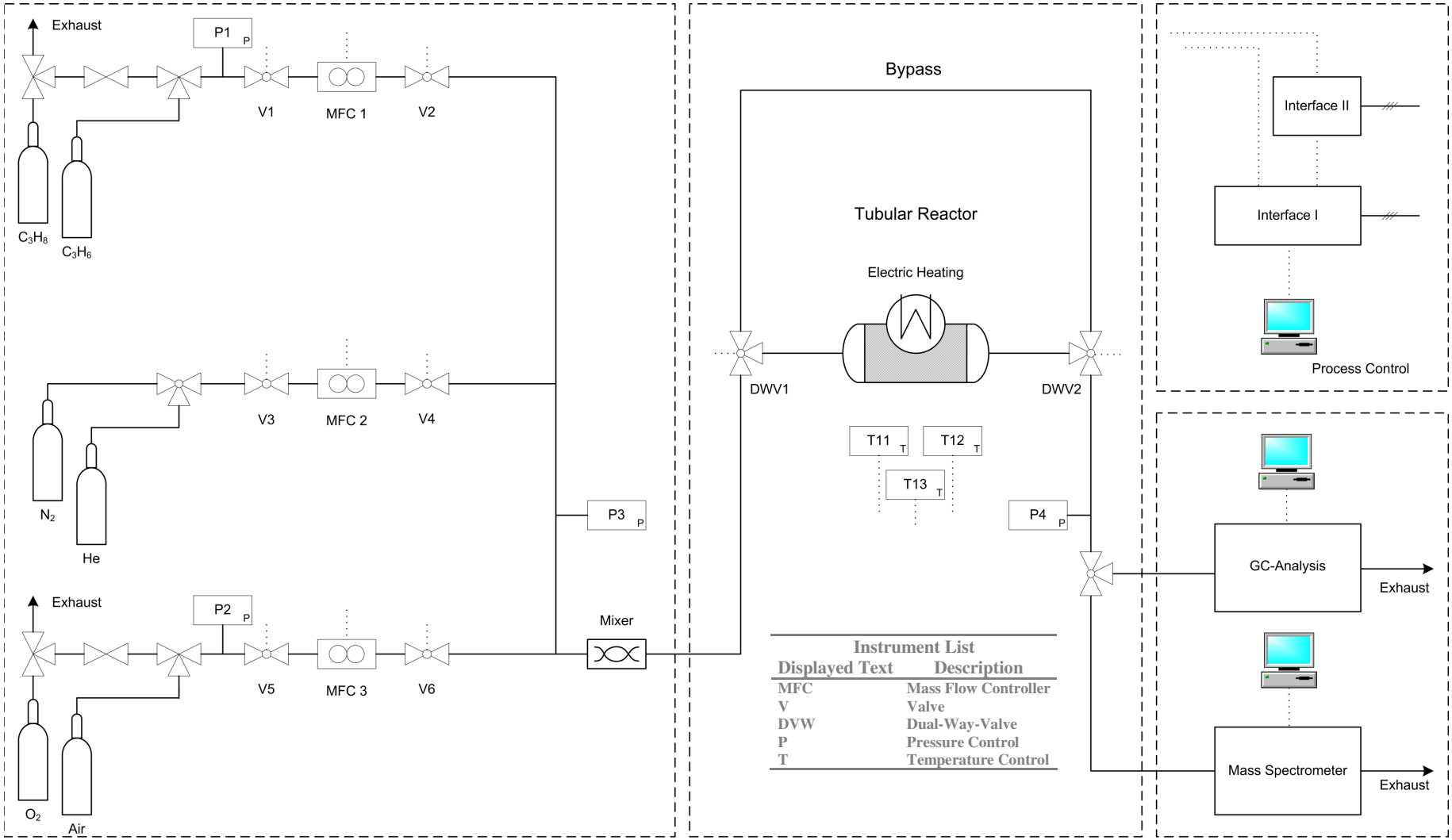

Figure 2-5. Flow scheme of the catalyst screening setup

In case of the study on the effect of the support material on ODP, the kinetic study on V-SBA-15 and the study of reduced sites, experimental runs were carried out at temperatures between 673 and 773 K using U-shaped fixed bed quartz reactors at atmospheric pressure. For the measurements, catalyst amounts between 1 - 1000 mg were portioned to 6 different channels. Using synthetic air as oxygen source, propane and oxygen were fed in the ratio 1:1 ($C_3H_8/O_2/N_2$ = 16.9/16.9/67.5), 2:1 ($C_3H_8/O_2/N_2$ = 29.1/14.5/56.4), 4:1 ($C_3H_8/O_2/N_2$ = 45/11.3/45), 8:1 ($C_3H_8/O_2/N_2$ = 62.3/7.8/31.2), and 2:4 ($C_3H_8/O_2/N_2$ = 9.2/18.4/73.7) with a gas hourly space velocity (GHSV) of 6.6 10^2 – 10^4 h^{-1}. The propane conversion was kept below 10 %, which enables for isothermal and differential conditions. Mass transfer limitations were avoided by working with particle sizes of 200 to 300 µm. This is described in more details elsewhere.[34] In addition, diffusional limitations were identified by effectiveness factor η and Weisz modulus Ψ' (Chapter 1.3.3) considering propane as the limiting reactant. The parameters for the calculation are given in Table 2-1.

Table 2-1. Parameters used for the calculation of the Weisz modulus.

Parameter	Value	Unit
L	10^{-4}	m
M	1	-
r_{eff}	$6x10^{-3}$	mol s^{-1} kg^{-1}
P	$2x10^3$	kg m^{-3}
D_{eff}	10^{-5}	m^2 s^{-1}
C	8	mol m^{-3}
T	500	°C

With a propane conversion of 10 % and the data given above a Weisz modulus of 0.15 is calculated indicating that the reaction proceeds much slower than the propane diffusion and no mass transfer limitation needs to be considered at 500 °C or lower temperatures. Concentrations of the individual components were calculated from a GC analysis of the product gas and expressed in mol m^{-3}.

The product mixture leaving the reactor was analyzed by an on-line gas chromatograph (GC, Satochrom 5873), equipped with Poraplot Q and Molsieve 5 columns as depicted in Figure 2-6**.** Light gases (O_2, N_2, CO, CH_4, CO_2) were detected with a thermal conductivity detector, C_2 and C_3 hydrocarbons and oxygenates were quantified using a flame ionization detector. Using nitrogen as an internal standard, the

reproducibility of conversion and selectivity measurement and calculation is sufficient (relative deviation < 5% for ODP). The duration of one GC analysis was about 20 min, which is longer than the time to achieve pseudo-steady state conditions, as confirmed by repeated measurements in one channel.

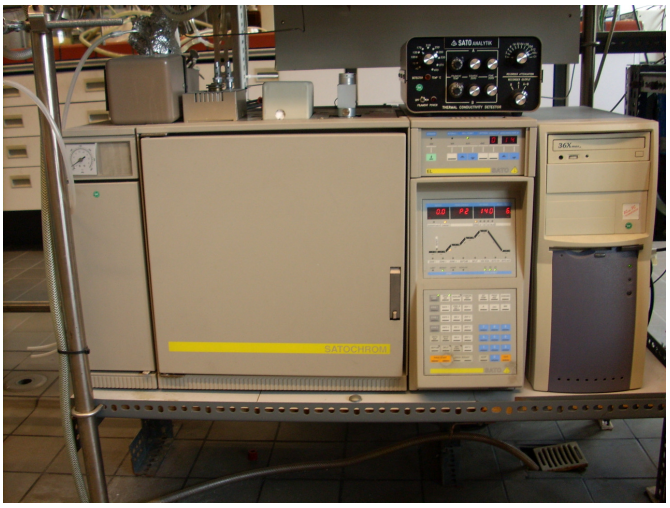

Figure 2-6. GC for analysis of ODP products.

Non-steady state reaction of ethane was carried out at one atmosphere and 773 K using a U-shaped fixed bed, quartz reactor filled with 400 mg of catalyst diluted with 1g of quartz, both with a particle size between 75 to 150 µm in order to avoid hot spots in the reactor. The reactor setup is depicted in Figure 2-7.

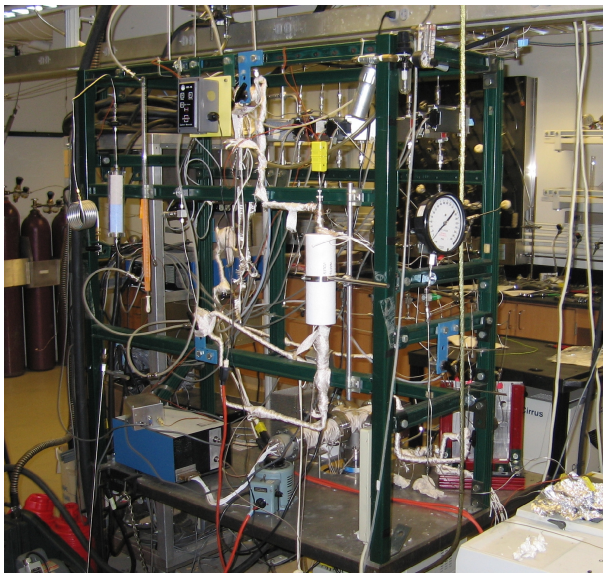

Figure 2-7. Reactor setup used for the investigation of ODE.

A mixture of C_2H_6 in He and Ar was fed into the reactor (C_2H_6/He/Ar = 16.2/84.2/0.85) at a GHSV of 3.6x103 h-1. The reactor effluent was analyzed by an MKS Mini-Lab quadrupole mass spectrometer as illustrated in Figure 2-8. Data collection was done for four masses every 2 s. Response factors were determined for C_2H_6, C_2H_4, CO_2 and CO relative to Ar, which was used as an internal standard (Atomic mass units recorded were 44, 30, 28 and 26). A matrix deconvolution program was used to deconvolute the data.[35] Numerical analysis of transient data was done with MAPLE V Release 4 Student Edition.

Figure 2-8. MKS Minilab used for product analysis.

3 Different Support Materials and Their Influence on Kinetic Parameters

3.1 Introduction

Intelligent catalyst design requires a profound knowledge of the reaction mechanism. However, a detailed understanding of the influence of the support material on the reaction mechanism of the ODP is still missing, despite numerous studies on the influence of support materials on the catalytic performance as well as the kinetics of this reaction.[2,9,36,37-41] A quantitative comparison of these results requires careful consideration of heat and mass transfer limitations. Because of a lack in structural characterization of many catalysts used for kinetic studies, reproducibility of gathered data is, however, not always granted. In the past only few studies were devoted to selectivity aspects of the ODP,[42,43] even though they state a powerful tool to ascertain models of possible reaction networks.

One of the objectives of catalysis research is to develop a detailed description of the relationship between structure and reactivity by bridging the gap between kinetic modelling, quantum chemistry calculations and analytical characterization. Kinetic investigations reveal a low reaction order for oxygen and reaction orders in the range of one for propane.[34,39] Previous studies underline the theory of a MvK mechanism as a microkinetic model, which suggests that lattice oxygen takes part in the reaction.[44,45] Quantum chemistry calculations by means of density functional theory (DFT) are currently exploring energetically favourable reaction sites in ODP. For silica supported vanadia catalysts calculations considered monomeric and/or dimeric vanadium oxide surface species to take part in ODP.[16] For a model (010) surface of a V_2O_5 system it was suggested that at least two V=O groups bonded by a V-O-V bond are required for the dissociative adsorption of propane.[15]

This chapter exhibits data concerning kinetics and selectivities for the ODP on differently supported vanadia catalysts. The impact of mass- and heat transfer effects on ODP even over a low (< 2 V nm-²) loaded alumina supported catalyst has recently been reported.[34] The focus of this study are highly dispersed supported vanadia catalysts with the objective of a comparison of the gathered kinetic data with that originating from quantum chemistry calculations and other well characterized catalyst systems.[16,46] The disadvantage of catalysts providing a low surface density of vanadium is the

possibility of propene adsorption on acidic sites of the bare support material, its consecutive decomposition and deep oxidation. On the other hand, these catalysts are considered to present a good starting point for a comparative study due to their high vanadium dispersion. The influence of pure support material was also taken into account in order to observe perturbing support influences besides acidic sites.

3.2 Results

BET surface areas for catalysts and support materials as well as apparent VO_x surface densities and TPR peak maxima are shown in Table 3-1. Only a slight decrease in surface area after impregnation and calcination treatment is observed.

Table 3-1. Surface areas, vanadia content and TPR peak maxima of differently supported catalysts.

	Surface Area		**Loading**		**TPR Max**
support	m^2/g_{cat}	$m^2/g_{support}$	V/nm^2	wt% V_2O_5	°C
TiO_2	66	68	1,5	1,6	498
Al_2O_3	96	100	1,4	2,1	515
ZrO_2	108	110	1,0	1,6	456
SiO_2	151	154	0,3	0,6	557
CeO_2	60	62	1,5	1,4	538

Figure 3-1 shows the results of TPR experiments. They show only one reduction peak for each catalyst, except for V-CeO_2, which shows a second weak peak at about 700 °C. Please note, that there are no TPR signals for the bare support materials, except for CeO_2 as discussed below.

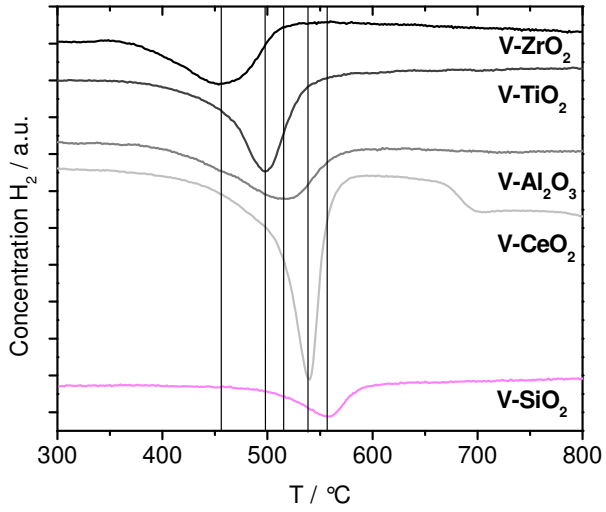

Figure 3-1. TPR spectra of V-Al_2O_3, V-TiO_2, V-CeO_2, V-SiO_2, V-ZrO_2. Lines indicate maxima of reduction peaks. Spectra are offset for clarity.

XRD patterns of the supported vanadium oxide catalysts are depicted in Figure 3-2 together with the diffraction pattern of V_2O_5. The catalyst patterns are identical to those of the respective support material (only catalyst spectra shown here). The peak pattern of bulk V_2O_5 differs from that of the catalysts.

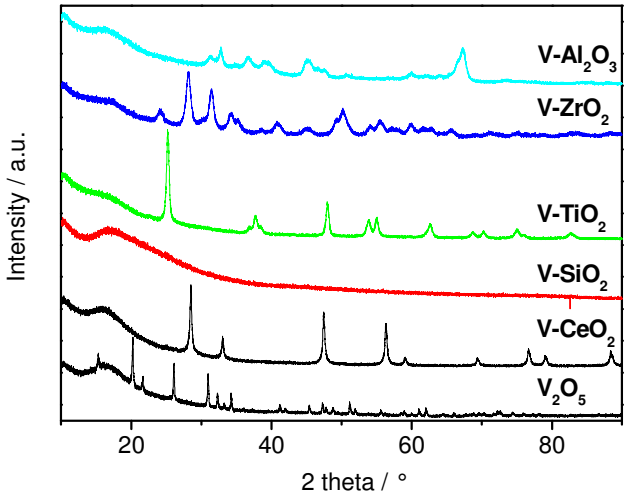

Figure 3-2. XRD patterns of V-Al_2O_3, V-TiO_2, V-CeO_2, V-SiO_2, V-ZrO_2, and V_2O_5. The patterns are offset for clarity.

Figure 3-3 depicts Raman spectra of dehydrated V-Al_2O_3, V-TiO_2, V-CeO_2, V-SiO_2, V-ZrO_2 before and after exposure to the reaction mixture and also contains a spectrum of V_2O_5 as reference. Before the reaction all catalysts exhibit vanadia-related Raman bands within 1015-1045 cm-1. For some of the after-reaction samples these bands peaks are weaker or have completely disappeared.

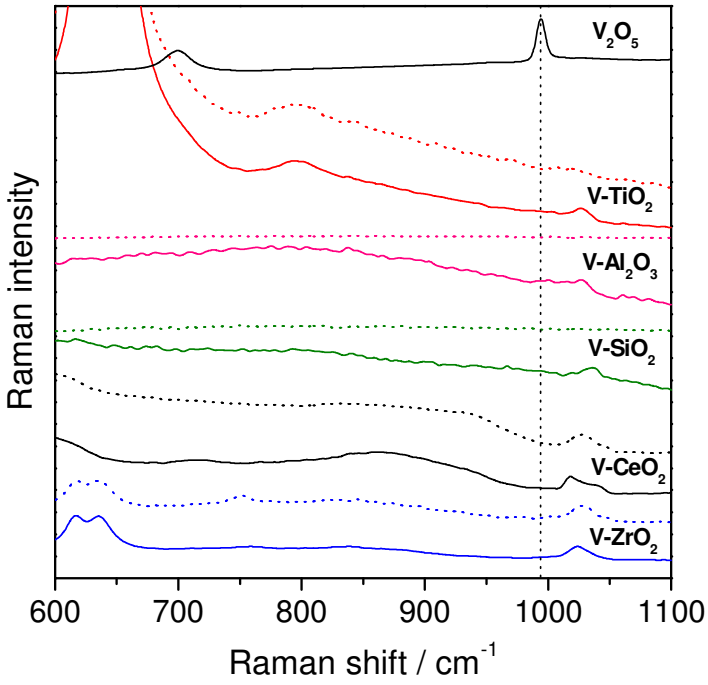

Figure 3-3. Raman spectra of dehydrated V-Al_2O_3, V-TiO_2, V-CeO_2, V-SiO_2, V-ZrO_2 before (solid lines) and after reaction (dashed lines). V_2O_5 depicted as a reference. Spectra are offset for clarity.

Figure 3-4 gives a detailed view of the range of the vanadyl stretch vibrations and reveals that the position as well as the shape of the Raman bands is quite different for the different support materials.

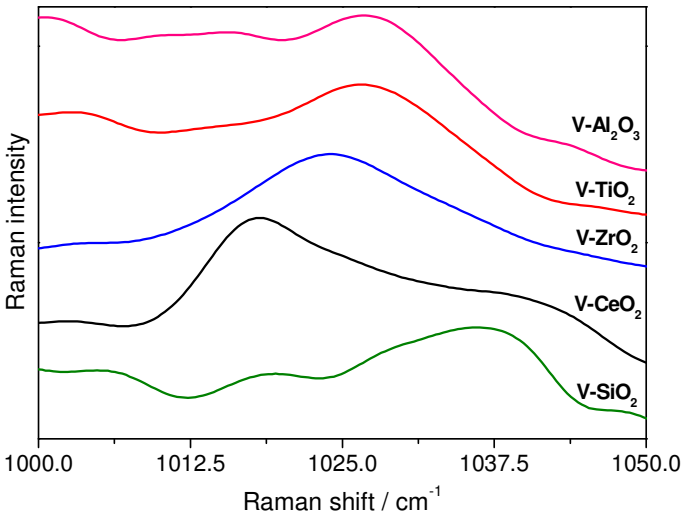

Figure 3-4. Raman spectra of dehydrated V-Al_2O_3, V-TiO_2, V-CeO_2, V-SiO_2, V-ZrO_2 before reaction. Spectra are offset for clarity.

For V-ZrO_2 the catalyst showed major Raman bands at 179, 190, 334, 347, 382, 477, 617 and 635 cm^{-1} before the reaction, which are characteristic of monoclinic zirconia.[47] For the after-reaction sample additional small bands at 417, 576 and 750 cm^{-1} were observed (Figure 3-5).

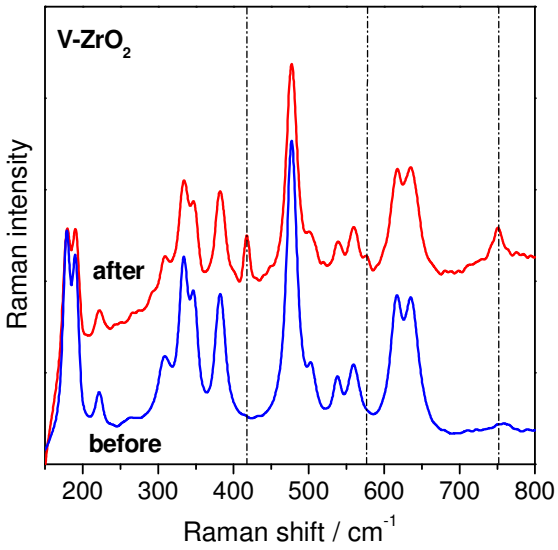

Figure 3-5. Raman spectrum of V-ZrO_2 before and after reaction.

To ensure isothermal conditions, the reactor temperature profile of propene combustion on a zirconia supported vanadia catalyst was measured (Figure 3-6), as this reaction represents the most exothermic partial reaction of the ODP reaction network on the most active catalyst. It was used to acquire the worst case reactor temperature profile. This ensures less pronounced profiles for all other reactions.

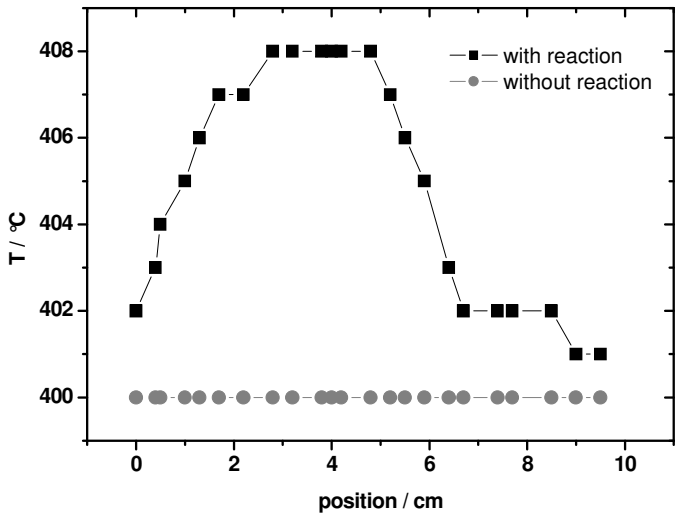

Figure 3-6. Temperature profiles within the catalyst bed with and without reaction for the propene combustion on V-ZrO_2 at 400 °C. With reaction: Composition: $C_3H_6/O_2/N_2$ = 29.1/14.5/56.4; gas flow: 60 ml min^{-1}; without reaction: Composition: N_2 = 60, gas flow: 60 ml min^{-1}, respectively.

In order to exclude mass transfer limitations, selectivity-conversion trajectories for the most active catalyst V-ZrO_2 were recorded for different particle sizes. As described previously,[34] similar trajectories depicted in Figure 3-7, reveal, that the effect of mass transfer limitations at 400 °C is negligible. Figure 3-8 shows the selectivity conversion trajectories of the differently supported catalysts at 400 °C. It is evident that there are large differences in selectivity towards propene in the studied conversion range. The order of selectivities at isoconversion at 400 °C is V-Al_2O_3 > V-TiO_2 > V-CeO_2 > V-SiO_2 > V-ZrO_2. For all catalysts except V-ZrO_2, propene selectivities seem to approach selectivites near 100% at zero conversion.

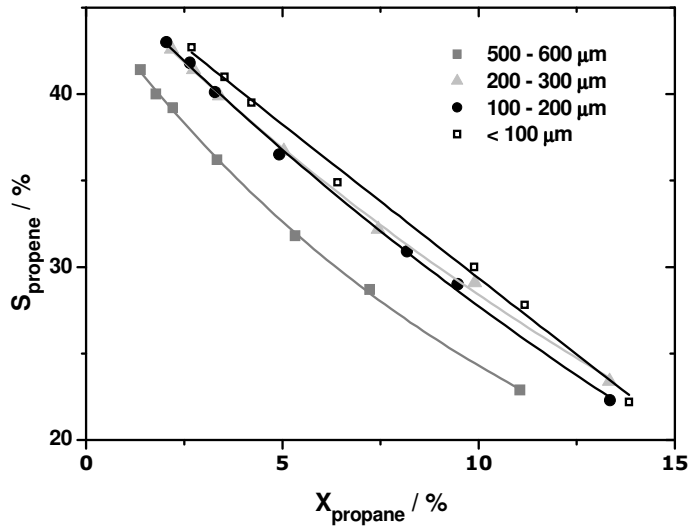

Figure 3-7. Selectivity-Conversion trajectories for V-ZrO_2 at 400 °C for different particle sizes. $C_3H_8/O_2/N_2$ = 29.1/14.5/56.4 at a total gas flow of 60 ml min^{-1}. Lines are to guide the eye.

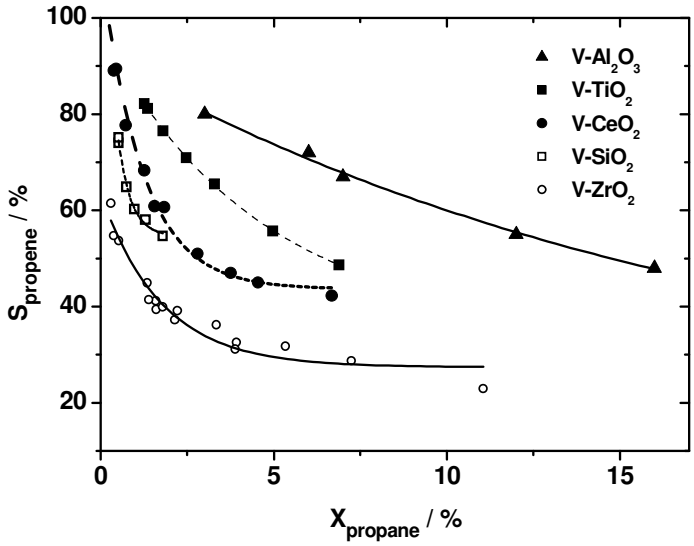

Figure 3-8. Selectivity-conversion trajectories for V-Al_2O_3, V-TiO_2, V-CeO_2, V-SiO_2 and V-ZrO_2 at 400 °C. $C_3H_8/O_2/N_2$ = 29.1/14.5/56.4 at a total gas flow of 60 ml min^{-1}. Lines are to guide the eye.

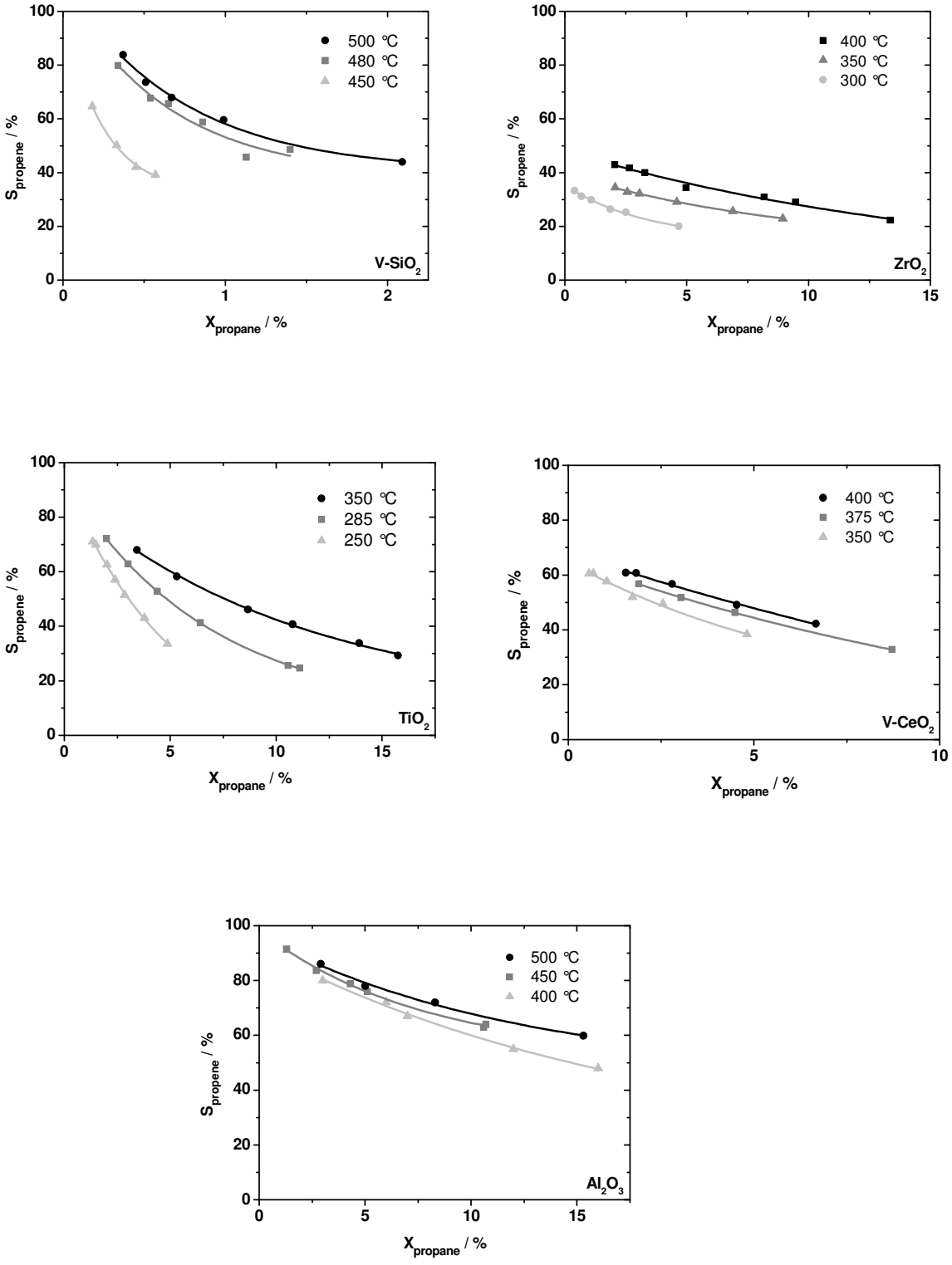

Figure 3-9. Selectivity-Conversion trajectories at different temperatures for V-Al_2O_3, V-TiO_2, V-CeO_2, V-SiO_2 and V-ZrO_2. $C_3H_8/O_2/N_2$ = 29.1/14.5/56.4 at a total gas flow of 60 ml min^{-1}.

For all catalysts, the selectivity increases with temperature as depicted in Figure 3-9. However, zero conversion intersections are independent of temperature and approach 100% selectivity values at low conversions.

Activation energies of the partial reactions were investigated by measuring initial reaction rates of ODP and propene combustion separately as function of temperature. Activation energies were then derived from Arrhenius-plots. The results are summarized in Table 3-2.

Table 3-2. Activation energies and TOF (400 °C) of ODP and propene combustion on differently supported vanadia catalysts. $C_3H_x/O_2/N_2$ = 29.1/14.5/56.4 at a total gas flow of 60 ml min^{-1}.

Catalyst	$E_{A,C3H8}$ kJ mol^{-1}	$E_{A,C3H6}$ kJ mol^{-1}	TOF_{C3H8} 10^{-2} s^{-1}	TOF_{C3H6} 10^{-2} s^{-1}
V-TiO_2	56 ± 5	147 ± 7	5.8 ± 0.2	47 ± 0.2
V-CeO_2	68 ± 6	101 ± 6	3.4 ± 0.2	14 ± 0.2
V-ZrO_2	78 ± 6	100 ± 6	5.6 ± 0.3	5.7± 0.3
V-Al_2O_3	113 ± 6	87 ± 5	0.68 ± 0.4	0.9 ± 0.2
V-SiO_2	146 ± 6	95 ± 5	0.13 ± 0.1	0.7 ± 0.1

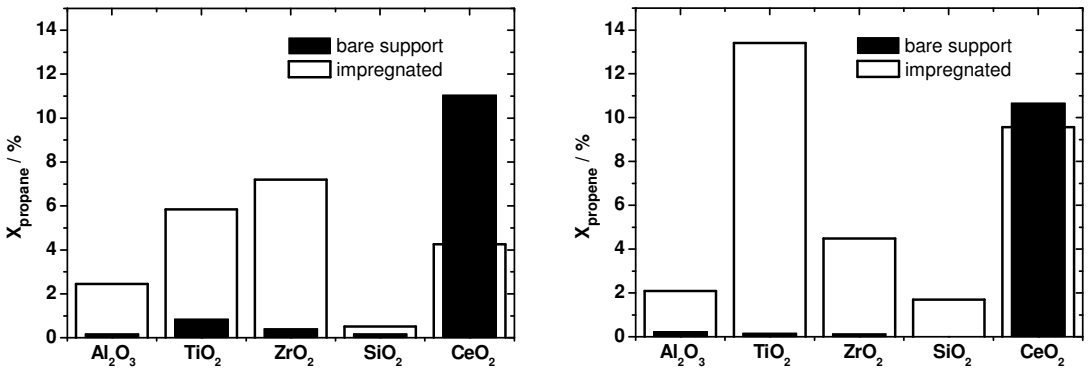

Figure 3-10. Propane (left) and propene (right) conversions at 400°C and 350 °C, respectively, over V-Al_2O_3, V-TiO_2, V-CeO_2, V-SiO_2, V-ZrO_2 (open) and Al_2O_3, TiO_2, CeO_2, SiO_2, ZrO_2 (filled), respectively. $C_3H_x/O_2/N_2$ = 29.1/14.5/56.4 at a total gas flow of 60 ml min^{-1}.

Generally, if different support materials have been compared in the literature with respect to their influence on ODP, contributions of the bare support material were not considered. Figure 3-10 shows the propane and propene conversion on the bare supports used in this study in comparison to the corresponding vanadia loaded materials. It can be seen that the contribution of the support material can be neglected for most of the catalyst/support combinations. An exception is CeO_2, which reveals a high activity. Most surprising pure CeO_2 exhibits even a higher activity than V-CeO_2. Since CeO_2 is an oxidation catalyst itself[48], this could be explained by surface vanadium species affecting the CeO_2 active surface sites. In this case propane would react on ceria sites on CeO_2 as well as on V-CeO_2 and is therefore not comparable to the other support materials used for our ODP study. Because bare support and catalyst exhibit about the same surface area, the higher conversion of the support cannot be ascribed to a loss of surface area during the preparation (calcination) of the catalyst. If propane would react only at a vanadia active site, the lower conversion on V-CeO_2 compared to the bare support could not be explained. However, the reason for this behaviour might be that there is still uncovered support material expected to be accessible for the reactants.

3.3 Discussion

Previous studies have shown a strong correlation of the catalytic performance with the surface concentration of vanadia species.[2,49,50] Low surface densities (< 2 V nm^{-2}) were determined by ICP for all catalysts in this study, in case of the SiO_2 support material being only 0.3 V nm^{-2} (Table 3-1). This might indicate a lower density of docking sites for vanadia species on SiO_2. A study by Weckhuysen et al.[8], which shows that the maximum surface vanadium loading without generation of V_2O_5 is especially low for SiO_2 (1-2 V nm^{-2}) compared to other support materials (7-8 V nm^{-2}), confirms this assumption. Very similar specific surface areas for the support materials and catalysts were observed by BET measurements, which indicate that clogging of pores by vanadium surface species is negligible.

Our TPR experiments show only one distinct reduction peak below 630 °C. This indicates that the reducibility of all catalytic active sites is similar and the presence of V_2O_5 may be excluded which is confirmed by Frank et al.[34] The additional shoulder, which is found in the case of V-CeO_2 may be assigned to CeO_2 surface species.[51] XRD patterns also do not show any V_2O_5-related peaks. However, due to the limited

sensitivity of XRD for the detection of V_2O_5 micro crystals, visible Raman spectra were additionally recorded.

The Raman spectra of dehydrated V-Al_2O_3, V-TiO_2, V-CeO_2, V-SiO_2 and V-ZrO_2 show bands within 1015-1045 cm^{-1}, which are assigned to the vanadyl stretch vibrations of dispersed vanadium oxide in agreement with literature data.[8] The small peak at 994 cm^{-1}, observed for V-Al_2O_3, indicates the presence of small amounts of crystalline V_2O_5 species (see Figure 3-3). Please note, that the amount of V_2O_5 detected is significantly lower than the fraction of peak areas, because the Raman cross section of the vanadyl band of these species is at least 5 times larger than that of the dispersed vanadia species.[19] The reason for the disappearance of some Raman bands after the reaction may be that the deposited coke was not completely combusted after the special treatment prior to Raman experiments. The residual carbon then absorbs most of the Raman light. In addition, carbon may cover part or even all of the surface vanadium oxide species, which may lead to a further decrease in the Raman intensity. The origin of the new Raman bands for V-ZrO_2 arising after reaction is currently under investigation. However, it should be pointed out that they neither match the known Raman band positions of tetragonal and cubic zirconia phases nor those of ZrV_2O_7. [47,52]

Summarizing, the results discussed above demonstrate that at most small amounts of crystalline V_2O_5 are present at the support and a highly dispersed system is available. This is an important observation, because bulk vanadia leads to a decrease in specific activity as buried vanadium atoms are not accessible for catalysis, while they would still be counted for the calculation of TOF. On the other hand, studies by Kondratenko et al.[50,53] showed that crystalline particles also decrease the selectivity towards propene. Therefore, if different amounts of crystalline V_2O_5 are deposited on a support surface during catalyst preparation, the catalytic performances of the different catalysts would not be directly comparable. Additionally it was shown that the V-ZrO_2 catalyst was not stable under reaction conditions. This has not been pointed out so far in the literature. Most important, the difference in position and shape of the vanadyl-related Raman bands of the prepared catalysts clearly indicate structural variations of the surface vanadium oxide species on the different support materials. This observation is at variance with the theories about the influence of support material that have been stated in literature so far. In these models identical vanadyl species were supposed to exist, independent of the respective support material. Studies to identify the different species observed are in progress.

One of the most important observations of this study is the strong influence of the support material on the catalytic performance in ODP. In case of SiO_2 it was furthermore verified, that no change in selectivity-conversion dependence could be detected when modifying the support structure.[54] Apparently structural changes alone do not affect the catalytic performance of ODP. One would be tempted to relate this negative result to the observation of Iglesia et al.[55] and Hess et al.[18], suggesting that water hydrolysis the V-O-support bond on SiO_2 and forming $V_2O_5 \cdot H_2O$ gels, which are disconnected from the support material. However, under reaction conditions this cannot occur because of high temperatures and resulting low H_2O surface coverage.

The low loadings (< 2 V nm^{-2}) for this study were chosen to detect support effects, which are hidden with higher vanadia loadings, as was shown by Khodakov et al.[2] They concluded that the initial influence of the support material on the distribution of monomeric and oligomeric vanadia species decreases with the formation of polymeric vanadia species, because at higher loadings differences in cluster formation can no longer influence the result. This argument is supported by Shee et al.[11] They recently found the same selectivity-conversion behavior for a titania and alumina supported catalyst at higher loadings (5 V nm^{-2}), excluding the influence of V_2O_5 surface species and mass transfer limitations.

Concerning the activity of supported vanadia catalysts, which is determined by the active site taking part in the rate determining step, two models can be found in the literature: Wachs et al.[56] found a substantial impact of EN of the support on the catalytic activity of the methanol oxidation, expressed as an exponential dependence of TOF on EN. They concluded that the V-O-support bond is the crucial reactive site. For ODP, however, theoretical calculations predict the V=O to take part in the rate determining step. On the basis of DFT calculations, Rozanska et al.[16] find the vanadyl oxygen to be responsible for the selective dehydrogenation of propane over silica supported vanadia catalysts. Although similar calculations have not been done so far for other support materials, a study of Gilardoni et al.[15] for unsupported V_2O_5 also assign the V=O as the crucial active site for the first hydrogen abstraction as the rate determining, though the second hydrogen abstraction may involve a V-O-V bond. In order to obtain additional information to enable discrimination between these models, we determined the dependence of ODP TOFs and activation energies on the EN of the cation of the respective support material.

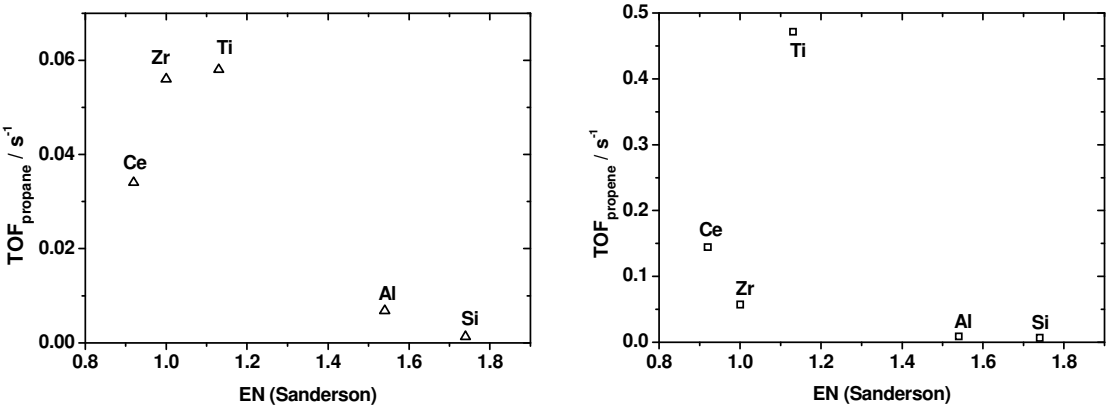

Figure 3-11. Turn-over frequencies of ODP (top) and propene (bottom) combustion on V-Al_2O_3, V-TiO_2, V-CeO_2, V-SiO_2 and V-ZrO_2 plotted against electronegativity of the support material cation.

Figure 3-11 illustrates that the TOF values vary by one order of magnitude, which demonstrates the strong influence of the support material on ODP. The TOF values of propene combustion are about one order of magnitude higher than those for ODP as it was expected due to the low selectivity caused by a fast consecutive combustion of propene in ODP. However, a general problem of a discussion of activities on the basis of TOF values is given by the fact that for TOF calculations it is assumed that all surface vanadia species contribute equally to the catalytic reaction. This would only be the case if all catalytically active species were structurally identical. Furthermore, vanadium atoms, enclosed in V_2O_5 particles contribute to the calculated TOF values as well and therefore could prevent correct interpretation. As alternative, we discuss the dependence of activation energies on EN, avoiding this problem. In Figure 3-12 activation energies for ODP, which were determined in our study, were plotted against EN values of the cation of the support material. They clearly increase with EN, whereas activation energies of the consecutive propene combustion are practically independent of EN (100 kJ mol^{-1}) except for V-TiO_2. The difference between activation energies of propane dehydrogenation and propene combustion is quite large in the case of V-TiO_2.

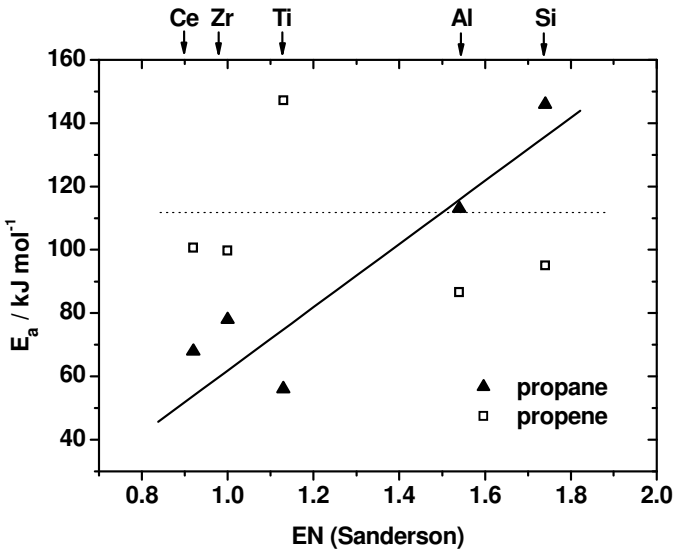

Figure 3-12. Activation energies of ODP and propene combustion on V-Al_2O_3, V-TiO_2, V-CeO_2, V-SiO_2, and V-ZrO_2 plotted against electronegativity of the support material cation. $C_3H_8/O_2/N_2$ = 29.1/14.5/56.4 at a total gas flow of 60 ml min^{-1}.

The dependence of activation energies on EN for the ODH step indicates a strong correlation of the catalytic reaction with physical properties of the support materials used for catalyst preparation. However, as well as TOFs, the activities for the ODH reaction do not seem to depend on the electronegativity of the support cation in a simple way. The results obtained here lead to the conclusion that the influence of support materials on ODP is of a more complex nature, than was indicated by the interpretation of methanol oxidation. However, comparing the measured activation energy of ODP for V-SiO_2 (~150 kJ mol^{-1}) one finds a good correlation with the values calculated by DFT calculation for the monomeric V=O bond be the crucial active site in the rate determining step (~123 kJ mol^{-1} at 750 K). The values are even more consistent, if one takes into account, that DFT calculations are known for underestimation of calculated values.[57] In this study a deviation of 0.4 eV (~40 kJ mol^{-1}) was found. For V-O-support bonds being the active site, the calculations revealed activation energies being about 60 kJ mol^{-1} higher.[16] For an unsupported V_2O_5 cluster a value of about 160 kJ mol^{-1} was calculated.[15]

The selectivity of ODP may be influenced by one or several of the following three attributes: (i) Different oxygen-vanadium bonds, e.g. the relative amount of

support-O-V, V-O-V or V=O groups, (ii) the surface acidity of the respective support material and (iii) differently structured surface vanadium species. These catalyst properties and their possible influence on the product selectivities will be discussed in the following. In many previous studies, especially if low loaded catalysts are investigated, monovanadate species are assumed to be the predominant active sites and therefore assigned to determine the selectivity of ODP.[24,58] In a new study of Bronkema et al.[59] using EXAFS, it was shown that only monovandate species to be existent on a SBA-15 supported catalyst. Recent studies of Klose et al.[60], however, suggested a new structural model for vanadium surface species on alumina supported vanadium catalysts. In their work a trimeric surface species, containing V^{5+} and V^{4+}, is proposed under moderate oxidizing conditions even at vanadium loadings less than 2 V nm^{-2}. These species would exhibit support-O-V, V=O as well as V-O-V bonds. Due to the known influence of support material of vanadia catalysts on ODP, they assumed the support-O-V bond to be the main active site. Furthermore, Hess et al.[17] observed associated vanadia species on SBA15 supported catalysts at very low loadings (0.7 V nm^{-2}) by probing with NO and CO molecules. The different results discussed above show that support-O-V and V=O bonds either with or without additionally available V-O-V bonds could influence the product selectivities in the case of low loaded catalysts.

An additional effect, which is expected to influence the reaction rate and selectivity to propene is the surface acidity. The attempt to relate surface acid-base properties of the support to activity and selectivity of ODP has already been a subject of previous investigations.[61,62] However, these results have to be considered with care because of missing analytical characterization and the neglect of mass and heat transfer effects. Furthermore, in both studies, TPR experiments reveal the presence of different reducible vanadium surface species as well as surface V_2O_5 species, which makes a comparison of the catalysts difficult. In order to rationalize the observed relative selectivities, we first exclude the V-CeO_2 and V-SiO_2 data. CeO_2 reveals a higher propane conversion on the bare support material than the corresponding catalyst, which indicates cerium sites instead of vanadium sites to be active. The documented differences in loading properties of SiO_2 also suggest a generally different site structure. The apparent similarity of the Raman of the remaining group supports our choice to discuss the catalytic properties within this restricted set. The pH at which the surface possesses zero surface charge shows the following trend:

$$V\text{-}ZrO_2 < V\text{-}TiO_2 < V\text{-}Al_2O_3$$

This is the same trend as has been observed for the selectivities of these catalysts, even though it is not as pronounced. Thus, a consideration of surface acidity of the catalyst may connect propene selectivity to surface acidity of the support. (In this context we want to mention that the relative order of reducibilities determined by TPR predicts the observed trend of catalyst activities expressed in TOF). At vanadium loadings below 2 V nm^{-2}, Broensted acid sites can be excluded referring to the literature.[63,64] In these studies the presence of surface acid sites for V-ZrO_2 and V-Al_2O_3 was investigated. At vanadium surface densities < 2 V nm^{-2} no Bronsted sites were found and the number of Lewis acid sites was slightly decreased compared to the bulk support material.

It is noteworthy that high resolution Raman spectra give clear evidence for a certain heterogeneity of vanadium sites under low loading conditions. This leads to spectral differences even for the restricted set of support materials. For this reason the current experimental data are not sufficient to exclude that this distribution of local site structure could also be influencing the relative order of activities and selectivities.

Additional studies on the selectivities of ODP towards propene make it possible to decide whether parts of the reaction network may be neglected leading to a significant simplification of the kinetic simulations. This information can be derived from the selectivity towards propene at low propane conversions. Except for ZrO_2, the ODP selectivity-conversion trajectories for the different catalysts approach selectivities of about 100% at low conversions. If there was significant parallel combustion of propane to carbon oxides, selectivities should be lower also at low conversions. This leads to the hypothesis that the consecutive reaction of propane is the main factor that determines selectivity. For V-Al_2O_3 and V-TiO_2 this is confirmed by studies described in the literature. For alumina supported catalysts the selectivity also approached 100% selectivity at low conversions.[65] In a further kinetic study Viparelli et al.[66] considered the rate constant k_2, which describes the rate of the parallel propane combustion (scheme 1) to be zero for a titania supported vanadia catalyst. In contrast, zirconia supported catalysts show poor selectivities even at very low conversions. This could be explained by parallel combustion of propane. A different explanation would be that propene formed at low conversions may not desorb from the active site or adjacent Lewis acid sites due to a strong adsorption resulting in a deep oxidation to CO and CO_2. According to results of isotopic tracer experiments performed by Chen et al.[22], a parallel combustion of propane seems to be more likely. This study reports CO_2 being formed via direct combustion of propane. However, it has to be mentioned that the fraction of

parallel combustion is low. It may also be possible that both, deep oxidation of propene even at low conversions and parallel combustion may be part of ODP over V-ZrO_2.

The increase in selectivity with increasing temperature indicates a stronger reaction rate increase of propane dehydrogenation than consecutive propene combustion and other side step reactions, respectively. Based on these results one would expect the highest activation energy within the reaction network for the ODH step. For alumina supported catalysts the selectivity increase with temperature was confirmed by Khodakov et al.[58] In this kinetic study, the ratio of k_3/k_1 was found to decrease with increasing temperature corresponding to higher activation energy for oxidative dehydrogenation of propane than for the consecutive combustion. However, the separate investigations of ODP and the combustion of propene with different supported catalysts do not follow the expectation mentioned above. V-CeO_2, V-ZrO_2 and V-TiO_2 activation energies for ODP are lower than those for the consecutive propene combustion (Table 2). This indicates that the two reactions may not be described as separated individual reactions at least in case of V-CeO_2, V-ZrO_2 and V-TiO_2. Usually subdivision is an accepted tool for kinetic investigations.[67] For V-SiO_2 and V-Al_2O_3 the correspondence of the selectivity-temperature dependence and activation energies may allow the two reactions to be investigated separately.[34] But the agreement of the results may be a coincidence. This has to be taken into account for future kinetic investigations. A reason for this may be the different average oxidation state of the catalyst during the separately studied oxidation of propane and propene, respectively. This is due to propene consuming more lattice oxygen during its combustion than propane during its dehydrogenation. Furthermore, the combustion of propene is faster than the ODP. Since the rate of propene combustion is also proportional to the number of active lattice oxygen site, it gets slow as its concentration decreases, and the reoxidation of the catalyst becomes the rate determining step. This consideration is supported by mechanistic studies,[37,68,69] in which a Mars-van Krevelen (MvK) approach is used to describe the kinetics of ODP (eqns. (3.1) – (3.3)).

$$r_1 = k_1 p_{C_3H_8} (1-\beta) \tag{3.1}$$

$$r_2 = k_2 p_{C_3H_6} (1-\beta) \tag{3.2}$$

$$r_3 = k_3 p_{O_2} \beta \tag{3.3}$$

with k_i the respective rate constant and p_i the respective partial pressure. The degree of reduction β is hereby defined as the ratio of catalyst reducing reactions and the sum of reducing and reoxidizing reactions, given by the steady-state mass balance of active sites (eqn. (3.4)).

$$\beta = \frac{0.5k_1 P_{C_3H_8} + 3k_2 P_{C_3H_6}}{0.5k_1 P_{C_3H_8} + 3k_2 P_{C_3H_6} + k_3 P_{O_2}} \tag{3.4}$$

If catalyst reduction is fast, which is the case in propene combustion, the degree of reduction β is high. In a steady state for which rates of reduction and reoxidation are balanced, eqn. (3.5) is valid.

$$r_2 = r_3 \tag{3.5}$$

so k_3 would be small compared to k_2, which leads to the fact, that the reoxidation of the catalyst is the rate-determining step. Therefore the activation energies for propene combustion measured in this study reveal only apparent activation energies for this reaction, which corresponds to the activation energy of the reoxidation step.

It should also be noted that recent considerations concerning the application of MvK-approaches for kinetic investigations have to be used carefully in terms of a physical interpretation of experimental results.[70] However, the application of a MvK model for the above discussion may be an appropriate tool to describe the issue of ODP kinetics in a descriptive way.

3.4 Conclusion

Different support materials show a strong influence towards activity and selectivity of equally prepared catalysts for ODP. The catalytic performance seems to depend on a complex interplay of vanadium surface species and bulk supporting material, which cannot easily be modelled by invoking the corresponding electronegativities of cations involved. All catalysts expose differently structured and/or distributed vanadium surface sites (monomers / oligomers). Therefore a comparison has to be based on further detailed investigations on the vanadia structure.

We also find that V-ZrO_2 undergoes structural changes under reaction conditions. For a future microkinetic evaluation of the investigated catalysts a simplified reaction

network containing only consecutive propene combustion steps seems to be appropriate except for zirconia supported catalysts, and will simplify such investigations to a large extend. ODP cannot be separately investigated in terms of propane ODH and propene combustion. That is, for multiple parameter determination, several experimental data sets have to be acquired. The separated investigation of catalyst reoxidation is probably helpful and in addition, extensive *in situ* characterisation and isotopic tracer experiments will be necessary to unravel possible microkinetic models. To improve selectivity towards the desired product, high temperatures seem to be appropriate, independent of the nature of support material. Temperatures are limited by the fact that unselective gas phase reactions may occur above 550°C.

4 Reduced Vanadium Sites on Different Support Materials and their Influence on ODP

4.1 Introduction

The previous results describing the influence of the support material on the kinetics of ODP indicate that the given effects are of more complex nature. A more detailed study of the catalytic active sites, therefore, seemed to be interesting. The proposed reaction mechanisms (Figure 1-3) indicate that vanadium may change between its oxidation states V^{3+}, V^{4+}, and V^{5+}. Electron Paramagnetic Resonance (EPR) is an important analytical method to directly identify different oxidation states in a bulk sample, which might be generated by electronic crossover during the reaction cycle. In particular it may provide information about the oxidation states V^{4+} and V^{3+}, both being paramagnetic caused by unpaired d-electrons, while V^{5+} is EPR silent. Although V^{4+} in its spin doublet state can be detected by standard X-band (9-10 GHz) EPR, V^{3+} in its spin triplet state probably has a large fine structure (FS) interaction, thus preventing its detection by standard EPR. Other methods for the identification of V^{3+}, like X-Ray photoelectron spectroscopy (XPS), are mostly applied under ultra high vacuum conditions, which may lead to changes in the catalyst structure. The interpretation of such experiments might therefore be erroneous. Because of its characteristic hyperfine structure, the spin doublet state of V^{4+} is easily identified even at X-band, thus at least providing information about one of the oxidation states. However, an unambiguous interpretation of these spectra is impeded by the fact that several other paramagnetic species, generated during the reaction or even present in the pristine catalyst, lead to crowded spectra. These are difficult to unravel, because small differences in g values are not sufficient to separate spectra, when using the standard rather small external field of 0.3 T.

The application of High-Frequency EPR (HF-EPR) in the study is based on a major technological development of EPR in the past decades, not only introducing Fourier-transform (FT) and multi-pulse EPR as important analytical tools, but furthermore expanding its frequency range well above 100 GHz (W-band), which was commercially available already since 1995. At these elevated frequencies, the tiny dimensions of microwave resonators restricts sample dimensions to the sub millimetre range and, more important, excludes the investigation of materials with significant microwave losses. As an alternative, for more general applications, a resonator-free set

up, invoking transmission or reflection like in ordinary optical spectroscopy is the method of choice, in particular if one is not restricted by sample mass. The inherent loss in sensitivity can partially be compensated by using sample dimensions adapted to the cross section of microwave propagation. The successful application of high frequency EPR for the investigation of ferroelectric material was demonstrated recently.[71] Further examples for the use of HF-EPR were compiled in a special issue of Magnetic Resonance in Chemistry.[72] It was, therefore, anticipated that this technique could also be applied for the study of catalytically active materials, invoking vanadium as active centres. As was shown recently, V^{3+} can be observed using HF-EPR, leading to a full characterization of its spin Hamiltonian parameters.[73] A HF-EPR study of various supported vanadium catalysts was therefore initiated.

In most previous studies catalysts are characterized before they are used for the respective reaction,[2,40,50] although it would be much more informative if in-situ methods could be invoked. In this study results from a pseudo in-situ approach are presented: The samples were quenched under steady state reaction conditions by purging the catalyst with nitrogen and cooling it down under inert atmosphere. Subsequently the catalysts were refilled in glass vials and sealed under high vacuum conditions, preventing any air or moisture contact with the samples. A similar procedure was already described in a study by Chary et al.[74]

4.2 Results

All investigated catalysts have been characterized before.[13,17,19] The catalysts were found to expose highly dispersed vanadium oxide surface species. Both isolated and polymeric vanadium oxide species are present. The V-Al_2O_3 catalyst sample contained negligible amounts of V_2O_5 as evaluated on the basis of results from Raman spectroscopy. The loadings, surface areas and vanadium densities of the samples as well as reaction conditions are summarized in Table 4-1. The vanadium oxide loadings (in wt% V_2O_5) were in the range of 1.6 – 4.7 wt% resulting in surface densities of 0.7 for V-SBA-15 and about 1.5 V nm^{-2} for V-Al_2O_3 and V-TiO_2. It was shown in previous studies that in case of V-SBA-15 no significant effects of the vanadium loading on the structure of vanadium sites was observed for low vanadium loadings (< 2.3 V nm^{-2}).[19]

Table 4-1. Parameters during reaction before samples were quenched with nitrogen and sealed in a pseudo-in-situ state.

Catalyst	Mass mg	T °C	Loading V nm^{-2}	Feed C_3H_8:O_2	X_{C3H8} %	X_{O2} %	S_{C3H6} %
V-SBA-15	250	500	0.7	2:4	25	40	21
V-SBA-15	250	500	0.7	8:1	4	63	57
V-Al_2O_3	150	450	1.4	2:4	18	24	33
V-Al_2O_3	150	450	1.4	8:1	5	69	61
V-TiO_2	90	450	1.5	2:4	20	30	26
V-TiO_2	90	450	1.5	8:1	3	56	54

In the case of the V-SBA-15 sample, a higher reaction temperature was applied in order to reach comparable degrees of propane conversion at concurrent homogeneity of the catalyst part The differences in the selectivity-conversion behaviour at equal reaction conditions have been discussed in detail before.[13] The results of this study show, that there is a strong influence of the support material on the catalyst activity and product selectivity. The selectivity at a given propane conversion decreases in the order of V-Al_2O_3 > V-TiO_2 > V-SiO_2.

In the following, EPR spectra of these catalyst materials before and after reaction will be shown. For all samples studied spectra with a signal to noise ratio better than 20 could be obtained with a single sweep of approximately 30 min duration. Except for field sweeps covering the full range from 0 to 15 T, a linear base line correction was sufficient thus allowing reliable numerical integration of the field derivative spectra without truncation of data. All EPR spectra are depicted after integrating the field-modulated data thus showing the EPR absorption pattern. This is a prerequisite if attempting to compare relative intensities of spectral components of different line width. This was most important for the interpretation of the TiO_2 based samples, because structures differing by more than two orders of magnitude difference in line width were present in this sample. As an example, the original, field modulated EPR spectrum of V-TiO_2 with its familiar first derivative line shape is compared with its single and double integrated form in Figure 4-1. Whereas the original spectrum is completely dominated by the narrow component, the integrated absorption spectrum

exhibits an additional broad component, which clearly dominates the EPR spin susceptibility as seen after the second integration.

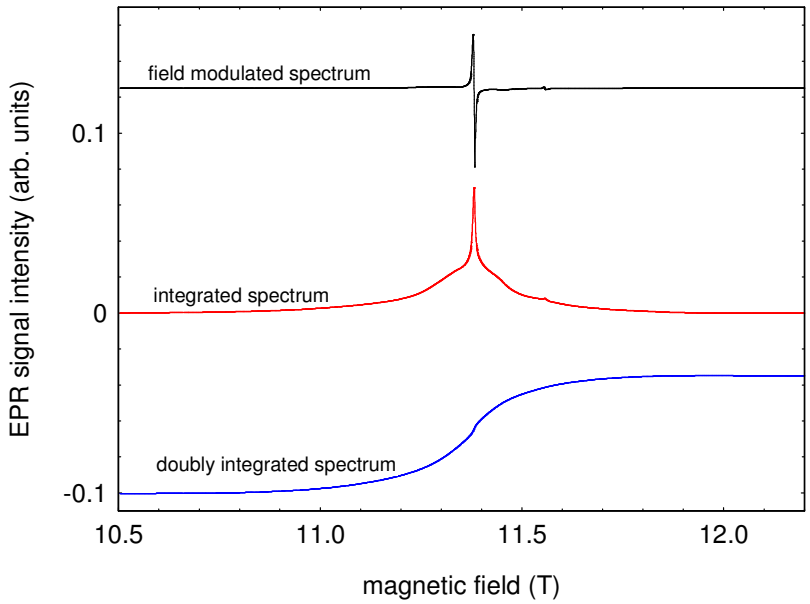

Figure 4-1. Comparison of the (original) field modulated 319.2 GHz EPR spectrum of V-TiO_2 with its single and doubly integrated data.

Figure 4-2 shows the EPR spectra of bare support materials and catalysts after calcination under ambient conditions. All EPR spectra shown in Figure 4-2 were measured using approximately the same amount of material. The spectra are depicted after integrating the field-modulated data thus showing the EPR absorption pattern. As stated above the number of paramagnetic centres, which is proportional to the EPR susceptibility, can only be obtained by performing a second integration. To facilitate the interpretation, the data are shown by invoking a g value axis instead of the more familiar field dependence. This is equivalent to the use of a chemical shift axis in NMR and allows comparing spectra measured with different microwave frequencies. (The direction of the g value axis is inverted to facilitate comparison with spectra presented as conventional field plots.)

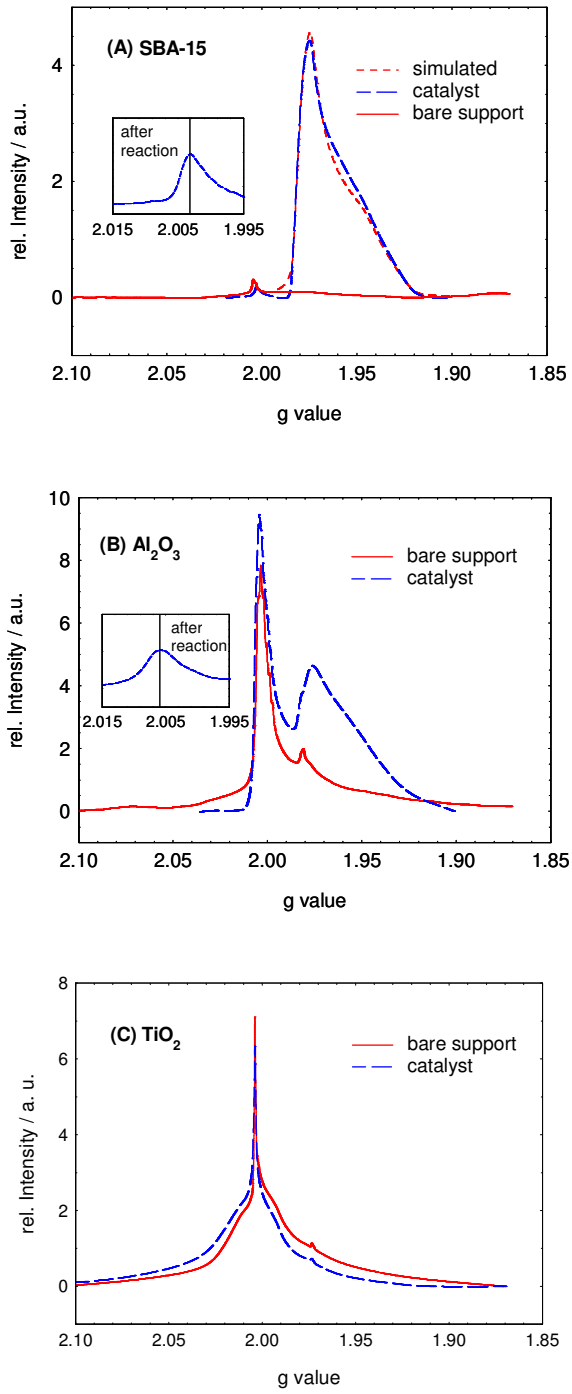

Figure 4-2. HF-EPR spectra (319.2 GHz, 20 K) of the bare support material and of respective catalyst (A) SBA-15/ V-SBA-15, (B) Al_2O_3/ V-Al_2O_3, (C) TiO_2/ V-TiO_2 "as is" after calcination. Experimental conditions used for all spectra were kept equal thus allowing for comparison of the relative intensities of (A) to (C). The simulation of the V^{4+} spectrum shown in (A) was performed using g matrix and vanadium hyperfine tensor values given in the text. Inserts with increased g resolution indicate the position of signals close to g = 2. Weak signals originating from Mn^{2+} impurities are also visible.

The resonance field position of all signals was found to be proportional to the microwave frequency used, thus proving assignment to spin doublet radicals ($S_{eff} = 1/2$). All spectra of the bare support materials show signals in the region of g = 2, close to the free electron value. The intensities of these signals at g = 2 are increasing in the order SBA-15 < $Al_2O_3 \approx TiO_2$. Whereas only a single component can be identified for (A) and (B) in the g = 2 region, at least two components, also centred at g = 2 but differing in g spread can be identified for TiO_2. A small peak can be seen at g = 1.982 for Al_2O_3 and TiO_2. The bare SBA-15 support material is nearly free of paramagnetic centres (A). The spectral change after coating allows an unambiguous assignment of the signal observed for V-SBA-15 as related to V^{4+} in its spin doublet state. The powder pattern can be fitted with a g matrix of nearly axial symmetry with $g_1 = 1.98077(2)$, $g_2 = 1.97380(2)$, and $g_3 = 1.93300(2)$ in combination with a vanadium hyperfine tensor with elements 104 (2), 64(5), 550(10) MHz. In particular the large hyperfine interaction in the "parallel" orientation with the I = 7/2 spin is characteristic for V^{4+}.[75] In the case of V-Al_2O_3, the V^{4+} signal can also be identified on top of a broad background signal, which is present already in the uncoated Alumina support material. It is noteworthy that a signal, which could be attributed to V^{4+} with its characteristic spin parameters as listed above is completely absent in the case of V-TiO_2. The narrow spike at approximately g = 1.97 cannot be assigned yet.

Figure 4-3 illustrates spectra of sealed samples of V-SBA-15, V-Al_2O_3 and V-TiO_2 after being used as catalysts using propane and oxygen in a ratio of 8:1. The emerging spectra clearly depend on the support material. Signal intensities, however, cannot be compared because different scaling factors were used (signal intensities in case of V-SBA-15 were multiplied by a factor of 10). For V-TiO_2 a new signal emerged at g = 1.935, which is assigned to Ti^{3+} (see discussion below).

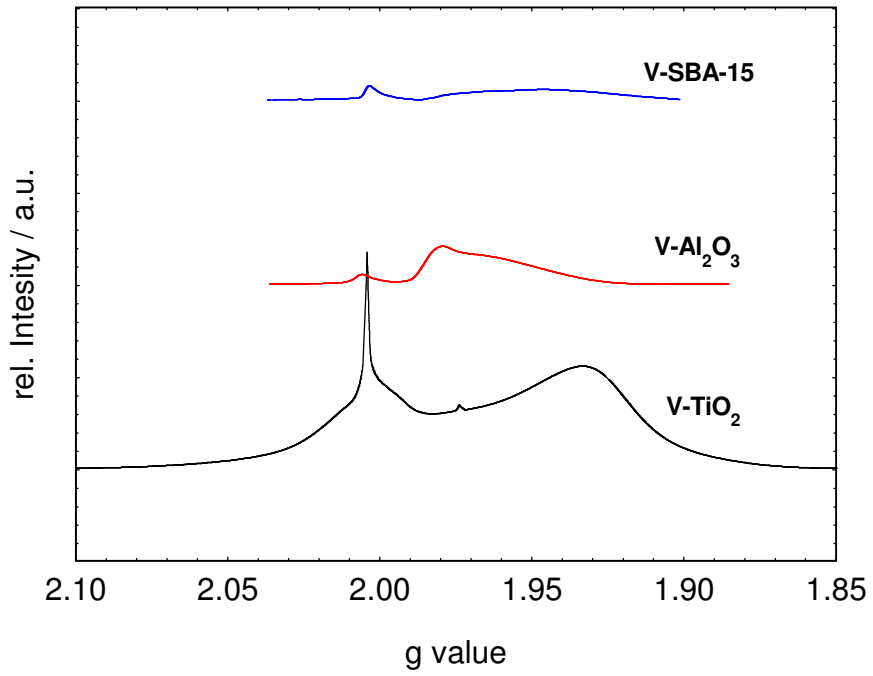

Figure 4-3. EPR spectra (319.2 GHz, 20 K) of sealed catalyst samples in their pseudo-in-situ condition, after being exposed to propane and oxygen in a ratio of (A) 8:1 and (B) 2:4 under reaction conditions.

In Figure 4-4 (A, B, C), the influence of different reaction conditions is shown separately for all three support materials. In the case of V-SBA-15 (A) it can be seen that the signal intensity of the signal at g = 2.0039 increases by an order of magnitude. The signal intensities can be directly compared, because the differences in sample mass have been used to scale the EPR data. Since these signals are observed only after exposing the catalyst to ODP and considering the very small g shift from the free electron value, we assign this signal to carbon-centred radicals on the surface of V-SBA-15. Such radicals are a consequence of cracking reactions occurring at elevated temperatures. The powder pattern of V^{4+} is slightly changing and the apparent peak maximum is decreasing from g = 1.976 for the fresh sample to g = 1.96 and 1.955, for the 2:4 and 8:1 sample, respectively. For V-Al_2O_3 (Figure 4-4 B), the intensity of the signal at g = 2.0062(3) is nearly constant for fresh and pseudo in situ samples. The signal apparently originates from paramagnetic centres of the bulk material, which are not influenced by reactions on the surface.

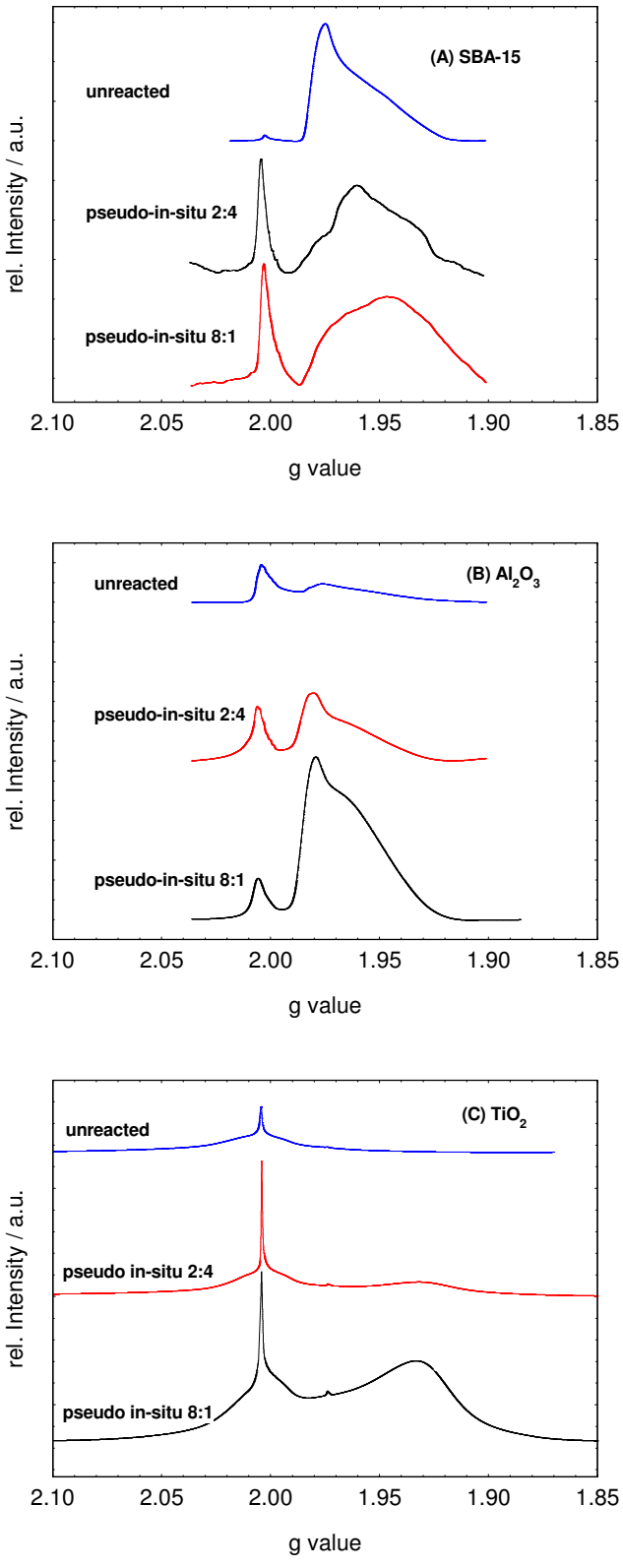

Figure 4-4. EPR spectra (319.2 GHz, 20 K) of unreacted and reacted catalysts, after being exposed to propane and oxygen in a ratio of 8:1 and 2:4. (A) V-SBA-15, (B) V-Al_2O_3, (C) V-TiO_2.

This indicates that they are not mobile under typical high temperature reaction conditions. The significant up shift of g from the free electron value suggests that these signals originate from oxygen vacancies. After reaction, a shoulder develops at a slightly smaller g value. Spectral resolution, however, is not sufficient to confirm the anticipated presence of additional carbon centred radicals. Signal intensities attributed to V^{4+} increase under oxygen deficient reaction conditions. Compared to the well defined pattern observed for the unreacted V-SBA-15 catalyst, it is obvious that a distribution of different V^{4+} sites is present, their relative intensity being influenced by the reaction. In the case of V-TiO_2 (Figure 4-4 C), the striking change in the spectrum caused by exposing the material to reaction conditions is the appearance of a strong signal with a new peak at g = 1.93. Considering the different g value and the lack of g anisotropy characteristic for the V^{4+} species, we assign this signal to Ti^{3+} instead (vide infra). The intensity of the spectral features close to g = 2 is also increasing, which may also be a consequence of the formation of carbon centred radicals. A detailed discussion of the signal consisting of at least two components is given below.

A direct test for the anticipated possibility to detect weak triplet state signals with the experimental set-up used is given in Figure 4-5.

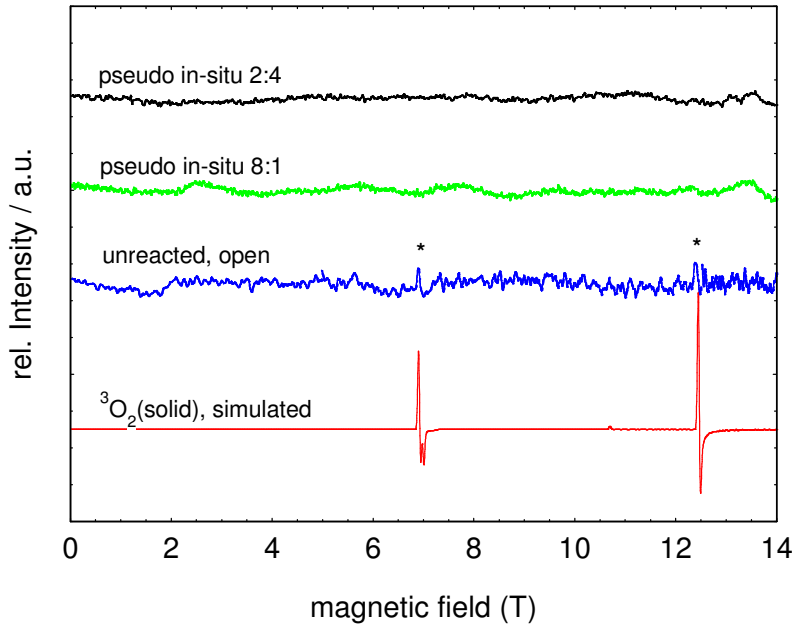

Figure 4-5. Experimental and simulated EPR powder spectra of a fictitious $\mathbf{V^{3+}}$ center with (A) D = 336 GHz, E = 57.4 GHz, (B) D = 280, E = 57.4 GHz, (C) D = 224, E = 57.4 GHz. The microwave frequency used in the experiment and for simulation was 406.4 GHz.

This graph shows the simulated and experimentally detected signals of triplet state molecular oxygen, adsorbed on the surface of the open, unreacted sample. The weak signals seen only for the "open" sample can unambiguously be assigned to molecular oxygen. For spectral simulation a ZFS constant of 106.4 GHz was used. A search for signals, which could have been assigned to V^{3+} was unsuccessful for all samples studied. In contrast to EPR spectra of doublet state paramagnetic centres, for which the dominant term in the spin Hamiltonian is given by the Zeeman interaction, the leading term in the spin Hamiltonian of triplet state compounds can be the fine structure interaction, usually termed "Zero Field Splitting" interaction.[76] Whereas for powder samples the spectral width in the case of S = 1/2 centres is determined by the g matrix anisotropy, the spread of absorption signals of S = 1 spectra might be dominated by ZFS and might be broadened beyond detection limits. In contrast the position of formally "forbidden" $\Delta m_S = \pm 2$ transitions are invariant (in first order) with respect to orientation, and therefore these lines are most prominent in powder samples. Figure 4-6 shows the simulated triplet state powder spectra, based on typical values for the ZFS splitting of V^{3+} centres with low site symmetry.[73]

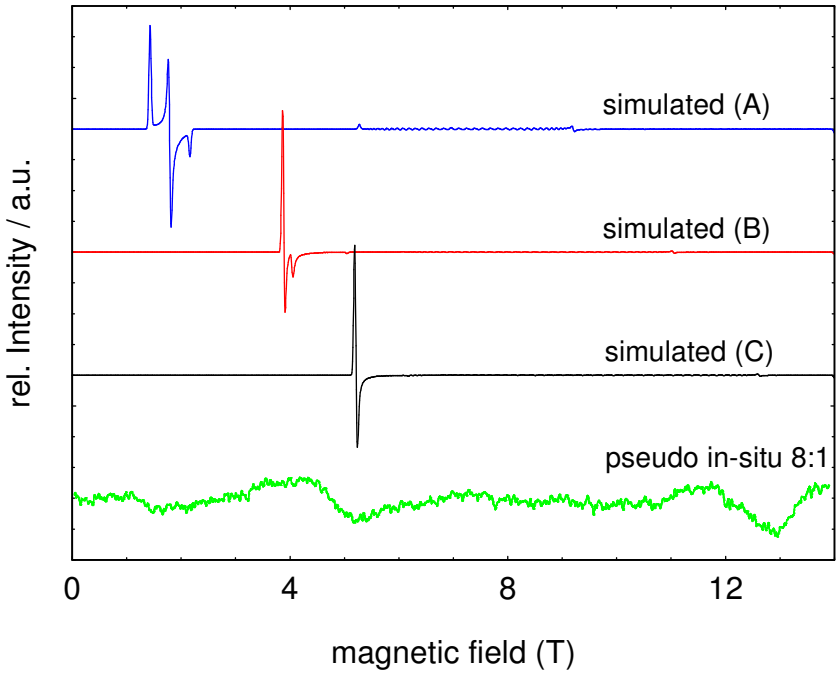

Figure 4-6. Full range experimental EPR spectra (319.4 GHz, T = 20 K, respective signals marked with *) of sealed and open catalyst samples (alumina support) in comparison with a simulated $^3O_2$ spectrum.

Whereas for ZFS of "medium" size the signals are observed close to g = 4 ("half field condition", here B = 7.1 T), increasing ZFS values lead to a down shift of the signals, until they are no longer observable. The lack of observation of these lines for the catalyst samples using a microwave frequency of up to 406 GHz puts a lower limit of 340 GHz for the ZFS constant of potentially present V^{3+} centers.

4.3 Discussion

The focus of this study was the impact of the support material on the formation and modification of paramagnetic centres during catalytic reaction. Because of the enhanced resolution of HF-EPR signals on a g-value scale, spectral components around g = 2 and those in the range below 1.98 can be separated. In this low g value range, signals from V^{4+} and also from Ti^{3+} are expected. In the region of smaller g values, signals which can be attributed to V^{4+} are observed only when using SBA-15 and Al_2O_3 as support. This assignment is based on the characteristic powder pattern most clearly seen for the V-SBA-15 material. The spectrum of the unreacted sample can be fitted with a g matrix of near axial symmetry and a large, unresolved vanadium hyperfine interaction. Fit parameters (g = (1.98077, 1.97380, 1.93300) and A = (104, 64, 550) MHz) are both typical for V^{4+}. In the case of V-SBA-15, the apparent peak maxima of V^{4+}, corresponding to the perpendicular orientation, are decreasing from g = 1.976 for the fresh sample to g = 1.96 and 1.955 for the reacted sample, respectively. This can be attributed to the fact that the well defined local site symmetry of V^{4+} on the surface of the fresh catalyst is modified by the generation of additional paramagnetic centres and probably also by the deposition of diamagnetic reaction products. The characteristic EPR signature of V^{4+} is preserved, however. In case of the alumina supported catalyst we also observe an increase in signal intensity of the characteristic V^{4+} pattern under oxygen-lean conditions. Because of the underlying broad background signal already present in the pure support material and in the fresh, unreacted V-Al_2O_3 sample, a spectral fit of the V^{4+} was not attempted. However, the comparison with the V-SBA-15 spectra indicates that a distribution of sites with different local symmetries is generated.

A striking difference in EPR pattern is observed for the TiO_2 support material before as well as after the reaction. A strong unstructured signal with maximum at g = 1.93 is created by the catalytic reaction, being completely absent for the other support materials. Previous EPR studies on TiO_2 in its anatase and rutile phases have revealed

unique local sites for lattice trapped electrons in the bulk material, resulting in well-defined values for the g matrix of such Ti^{3+} centres. ($g^{(anatase)}_{perpendicular}$ = 1.976, $g^{(anatase)}_{parallel}$ = 1.990; $g^{(rutile)}_{perpendicular}$ = 1.976, $g^{(rutile)}_{parallel}$ = 1.941).[77] For surface trapped electrons, however, a broad signal with peak at g = 1.93 was observed instead.[78] A similar pattern was also observed for surface Ti^{3+} cations in a tetragonally distorted environment in different matrices such as oxide of fluoride glasses.[79] The observed g value of 1.933 in our sample would be consistent with the assumption that electrons trapped at Ti^{4+} sites on the surface during the catalytic reaction give rise to the EPR signal, which is specific for the TiO_2 supported catalyst. The wide distribution of g values leading to the broad signal is indicative of a large variation of local symmetries. This assignment is further supported by our recent observation that the peak maximum of this characteristic signal is shifted from 1.933 to g = 1.965, if methanol instead of propane is used as a substrate. This shift is explained by considering the partial substitution of oxygen anions by hydroxyl groups.[80] The remaining spectral properties centred at g = 2 were not affected, even when changing the substrate.

Doublet radicals with a g value close to the free electron value are either already present for the pure support material or generated during the reaction. The nature of the signals seen for the SBA-15 and Al_2O_3 support close to g = 2 is yet unknown. By using HF-EPR with its inherent increase in g resolution, it was possible to identify unambiguously a difference in g values for these radicals on the two support materials. Whereas the small positive g shift +0.0016 seen for V-SBA-15 after reaction is indicative for carbon centered radicals, the larger g shift of +0.0039 found for the alumina supported catalyst even before catalytic reaction indicates partial spin localization at oxygen atoms, also referred to as “oxoradicals”, with their increased spin orbit coupling in the Al_2O_3 lattice.

The pure TiO_2 support material as well as the catalyst before and after reaction exhibit a narrow line superimposed on a broad signal close to g = 2, with line width parameters completely different from the pattern observed for SBA-15 and alumina. It should be noted that the total spin susceptibility, i. e., the number of paramagnetic centres derived from the broader component is larger by a factor 10 than that from the narrow line (see Figure 4-2 C). The spectral pattern is nearly invariant, but the signal intensity is significantly larger after the samples were exposed to reaction conditions. These g = 2 centres are tentatively ascribed to oxygen vacancies in the bulk support material and to paramagnetic centres on the surface. This assignment is supported by a

recent EPR study of titania anatase nanoparticles, giving evidence for trapped electrons on oxygen vacancies.[81] The g value reported for these F centres (g = 2.0034) are close to the g value of the narrow component (g = 2.0043(4)). The dominant broader component exhibits an asymmetric powder line shape, which is more pronounced when taking spectra with the highest available microwave frequency 406.4 GHz. Although not fully resolved, the spectrum can be described with an anisotropic g matrix (g_1 = 2.027(25), g_2 = 2.011(15), g_3 = 1.992(6)). This set is similar to the values reported for $O_2^{(-)}$ absorbed on the surface of anatase particles.[82] It thus seems possible that electrons can be trapped at Ti^{4+} as well as on surface bound molecular oxygen on the titania surface, significantly influencing the catalytic redox cycle and/or leading to additional unselective reaction pathways. It can be excluded that the broad component results from $O_2^{(-)}$ radicals directly coordinated to vanadium, because the signal is already present before coating the support material. The additional presence of bulk oxygen vacancies which probably are mobile at elevated temperatures might also influence the catalytic behaviour, although their relative abundance is small.

A recent study of Ganduglia-Pirovano et al.[83] identified oxygen vacancies as being possibly involved in catalytic processes during oxidative dehydrogenation reactions. In addition, a recent study of Goodrow et al.[84] investigated the influence of oxygen vacancies on the methanol oxidation on titania supported catalysts by means of DFT calculations. They came to the conclusion that oxygen vacancies are part of the active center and serve to reduce the activation energy of the rate determining step for the oxidation of methanol. Both studies indicate that the formation of oxygen vacancies could have a major influence on the catalytic performance of oxidative dehydrogenation reactions. An interesting aspect is that except for SBA-15, oxygen vacancies already exist in the bare support materials chosen for this study. Sekiya et al.[85] studied the behaviour of oxygen vacancies in TiO_2 single crystals (anatase) and found that they can be even stable under oxidizing conditions at elevated temperatures. This would explain the abundance of oxygen vacancies in the pseudo-in-situ samples, which were exposed to high oxygen partial pressures.

The absence of persistent V^{3+} signals in all samples does not exclude such sites being involved in ODP. As extremely short lived catalytic species they might generally evade detection by “post reaction” EPR as long as oxygen is present in the reaction mixture. This seems generally to be the case, because even under oxygen lean conditions more than 2 % of oxygen is left in the reaction mixture. Evidence for V^{3+}

surface species has been presented in previous XPS studies on the basis of a $V2p_{3/2}$ band around 515.9 eV.[19,86] However, recent time-dependent XPS experiments, which eliminate the influence of vacuum/X-ray radiation by extrapolating the temporal changes to $t = 0$, indicate the absence (contribution ~1%) of V^{3+} in the case of dehydrated (hydrated) silica supported vanadia samples.[19]

4.4 Conclusion

The application of HF-EPR for the investigation of catalysts was found to be very promising because of the significant improvement of spectral resolution. At microwave frequencies of 300 GHz and above with the corresponding magnetic fields in the range of 10 to 15 T, it is possible to separate spectral components originating from various transition metal ions from carbon centred radicals or from oxygen vacancies. High sensitivity for the detection of paramagnetic centres is provided at these high frequencies, because nearly complete spin polarization is obtained if spectra are taken below 20 K. This allows performing experiments without the use of a resonance cavity. EPR in "transmission mode" imposes much less restrictions on sample dimensions and dielectric properties, and can thus be invoked to study catalysts, because in general the amount of available samples is not restricted. It was possible to investigate probes extracted from the reactor under "inert" conditions, sealed in quartz sample tubes of 6 mm o.d. and 50 mm length. The comparison of pure support materials with unreacted and catalysts exposed to reaction conditions helped to identify paramagnetic centres which might be related to catalytic active sites in ODP.

In this study silica (SBA-15), alumina, and titania supported vanadium oxide catalysts were investigated. Before being used as catalysts, one well defined V^{4+} surface site was found in case of the SBA-15 support and a variety of different V^{4+} sites in case of the alumina support material. No V^{4+} centres are detected in case of the titania supported catalyst. For this material, strong signals originating from F centres, indicating the presence of oxygen vacancies, and, more abundant, from surface trapped $O_2^{(-)}$ radicals are also observed. After being exposed to reaction conditions, additional signals are detected due to the presence of carbon centred radicals for SBA-15 and partial electron localization on the alumina lattice (oxoradicals) in the case of alumina supported catalysts. In contrast, a signal attributed to surface trapped electrons forming Ti^{3+} centres is generated by the catalytic reaction of TiO_2 supported samples. The

number of F centres and trapped $O_2^{(-)}$ radicals increased during the reaction of the titania supported catalyst. We therefore conclude that the reaction scheme depicted in Figure 1-3 has to be appended by including the electronic properties of the support materials. The suggestion of Chen et al.[27] relating catalytic activity to the extent of electron delocalization on a given catalyst could be extended by predictions about the different mechanisms of such delocalization on the respective support material. However, such conclusions need to be considered carefully because of the fact that the catalysts in this study were investigated under post-reaction conditions, thus making predictions about catalytic relevant steps erroneous.

No indication of persistent V^{3+} could be found in any sample, although they could be present as short lived species during the catalytic reaction. However, a reaction mechanism of ODP without the participation of V^{3+} is generally possible for supported isolated and associated vanadium oxide species as shown in Figure 1-3 and was predicted to be energetically preferred by DFT calculations.

From our study there is evidence that titanium as a support material for vanadium oxide is involved in the key steps of ODP by trapping electrons either on Ti^{4+} surface states or on surface trapped molecular oxygen. In this context it will be of interest, if similar changes in the EPR spectra are observed when exposing the bare TiO_2 support material to reaction conditions. The results indicate that alumina participates in mechanisms of electron delocalization during catalytic turnovers through partial localization of electrons on oxoradicals. No participation of the support material on the catalytic reaction was found for the SBA-15 supported catalysts. In addition different structural properties of the active site have to be considered. This is suggested by Raman spectra of these catalysts presented in a previous publication.[13] In order to derive a correlation between persistent reduced states and catalytic performance a quantitative study invoking comparable reaction conditions will be performed in the future.

5 Kinetic Modelling using a Silica (SBA-15) Supported Vanadium Oxide Catalyst

5.1 Introduction

With respect to the previous chapters a more detailed kinetic study of V-SBA-15 was conducted to get more insight into the reaction mechanism. The choice was especially based on the fact that silica as a support material does not influence the reaction, as it is apparently the case for V-Al_2O_3 and V-TiO_2. In addition, quantum mechanical calculations done for parameter determination were mainly done for silica supported vanadia clusteres.[15,16] Furthermore, the V-SBA-15 catalyst has already been analytically characterized in previous studies.[17,19,28] These studies also take into account the influence of water on the dispersion of surface vanadium sites and describe the redox-behaviour of this catalyst via molecule probing in detail. For the kinetic description of ODP rate laws based on a MvK type reaction mechanism are often found in the literature.[11,23,70] However, first order rate expressions with respect to propane partial pressures may also be used for a sufficient experimental determination of turn over frequencies (TOF) and activation energies.[34]

The ODP reaction is a complex reaction network containing essentially the parallel and consecutive reactions depicted in eqns. (5-1) – (5-5).[22,39]

$$C_3H_{8(g)} + \overset{+V}{V}\,O_{(s)} \rightarrow C_3H_{6(g)} + H_2O_{(g)} + \overset{+III}{V}_{(s)} \quad (5\text{-}1)$$

$$C_3H_{8(g)} + (4+3x)\,\overset{+V}{V}\,O_{(s)} \rightarrow 3CO_{x(g)} + 4H_2O + (4+3x)\,\overset{+III}{V}_{(s)} \quad (5\text{-}2)$$

$$C_3H_{6(g)} + (3+3x)\,\overset{+V}{V}\,O_{(s)} \rightarrow 3CO_{x(g)} + 3H_2O + (3+3x)\,\overset{+III}{V}_{(s)} \quad (5\text{-}3)$$

$$CO_{(g)} + \overset{+V}{V}\,O_{(s)} \rightarrow CO_{2(g)} + \overset{+III}{V}_{(s)} \quad (5\text{-}4)$$

$$O_{2(g)} + 2\,\overset{+III}{V}_{(s)} \rightarrow 2\,\overset{+V}{V}\,O_{(s)} \quad (5\text{-}5)$$

Homogeneous gas phase contributions to this reaction scheme were observed only at temperatures above 773 K

Simplifications for eqns (5.1) – (5.5) are the following: The conversion/selectivity-trajectories presented in Figure 3-8 have an extrapolated intercept at nearly 100 % propene selectivity, indicating that primary propane combustion (B) can be neglected in this case (i) and (ii) the ratio of CO and CO_2 was nearly constant at a value of 1.5, independent from the propane conversion. This indicates a slow CO oxidation to CO_2 and the reaction scheme simplifies to eqns. (5.6) – (5.8).

$$C_3H_{8(g)} + \overset{+V}{V}\,O_{(s)} \rightarrow C_3H_{6(g)} + H_2O_{(g)} + \overset{+III}{V}_{(s)} \tag{5-6}$$

$$C_3H_{6(g)} + 7\overset{+V}{V}\,O_{(s)} \rightarrow 2CO + CO_2 + 3H_2O + 7\overset{+III}{V}_{(s)} \tag{5-7}$$

$$O_{2(g)} + 2\overset{+III}{V}_{(s)} \rightarrow 2\overset{+V}{V}\,O_{(s)} \tag{5-8}$$

Elimination of the catalytic species results in the stoichiometric equations for the stable compound, eq. 5.9 and 5.10.

$$C_3H_8 + 0.5O_2 \rightarrow C_3H_6 + H_2O \tag{5.9}$$

$$C_3H_6 + 3.5O_2 \rightarrow CO + CO_2 + 3H_2O \tag{5-10}$$

Please note that eqns. (5.1) – (5.5) are based on the following assumption: One catalytic turn over leads to a reduction of V^{5+} to V^{3+}. The assumption was made despite DFT calculations for silica supported vanadium oxide and bare V_2O_5 predicting a lower activation barrier for reaction pathways only including V^{4+}.[15,16] However, such mechanisms would not change the stoichiometry of eq. 5.9 and 5.10. Furthermore, reaction pathways including V^{3+} as short lived species could experimentally not be thoroughly excluded so far.

The material balances for stable reactants and products in a PFTR is given by eqns. (5-11) - (5-13).

$$\frac{dc_{C_3H_8}}{d\tau} = -r_1 \tag{5-11}$$

$$\frac{dc_{C_3H_6}}{d\tau} = r_1 - r_2 \tag{5-12}$$

$$\frac{dc_{O_2}}{d\tau} = 0.5r_1 - 3.5r_2 \tag{5-13}$$

Rate expressions for propane ODH and consecutive propene combustion r_1 and r_2, respectively, are given by eqns (5-14) and (5-15).

$$r_1 = k_{1,eff} \cdot \exp\left(\frac{-E_{A1,app}}{R \cdot T}\right) \cdot c_{C_3H_8}^{n1} \cdot c_{O_2}^{m1} \tag{5-14}$$

$$r_2 = k_{2,eff} \cdot \exp\left(\frac{-E_{A2,app}}{R \cdot T}\right) \cdot c_{C_3H_6}^{n2} \cdot c_{O_2}^{m2} \tag{5-15}$$

Numerical integration for data evaluation was done by using "Athena Visual Studio" Version 11.0 which uses the least square method for fitting.

For the determination of the equilibrium constants for the propane adsorption on V-SBA-15 a Langmuir equation was fitted a set of experimental data. The Langmuir isotherm is given in eqn. (5-16).

$$\frac{N}{N_0} = \frac{K \cdot p}{1 + K \cdot p} \tag{5-16}$$

with N the number of adsorbed molecules, N_0 the number of molecules for a monolayer coverage of the sample, p the pressure and K the equilibrium adsorption constant. The determination of the heat of adsorption was based on eqn. (5-17).

$$K = K_\infty \cdot \exp\left(\frac{\Delta H}{R \cdot T}\right) \tag{5-17}$$

with ΔH, the heat of adsorption.

5.2 Results

The grafting - ion exchange procedure used for the incorporation of vanadium into the porous silica matrix results in highly dispersed vanadia species.[28] For the sample used here (0.7 V nm^{-2}), no crystalline V_2O_5 was observed with visible Raman spectroscopy.[19] By combining Raman spectroscopy, DR UV-Vis spectroscopy as well as X-ray photoelectron spectroscopy (XPS) we recently demonstrated the strong increase in the dispersion of the supported vanadia species upon dehydration.[87] The changes in the dispersion are accompanied by distinct structural changes, i.e., changes in the vanadium coordination as well as the size of the vanadia aggregates. Detailed studies using

transmission IR spectroscopy using NO as probe molecule revealed the presence of bridged nitrates implying the presence of dimeric/polymeric vanadia species.[17]

Figure 5-1 shows the selectivity-conversion trajectories of V-SBA-15 as a function of temperature. It can be seen, that the selectivity increases with temperature, indicating a weaker temperature dependence of oxidation of propene in comparison to propene formation by ODP, i.e. $E_{A1,app} > E_{A2,app}$.

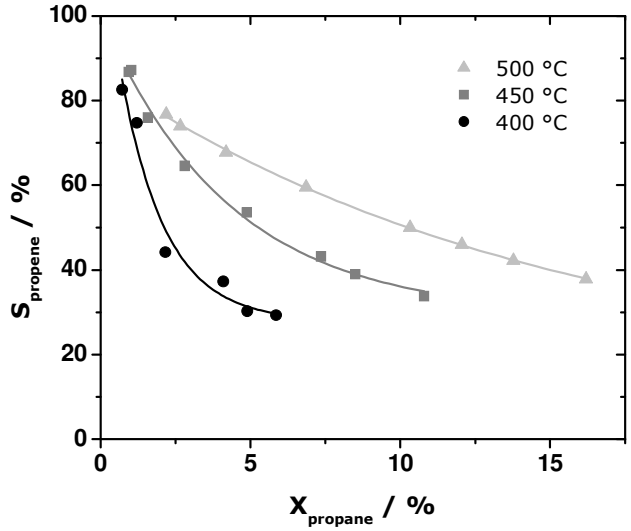

Figure 5-1. Selectivity-conversion behaviour of ODP at different temperatures for V-SBA-15.

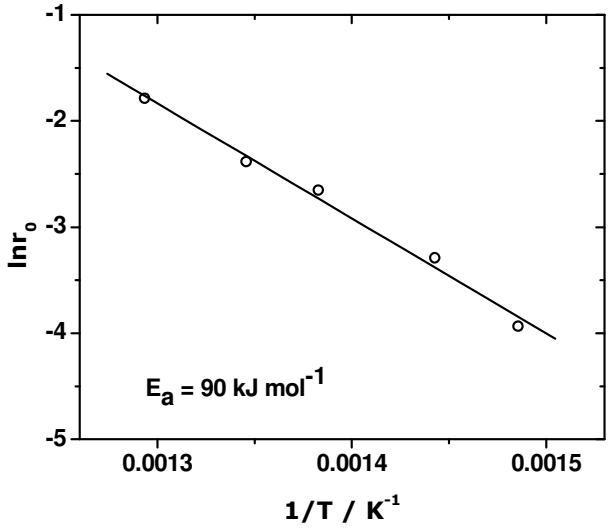

Figure 5-2. Arrhenius plot for the determination of the activation energy of ODP.

Figure 5-2 shows an Arrhenius plot for the determination of the apparent activation energy of ODP from the initial rates of propane conversion. The calculated value of 90 kJ mol^{-1} can be used as an orientation for the subsequent determination of the kinetic parameters for the complete reaction network.

The reaction orders for the oxidative dehydrogenation of propane were determined by a differential method studying the dependence of the initial rates on the individual initial concentration of the reactants. The logarithmic form of eqn. (5-14) yields eqn. (5-19).

$$\ln r_0 = \ln k_{1,eff} + n1 \ln c_{0,C_3H_8} + m1 \ln c_{0,O_2} \qquad (5\text{-}19)$$

with r_0 the rate, $k_{1,eff}$ the effective rate constant, c_0 the respective reactant concentration, n1 the reaction order of ODP with respect to propane and m1 the reaction order with respect oxygen. The reaction orders for propane and oxygen were determined by plotting the logarithm of the initial rate versus the logarithm of the concentration of the corresponding component. From the resulting slope the reaction orders were found to be 1 and 0 for propane and oxygen, respectively (Figure 5-3).

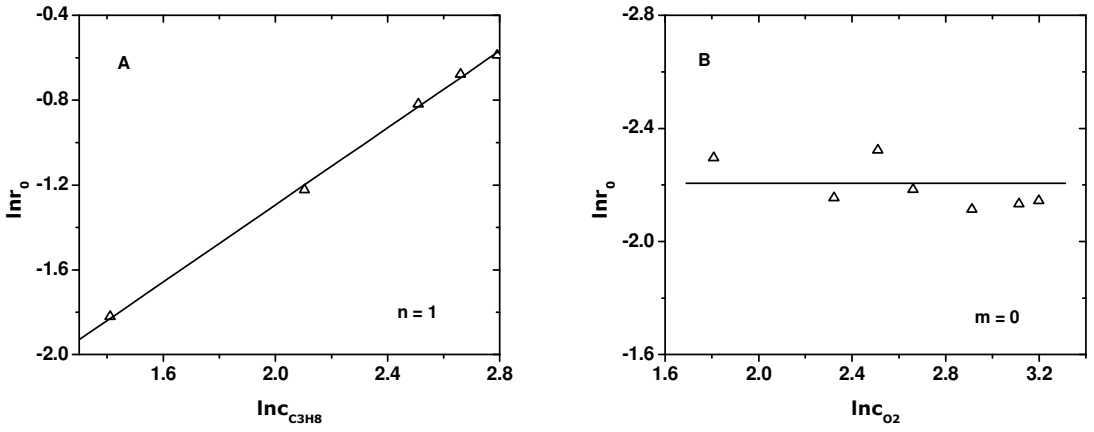

Figure 5-3. Determination of the reaction orders for propane (A) and oxygen (B) in the dehydrogenation step.

The reaction orders of the consecutive reaction of propene and oxygen cannot be determined in terms of the particular partial reaction. This is because of propene being a stronger reducing agent than propane, resulting in a lower average oxidation state of the

catalyst.[13] In order to get more insight into the consecutive propene combustion reaction and its reaction orders an indirect method was used. This is done by considering the selectivity dependence on the conversion of ODP at different partial pressures of propane and oxygen, respectively.

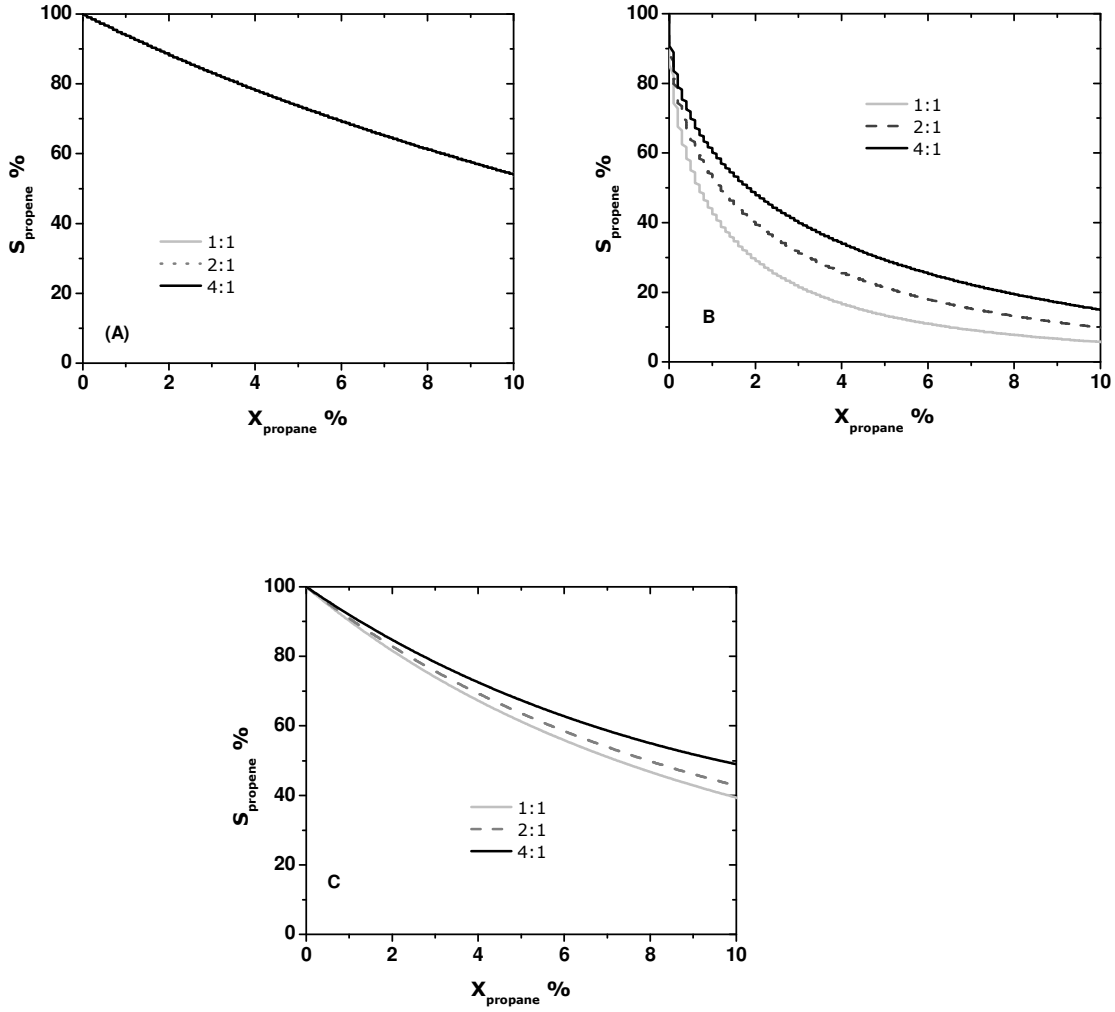

Figure 5-4. Simulation of Selectivity-conversion trajectories for ODP at 450 °C, for different reaction orders of propene and oxygen, respectively, in case of variable inlet concentrations of propane and oxygen. (A) Reaction order 1 for propene and 0 for oxygen, (B) reaction order 0.5 for propene and 0 for oxygen, (C) reaction order 1 for propane and 0.5 for oxygen. Simulations were performed for 1 bar overall pressure and the partial pressures of the reactants chosen for the experiments.

The propene selectivity dependence on the propane conversion indicates certain values of the reaction orders with respect to the reactants. For example, if a change in the feed ratio of the substrates at the reactor inlet does not affect the selectivity towards propene, the consecutive reaction must have an order of 1 and 0 for propene and oxygen, respectively. If this is not the case, selectivity would vary strongly with the partial pressure of the reactant gas. For further allocation a simulation of the propene selectivity with different reaction orders for propane, propene and oxygen is depicted in Figure 5-4.

Figure 5-5 shows the measured selectivity-conversion trajectories for different initial concentrations of propane and oxygen. It can be seen, that the propene selectivity is not affected by this variation. This leads to the conclusion that the reaction orders of the consecutive propene combustion are 1 and 0 for propene and oxygen, respectively, as shown by comparison with the simulation.

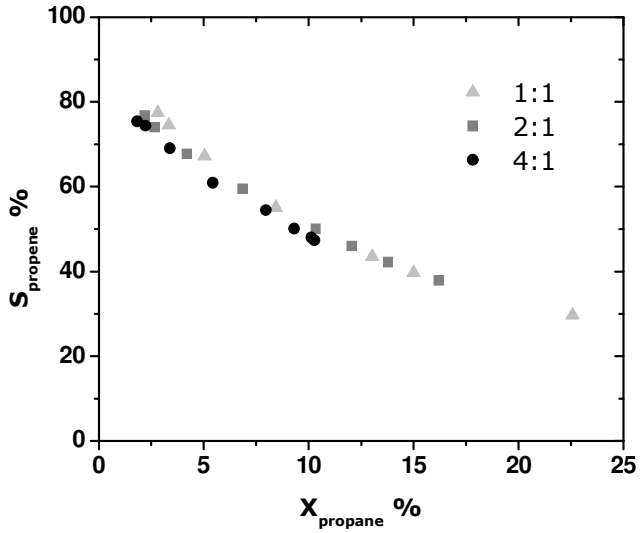

Figure 5-5. Experimental selectivity/conversion dependence for different propane/oxygen ratios.

The experimentally determined reaction orders, discussed above, were subsequently implemented into the kinetic model for the reaction network, which consisted of a simple consecutive reaction of propane to propene and propene to carbon oxides and water, respectively. The respective equations are given in eqns. (5-14) and (5-15). The

material balances for the stable compounds were fitted to of experimental data at five different temperatures (673K, 693K, 723K and 773K) and three different ratios of propane to oxygen (4:1, 2:1 and 1:1). Fitting variables were the apparent activation energies for ODP as well as for propene combustion and the respective pre-exponential factors $k_{1,eff}$ and $k_{2,eff}$. Parity plots, shown in Figure 5-6 indicate a good agreement of experimentally determined data and concentrations predicted by the derived model.

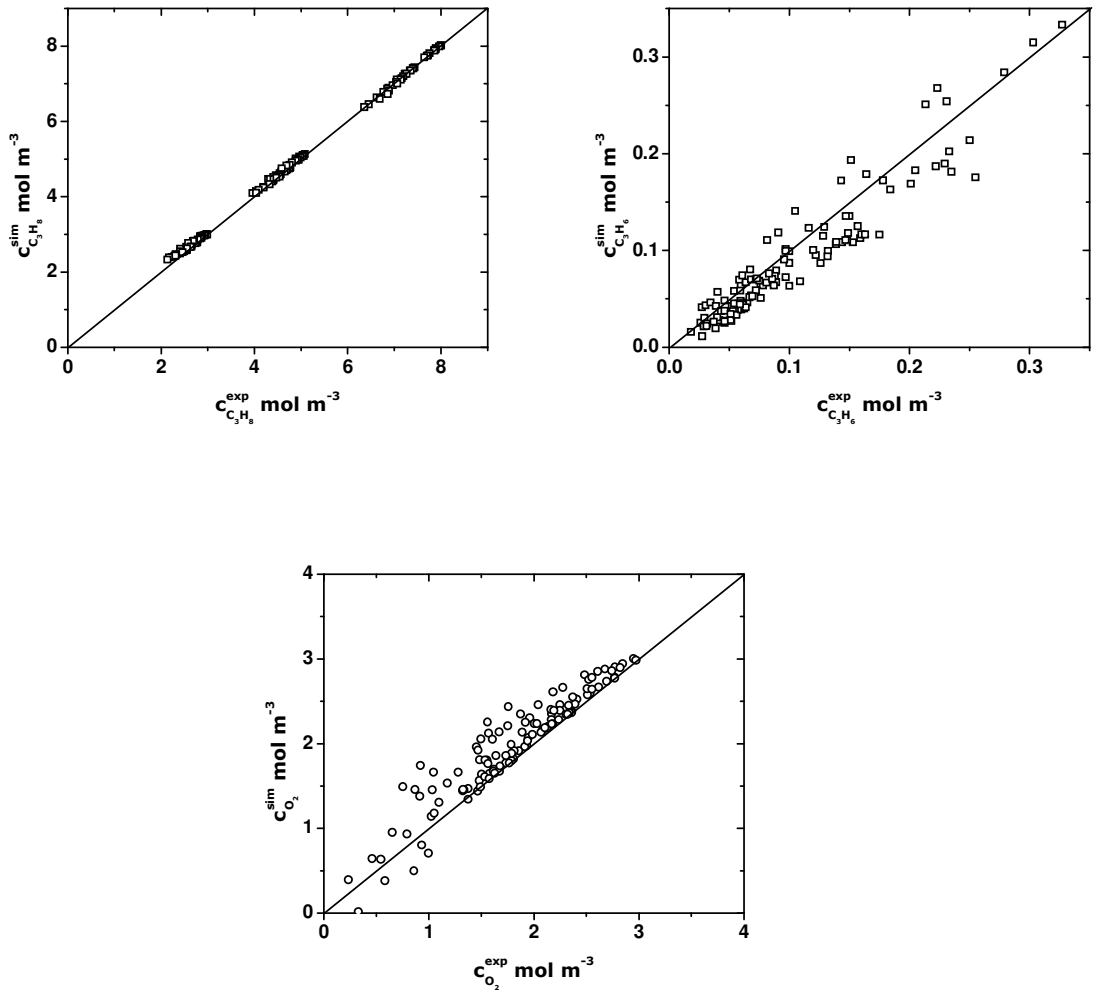

Figure 5-6. Parity plots for simulated and experimental concentrations. (A) Propane, (B) Propene, (C) Oxygen.

The pre-exponential factors, reaction orders and apparent activation energies, determined by fitting the concentration profiles to the experimental data are depicted in Table 5-1.

Table 5-1. Kinetic parameters for ODP reaction network.

x	$k_{0,eff,x}$ ml mg^{-1} min^{-1}	$E_{A,APP,x}$ kJ mol^{-1}	n_x	m_x
1	2260 ± 1270	103 ± 6	1	0
2	0.7 ± 0.5	34 ± 18	1	0

Figure 5-7 shows the differential heats of propane adsorption at V-SBA-15 as well as at the pure SBA-15 support. For both materials similar adsorption enthalpies in the range of 40 kJ mol^{-1} were determined.

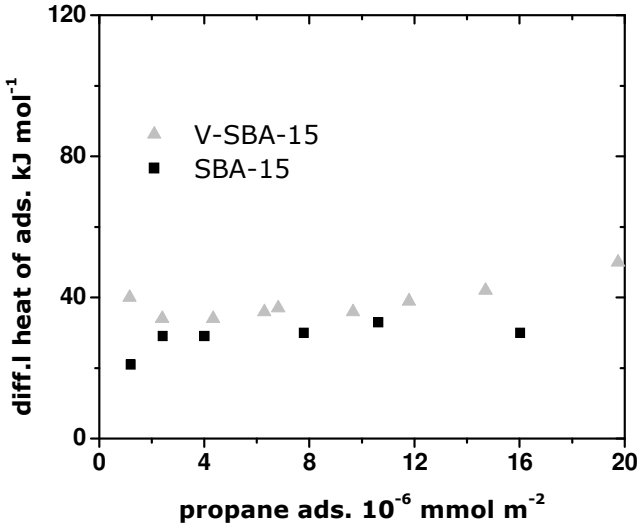

Figure 5-7. Differential heats of adsorption as a function of adsorbed propane for SBA-15 (pure support) and V-SBA-15.

For the determination of the adsorption equilibrium constant, a Langmuir isotherm was fitted to a set of experimental data with variation of propane pressure. The results are depicted in Figure 5-8. As can be seen, the simulation is in very good accordance with the experimental data. The parameters determined for the propane adsorption are given in Table 5-2.

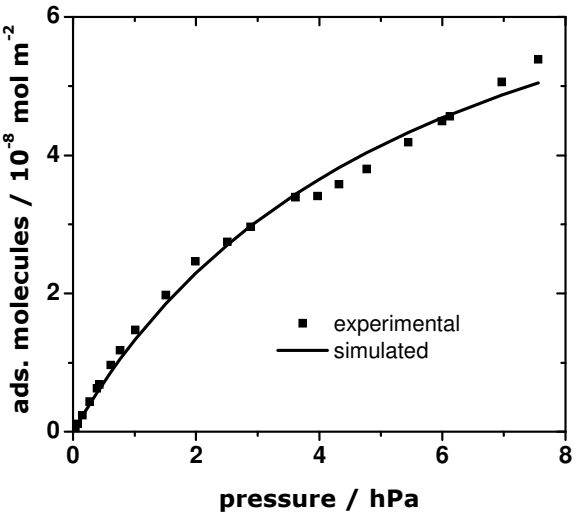

Figure 5-8. Experimental data and simulation of the adsorption isotherm (Langmuir) of propane on V-SBA-15 at T= 313 K.

Table 5-2. Thermodynamic parameters determined for the propane adsorption on V-SBA-15.

K_∞	ΔH
10^{-7}	kJ mol^{-1}
2.1 ± 0.2	40 ± 10

5.3 Discussion

Initial selectivities of almost 100 % allow for the conclusion that ODP is described by a simple consecutive reaction in case of using SBA-15 supported vanadium catalysts. The simplification of the reaction network leads to the chosen kinetic model described in eqns. (5-14) and (5-15). A further important aspect concerning selectivity is the observation that it strongly increases with temperature. This was already found in a previous study for various other supported vanadia catalysts.[13] Only if the activation energy of the oxidative dehydrogenation is higher than the activation energy of propene combustion, the propene formation rate increase stronger with temperature than the rate of the consecutive propene combustion, leading to a higher selectivity of the desired product. Therefore a low activation energy is expected for the propene combustion, which is also in agreement with the lower bond strength of the allylic C-H bond (~ 370

kJ mol^{-1}) in propene compared to the stronger secondary C-H bond (~ 410 kJ mol^{-1}) in propane (Figure 5-9). Please note that the difference in the weakest C-H bond strength (40 kJ mol^{-1}) corresponds approximately to the difference in activation energies of ODP and propene combustion (70 kJ mol^{-1}) as calculated in this study.

Figure 5-9. C-H bond strength in propane (left) and propene (right).

The reaction order of 1 for propane ODH indicates the participation of propane in the rate determining step, which was already proven by isotopic tracer experiments of Chen et al.[22] for different supported catalysts. The zero reaction order with respect to oxygen proves a fast reoxidation of the catalyst, which can also be found for other catalysts investigated in the literature.[23,39] The reaction orders determined above for the consecutive propene combustion of one for propene and zero for oxygen, respectively, suggest a participation of propene in the rate determining step of the consecutive combustion. This may be explained by the similarity of the active C-H bond in both molecules. The good agreement of modelled and experimental data in Figure 5-6 indicates that the assumptions made for the simplification of the reaction network are appropriate.

In order to calculate the real activation energies from the determined apparent activation energies the elementary steps of ODP and the heat of adsorption of propane at the catalysts have to be known. Based on isotopic tracer experiments by Chen et al.[22], the elementary reaction steps of a propane turn over were illustrated above (eqns. (1-17) - (1-21)) leading to rate eqn. (1-27). As found by Argyle et al.[29] by in-situ UV-Vis spectroscopy, the reoxidation rate of the catalyst, described by k_5 is about 10^5 times higher than the rate determining hydrogen abstraction, described by k_2 and K_1. Therefore eqn. (1-27) simplifies to eqn. (5-20).

$$r_{C_3H_8} = k_2 \cdot K_1 \cdot c_{C_3H_8} \qquad (5\text{-}20)$$

This rate law is equal to eqn. (5-15) in the case of a zero reaction order with respect to oxygen as found in the experiments presented here. Therefore, the first order rate law

with respect to propane, as applied in this study will result in the same kinetic describtion as a MvK type rate law does. Because of the high reoxidation rate constant k_5, the kinetic parameters K_4 and k_5 cannot be determined accurately from a MvK model. A variation in these parameters has almost no impact on the rate of propane consumption. The product of k_2 and K_1 may also be written as eqn. (5-21).

$$k_2 \cdot K_1 = k_{2,0} \cdot \exp\left(\frac{-\Delta E_{A,2}}{R \cdot T}\right) \cdot K_{2,0} \cdot \exp\left(\frac{-\Delta H_{ads,2}}{R \cdot T}\right) \qquad (5\text{-}21)$$

Thus, the measured apparent activation energy is the sum of the real activation energy of ODP and the heat of adsorption of propane on the active site. In order to calculate the real activation energies of ODP, the heats of adsorption of propane on V-SBA-15 were determined. The measured adsorption enthalpies indicate a weak interaction between propane and vanadium surface species. The above discussion leads to the conclusion that the real activation energy for ODP is approximately 140 kJ mol^{-1}.

Table 5-3 shows kinetic parameters determined by Grabowski et al.[88] for a high loaded silica supported vanadium catalyst. The apparent activation energy of the ODP is much lower (70 kJ mol^{-1}) than the values derived in this study (103 kJ mol^{-1}).

Table 5-3. Literature data for ODP on silica supported vanadia.

x	$k_{x,0}$ / s^{-1}	$E_{A,APP,x}$ / kJ mol^{-1}
1	512 ± 56	70 ± 7
2	32000 ± 3490	48 ± 5

This fact may be attributed to the high vanadium loadings in the mentioned study, which lead to formation of V_2O_5 for which the activation energy is actually measured in such case. Furthermore, mass transfer limitations, which especially occur at high vanadium loadings, were eventually not excluded. This makes the calculated kinetic parameters erroneous and leads to lower activation energies. The data, however also show, that the activation energy for the propene combustion is lower than for ODP, as it was found in this study. Reaction orders were not determined in the study discussed above, because it was based on an Eley-Rideal reaction model. The experimentally

determined apparent activation energies of the ODP are in good agreement with data derived from DFT calculations shown in Table 5-4.[16] Theoretically determined values for the propene combustion could not be found.

Table 5-4. Comparison of experimentally and theoretically determined apparent activation energies. [a]Activation energy corrected by the heat of adsorption (40 kJ mol^{-1}).

Reference	$E_{A,ODP}$ kJ mol^{-1}
This Study	103 ± 6
Gilardoni et al.[15]	112[a]
Rozanska et al.[16]	123 ± 5

5.4 Conclusion

The SBA-15 supported catalyst used for this study is an ideal model catalyst, because of its well investigated characteristics and the theoretically predictable reaction behavior. However, further preparative studies are necessary to understand the difference between vanadium monomers and associated species. The reaction order one for the oxidative dehydrogenation step of propane as well as for the consecutive propene combustion indicate similar reaction mechanisms for the activation of the two substrates. A total oxidation of propane and propene with adsorbed molecular oxygen can be excluded, because in such a case a higher reaction order for ODP and propene combustion would be expected. Zero reaction orders in the case of oxygen indicate a fast catalyst reoxidation for ODP and propene combustion. The fast reoxidation also justifies a formal kinetic model approach as a reliable method for the determination of the apparent activation energies. Higher activation energies of propane dehydrogenation as compared to the propene combustion indicate the participation of the weaker allylic C-H bond of propene in the rate determining step of the propene combustion. In addition, this leads to higher propene selectivities at elevated reaction temperatures. For further investigations of the reoxidation reactions transient experiments need to be conducted. As shown by the calorimetric experiments, the active sites have no influence on the adsorption behaviour of propane. The values of the heat of adsorption are in the expected range of heterogeneous reactions.

6 The Role of Lattice Oxygen in ODE on Alumina Supported Vanadium Oxide Catalysts

6.1 Introduction

The previous chapters highlighted the reaction mechanism of ODP considering the reactant and the reduced active site under steady state conditions. This chapter elucidates the active site under non-steady-state conditions and deals with selectivity aspects of ODH. Ethane was used as a probe molecule, because of its less complex cracking patterns, which lead to an easier deconvolution of the product response. So far, alkene selectivities up to 80% have been observed upon extrapolation of experimental data to zero alkane conversion, indicating that the intrinsic activity of supported vanadia is higher for alkane ODH than for direct alkane combustion.[2,13] However, the alkene selectivity decreases with increasing alkane conversion due to fast alkene combustion. When N_2O is used as the oxidant instead of O_2, a higher propene selectivity can be achieved at a given propane conversion level on alumina-supported vanadia.[50,65] To explain this observation, it is proposed that the rate of catalyst reoxidation by N_2O is slower than by O_2 and that the surface of a partially reduced catalyst is less active for olefin combustion. It has also been reported that under reducing conditions (i.e., when the concentration of the reducing agent is in stoichiometric excess of the oxidizing agent) the V^{4+} and V^{3+} cations produced by reduction of vanadia supported on alumina interact strongly with the support, leading to lower rates of CO and CO_2 formation, while the rate of ODH of ethane to ethene is not affected.[64] The aim of the present investigation is to investigate the effects of catalyst reduction prior to use on the rate of ethane ODH and the rate of secondary combustion of ethene to CO and CO_2. To this end, transient-response experiments were conducted on both fully oxidized and partially reduced alumina-supported vanadia catalysts.

6.2 Results and Discussion

The V_2O_5 weight loading of the catalysts was nominally calculated to be 10 wt%, which corresponds to a vanadium surface density of 7 V nm^{-2}, and the BET surface area of the catalyst was 100 m^2 g^{-1}. Characterization of the catalyst by Raman spectroscopy indicates that the vanadia is highly dispersed and the content of crystalline V_2O_5 is below 1%.[2,89]

Figure 6-1 shows the change in the "lattice" oxygen to vanadium (O/V) ratio during the course of H_2 TPR. The initial value of the O/V ratio is taken to be 2.5, under the assumption that all of the vanadium is in the 5+ state prior to the onset of reduction (see below). The change in the O/V ratio after reduction was then determined from the amount of O_2 required to reoxidize the catalyst. At 950 K, the O/V ratio decreased to 2.05, suggesting that all of the V^{5+} had been reduced to the V^{4+} or that half of the V^{5+} had been reduced to the V^{3+}.

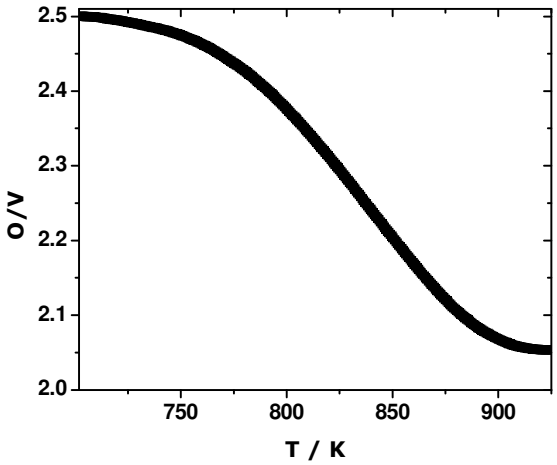

Figure 6-1. The decrease in O/V ratio with temperature observed during H_2 TPR of fully oxidized VO_x/Al_2O_3.

Several authors have discussed the initial oxidation sate of alumina supported vanadia.[60,90] Weckhuysen and Keller have reported that after treatment of alumina supported vanadium oxide (5 wt%) in air at 853 K analysis by X-ray photoelectron spectroscopy (XPS) indicates that all of the vanadium is in the 5+ state.[8] Klose et al.[60] have also used XPS to characterize samples of alumina supported vanadia. While the samples were not pre-oxidized, they were examined within 5 min of being transferred to the XPS chamber in order to minimize the loss of oxygen in vacuum. It was observed that for vanadia loadings of < 5 V/nm^2, the average oxidation state of vanadium was 4.3+, and for vanadia loadings of > 5 V/nm^2, the average oxidation state of vanadium was 4.8+. Characterization of fully oxidized alumina-supported vanadia by UV-Visible spectroscopy and XANES has also led to the conclusion that the vanadium in such samples is in the 5+ oxidation state. Argyle et al.[91] have reported that oxidized samples

of alumina-supported vanadia exhibit a UV-Visible band at 4.2 eV (33000 cm^{-1}) characteristic of compounds containing V^{5+}. A similar conclusion was reached by Olthof et al.[89] based on evidence from X-ray near edge absorption spectroscopy (XANES). In summary, it appears reasonable to assume that the vanadium in the V-Al_2O_3-H sample used for the experiments reported here was in the 5+ state, following oxidation.

The extent to which alumina-supported vandia can be reduced in hydrogen has also been a subject of discussion. Weckhuysen and Keller have reported that following reduction in H_2 at 853 K for 30 min, the average oxidation state of alumina supported vanadia (5 wt.%) decreased from 5+ to 3.8+, leading to an estimated O/V ratio of < 2.0.[8] Similar observations have been reported more recently by Wu et al.[92] Since the average oxidation state was determined by hydrogen consumption without correction, the reported O/V ratio after reduction is likely too low. If the same correction used in the study presented here is applied to the data of the two reports mentioned above, then the O/V ratio for the reduced catalyst would be ~ 2.0, in reasonable agreement with what is observed in Figure 6-1. Deconvolution of the XPS spectrum of the reduced catalyst reported by Weckhuysen and Keller indicated that the V cations are distributed in the following manner: V^{5+} - 21%; V^{4+} - 37%; and V^{3+} - 38%.[6] Evidence for V^{4+} following H_2 reduction was also supported by EPR spectroscopy.[93] Similar results have been reported by Klose et al.[60] for a sample of 4 wt% V/Al_2O_3.

The results of transient response ODH of ethane are illustrated in Figure 6-2 for a fully oxidized and a partially reduced sample of V-Al_2O_3-H. Partial reduction was achieved by heating the catalyst in H_2 at 823 K to remove half of the reducible oxygen from the vanadia, resulting in an initial O/V ratio of 2.25. The observed transient responses for C_2H_6, C_2H_4, CO, and CO_2 were qualitatively the same for both experiments. The concentration of C_2H_6 was zero initially, increased monotonically with time, and reached the inlet level of $6x10^{-6}$ mol/cm^3 after 150 s in both experiments. The concentration of C_2H_4 increased rapidly during the first 20-25 s and then decreased slowly to a level of $3x10^{-7}$ mol m^{-3}, independent of whether the catalyst was oxidized or partially reduced prior to the onset of the experiment. It was also noted that the peak in the concentration of C_2H_4 was roughly 50% higher for the pre-reduced catalyst. Sharp transients were observed for CO and CO_2. The maximum in both products was three-fold higher for the fully oxidized catalysts, but in both experiments the concentration of CO and CO_2 fell to zero at the end of the experiment.

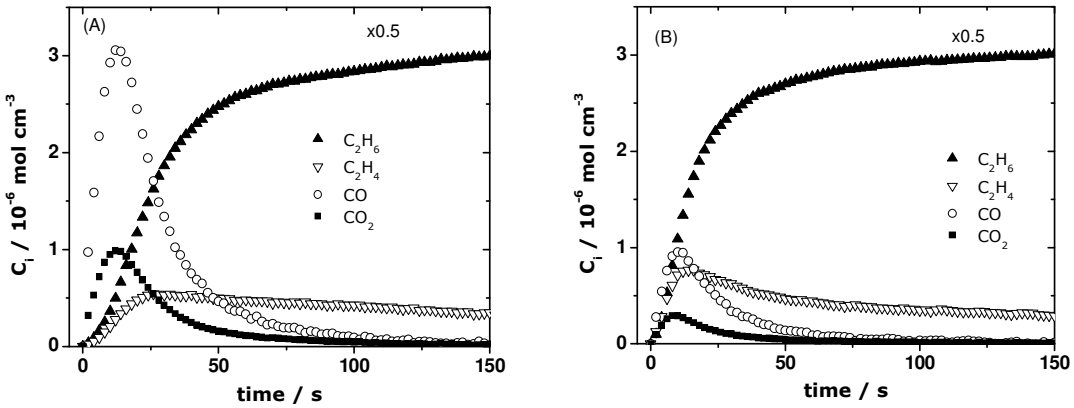

Figure 6-2. Product concentration profiles observed during exposure of fully oxidized (A) and pre-reduced (B) VO_x/Al_2O_3 to a mixture containing 16.2 %C_2H_6/84.2%He/Ar flowing at 0.5 cm^3 s^{-1}.

The residual amount of ethylene produced at the end of each experiment was attributed to non-oxidative dehydrogentation occurring on reduced catalyst sites via the process $C_2H_6 \rightarrow C_2H_4 + H_2$. Consequently, the values of ethane conversion and ethene selectivity ascribed to ODH had to be corrected for this process. To determine the contribution of non-oxidative dehydrogenation, a fully reduced catalyst was exposed to a flow of ethane at 773 K with a flow rate of 0.5 cm^3 s^{-1}. This resulted in an ethane conversion of 4 % and an ethene selectivity of 100 %. No reaction occurred on bare aluminium oxide under the same conditions. Therefore the corrected values of conversion and ethene selectivity are, therefore, given by eqn. (6-1) and (6-2).

$$X_{ODP} = X_{total} - X_{nonox} \tag{6-1}$$

$$S_{ODP} = \frac{S_{total}X_{total} - S_{nonox}X_{nonox}}{X_{total} - X_{nonox}} \tag{6-2}$$

X_i and S_i are the conversion and selectivity, respectively, for total and non-oxidative conversion of ethane.

The dependence of ethene selectivity on ethane conversion is shown in Figure 6-3 for experiments carried out with a fully oxidized catalyst and one in which half of the reactive oxygen had been removed by H_2 reduction at 823 K. In both experiments, the mass of catalyst was the same, 400 mg. It is evident that the ethene selectivity was

significantly higher when the catalyst was partially reduced than when it was fully oxidized. Figure 6-3 also shows data for an experiment in which the mass of fully oxidized catalyst was reduced from 400 mg to 200 mg. In this case, the conversion observed at the outset of the treatment with ethane was nearly the same as that for case in which half of the reactive oxygen had been removed by reduction; however, the trace of the ethene selectivity versus ethane conversion was nearly identical to that of the fully oxidized catalyst. These results suggest that the conversion of ethane to products depends only on the surface concentration of reactive oxygen but not on how that concentration was reached. On the other hand, the ethene selectivity is sensitive to the means by which a given concentration of oxygen was attained.

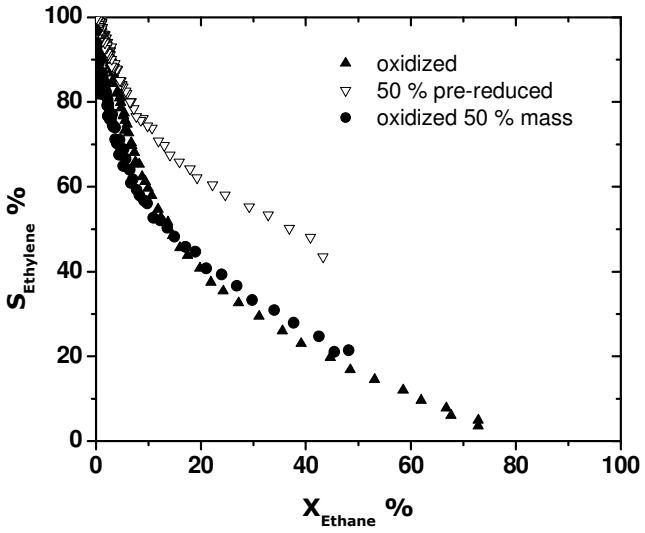

Figure 6-3. Plots of ethene selectivity versus ethane conversion for a fully oxidized and pre-reduced VO_x/Al_2O_3.

The conversion of ethane and the selectivity to ethene versus time for the first 150 s of each experiment are shown in Figure 6-4. In all cases, both the conversion and the ethene selectivity have been corrected for non-oxidative dehydrogenation. It is evident that the conversion of ethane was always lower but the selectivity to ethene was higher for the pre-reduced catalyst. Also shown in this figure are the results of an experiment in which the mass of the fully oxidized catalyst was reduced from 400 mg to 200 mg. In this case, the ethane conversion profile with time was identical to that for the case in which half of the reducible oxygen had been removed by reaction with H_2,

further supporting the conclusion presented above that the rate of ethane conversion is dependent solely on the surface concentration of reactive oxygen.

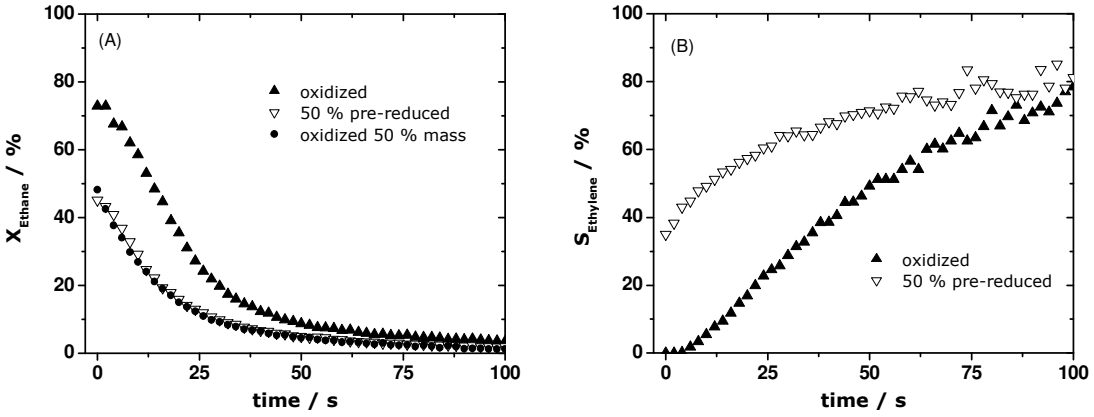

Figure 6-4. Temporal profiles of ethane conversion (A) and ethene selectivity (B) observed during exposure of fully oxidized and partially reduced VO_x/Al_2O_3 to a stream containing 16.2 $\%C_2H_6$/84.2%He/Ar flowing at 0.5 $cm^3\ s^{-1}$ at 773K.

The transients in product concentration were used to calculate the concentration of oxygen associated with vanadium as a function of time and the corresponding O/V ratio. The initial O/V ratio for the oxidized catalyst was 2.5 and that for the pre-reduced catalyst was 2.25. Figure 6-5 shows that in both cases the O/V ratio decreased from its initial value to a value of 2.1.

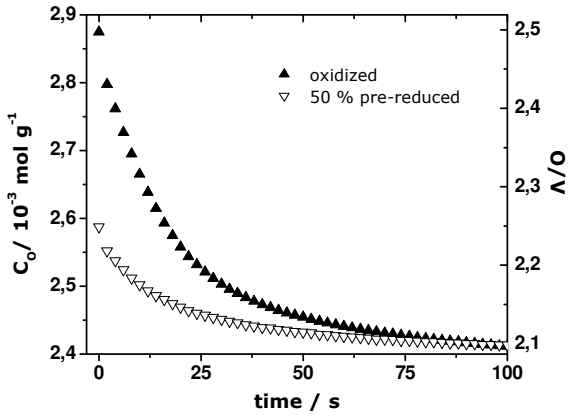

Figure 6-5. Temporal profiles of the lattice oxygen concentration and O/V ratio observed during exposure of fully oxidized and partially reduced VO_x/Al_2O_3 to a stream containing 16.2 $\%C_2H_6$/84.2%He/Ar flowing at 0.5 $cm^3\ s^{-1}$ at 773K.

The final O/V ratio was virtually the same as that achieved by reduction in H_2 (see Figure 6-1), indicating that the amount of oxygen associated with vanadium that can be removed by reaction with C_2H_6 and H_2 is the same. The results presented in Figure 6-2 to Figure 6-4 can be interpreted in terms of the following reaction scheme, specifying the general ODH reaction network illustrated in Figure 1-2:

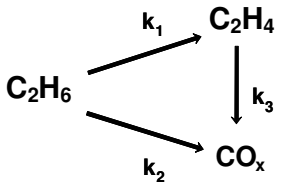

Reactions 1-3 are assumed to be first order in either C_2H_6 or C_2H_4 and first order in the surface concentration of reactive oxygen. Assuming the catalyst bed to behave as a plug-flow reactor, the partial differential equations describing the concentrations of C_2H_6 and C_2H_4, can be written as eqns. (6-3) and (6-4).

$$\frac{\partial C_{C_2H_6}}{\partial t} = -v\frac{\partial C_{C_2H_6}}{\partial z} - \rho_{cat}(k_1 + k_2)C_{O^*}C_{C_2H_6} \tag{6-3}$$

$$\frac{\partial C_{C_2H_4}}{\partial t} = -v\frac{\partial C_{C_2H_4}}{\partial z} + \rho_{cat}k_1C_{O^*}C_{C_2H_4} - \rho_{cat}k_3C_{O^*}C_{C_2H_4} \tag{6-4}$$

$C_{C_2H_6}$ and $C_{C_2H_4}$ are the gas-phase concentrations of C_2H_6 and C_2H_4, respectively; C_{O^*} is the concentration of reactive oxygen associated with vanadium; z is the distance from the inlet to the catalyst bed; t is time; v is the linear velocity; and k_i is the rate coefficient for the i^{th} reaction. Since the space time for the catalyst bed was 2 s, whereas the time scale of the experiment was ~ 150 s, eqns. (6-3) and (6-4) can be rewritten as quasi-steady state relations (6-5 and 6-6).

$$\frac{\partial C_{C_2H_6}}{\partial \tau} = -\rho_{cat}(k_1 + k_2)C_{O^*}C_{C_2H_6} \tag{6-5}$$

$$\frac{\partial C_{C_2H_4}}{\partial \tau} = \rho_{cat}k_1C_{O^*}C_{C_2H_6} - \rho_{cat}k_3C_{O^*}C_{C_2H_4} \tag{6-6}$$

Here, τ is defined as z/v. The initial conditions for eqns. (6-5) and (6-6) are that $C_{C_2H6} = C^o_{C_2H_6}$ and $C_{C_2H_4} = 0$ at $\tau = 0$. It was further assumed that the concentration of active oxygen is uniformly distributed along the length of the catalyst bed and changes with time slowly. This simplifications allows eqns. (6-5) and (6-6) to be solved

explicitly. Eqn. (6-5) was first used to determine $(k_1+k_2)C_{O*}$ from the experimental dataset ($C_{C_2H_6}$, $C^o_{C_2H_6}$, $C_{C_2H_4}$, τ and ρ_{cat}). Assuming that $k_2/(k_1 + k_2) = 0.2$ (based on the ethene selectivity observed at near zero ethane conversion), eqn. (6-6) was then used to determine k_3C_{O*} for each chosen time t, corrected for the effects of non-oxidative dehydrogenation. Figure 6-6 A and B show how $(k_1+k_2)C_{O*}$ and k_3C_{O*} change with C_{O*}.

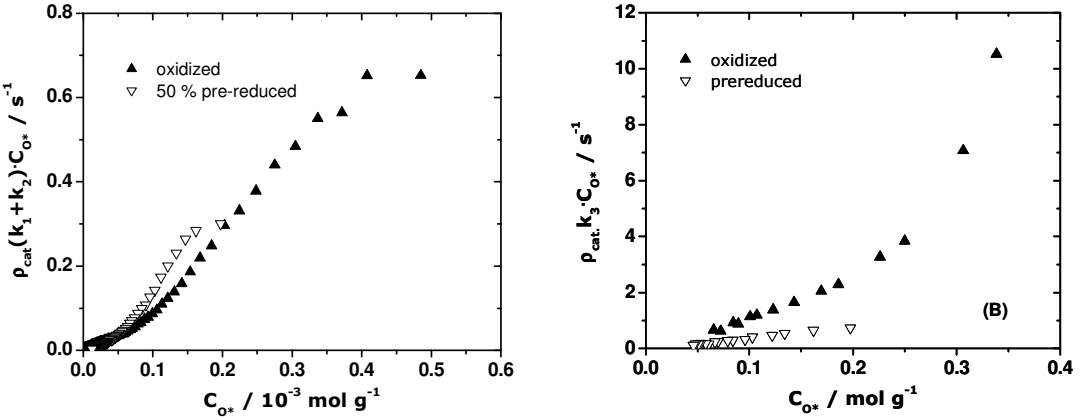

Figure 6-6. (A) Plots of $\rho_{cat}(k_1+k_2)C_{O*}$ versus C_{O*} for fully oxidized and partially reduced VO_x/Al_2O_3. (B) Plots of $\rho_{cat}k_3C_{O*}$ versus C_{O*} for fully oxidized and partially reduced VO_x/Al_2O_3.

The data in Figure 6-6 (A) show that $(k_1+k_2)C_{O*}$ increased nearly linearly with C_{O*} for both the oxidized and pre-reduced samples. The value of (k_1+k_2) was somewhat higher for the pre-reduced catalysts, 4.2×10^{-1} cm^3 g^{-1} s^{-1}, than for the oxidized catalyst, 6.8×10^{-1} cm^3 g^{-1} s^{-1}. These results suggest that pre-reduction does not have a strong effect on the ODH activity of the catalyst. Figure 6-6 (B) shows that k_3C_{O*} decreases rapidly with C_{O*} for values of C_{O*} below 0.4 mol g^{-1}, but then decreases linearly with C_{O*} for smaller values of C_{O*}. The plot of k_3C_{O*} versus C_{O*} for the pre-reduced sample is also linear for C_{O*} concentrations below 0.2 mol g^{-1}, but the slope is much smaller than that for the oxidized sample. For the range of C_{O*} where both sample show a linear relationship, the value of k_3 is 8.3 cm^3 g^{-1} s^{-1} for the oxidized sample and 7.0×10^{-1} cm^3 g^{-1} s^{-1} for the pre-reduced sample. Thus, pre-reduction reduces significantly the rate coefficient for ethene combustion.

The results of this study can be compared with those of Argyle et al.[24] and Zobray et al.[94] Since the latter two investigations were carried out at steady state, we

compared the reported steady-state rates of ethane consumption at 773 K and an ethane and oxygen partial pressure of 0.16 bar and 0.02 bar, respectively with the rate of ethane consumption determined for the fully oxidized catalyst at the start of the transient reaction carried out at 773 K in the presence of 0.16 bar of ethane (i.e., when C_{O*} was at its maximum value). Under these circumstances, the rate of ethane consumption per V atom exposed at the catalyst is $1.2x10^{-2}$ s^{-1} in our work, $2.6x10^{-2}$ s^{-1} in the study of Argyle et al.[24], and $2.0x10^{-2}$ s^{-1} in the work of Zboray et al.[94] Given the differences in methods of catalyst preparation the agreement of the maximum rate of ethane consumption reported here and the rate of ethane consumption reported in the studies of Argyle et al.[24] and Zboray et al.[94] is good. The value of k_3/k_1 reported here and those reported in the previous studies can also be compared. The value of k_3/k_1 found in this study is 10 to 14 versus 4.5 in the work of Argyle et al.[24] and 4.0 in the work of Zboray et al.[94] The reason for the higher value observed in the present work is likely due to means by which k_3/k_1 is determined here versus that used for the work up of the steady-state data.

The results of this study show that the ODH activity of the catalyst depends only on the concentration of reactive oxygen atoms, C_{O*}, and not on the way in which that concentration was achieved. Thus, as shown in Figure 6-4 (A), the same ethane conversion versus time trajectory is obtained for 200 mg of fully oxidized catalyst as for 400 mg of catalyst in which one half of the active oxygen had been removed by H_2 reduction prior to the onset of the transient-response experiment. This observation suggests that the ODH requires the presence of monomeric, or preferably oligomeric vanadate species, in which all of the vanadium is present in the 5+ oxidation state. By contrast, Figure 6-3 demonstrates that for the same ratio of C_{O*}/F_{C2H6} (where F_{C2H6} is the molar flow rate of ethane), corresponding to an ethane conversion of 40%, the ethene selectivity is significantly higher for the 400 mg catalyst sample from which half of the reactive oxygen had been removed by H_2 reduction relative to the 200 mg sample of fully oxidized catalyst.

The higher ethene selectivity observed on pre-reduced V-Al_2O_3-H might be explained in the following way: For ethene to combust via reaction 3, it must first adsorb from the gas phase. This might occur by reaction of C_2H_4 with V-OH groups produced during the formation of C_2H_4 from V-OCH_2CH_3 groups.[7] Alternatively, one could imagine that the adsorption of ethene could occur via interaction with Lewis acid centers, such as V^{5+}, V^{4+}, and V^{3+}. Evidence for ethene and propene adsorption on

vanadium cations has been presented by Che et al.[95] and Red'kina et al.[96], respectively. As the oxidation state of a vanadium cations decreases, its ionic radius increases together with number of electrons in the 3d orbital. These changes decrease the Lewis acidity of the cation and, hence, its ability to accept electrons from the p-orbital electrons of ethene, which should result in a decrease in the ability of the vanadium cation to adsorb ethene. As noted earlier, several investigators have reported the formation of both V^{4+} and V^{3+} upon reduction of alumina supported vanadia and that the distribution between these states of oxidation depends on the reducing agent.[86,97] Therefore, it is reasonable to propose that reduction in H_2 leads to a lower ratio of V^{4+} to V^{3+} than reduction in C_2H_6. If this hypothesis is correct, then the higher ethene selectivity observed for the H_2 reduced catalyst could be attributed to this effect. Another possibility is that a vanadium aluminate is formed upon reduction via the substitution of V^{3+} cations into the surface of the alumina support.[98] As noted earlier, Martinez-Huerta et al.[64] have suggested that the formation of such as species does not affect the formation of ethene but decreases the formation of CO and CO_2. Hence, there may be several reasons why H_2 reduction of dispersed vanadia leads to an increase in ethene selectivity without a loss in ethane ODH activity for a given concentration of active oxygen.

6.3 Conclusion

Hydrogen reduction of a monolayer of fully oxidized vandia dispersed on alumina can remove 0.5 oxygen atoms per vanadium atom, thereby reducing the O/V ratio of the vanadia layer from 2.5 to 2.0. A similar quantity of oxygen atoms can be removed during transient-response oxidative dehydrogenation of ethane to ethene at 773 K, starting with a fully oxidized catalyst. Removal of one half of the accessible (reducible) oxygen by H_2 prereduction does not alter the activity of the catalyst for ethane ODH but reduces significantly the secondary combustion of the resulting ethene. These results suggest that the combustion of ethene may involve adsorption of the olefin on Lewis acid centers, as opposed to adsorption by reaction with V-OH groups produced during the loss of hydrogen atoms from $V\text{-}OCH_2CH_3$ groups during the process leading to ethene. Since V^{4+} and V^{3+} cations produced by pre-reduction are less Lewis acidic than V^{5+} centers, ethene adsorption at these centers should be disfavored relative to V^{5+} centers. The results of the present study suggest that H_2 pre-reduction may favor

formation of V^{3+} versus V^{4+} cations compared to reduction by C_2H_6. This hypothesis could explain the higher ethene selectivity observed for H_2-reduced versus C_2H_6-reduced V-Al_2O_3-H containing the same concentration of active oxygen.

7 General Conclusion and Outlook

Different supported vanadium oxide catalysts were subject of a detailed investigation in order to establish a structure-reactivity-selectivity relationship for ODP and ODE. From analytical studies performed prior to this investigation it was known that these catalysts are composed of monomeric and/or associated vanadia species arranged on the respective support material.[8,17,20,21] Furthermore, isotopic tracer experiments and quantum chemistry calculations had shed light on the reaction mechanisms of ODH.[15,16,22,26] In kinetic studies, olefin selectivities up to almost unity had been observed at zero alkane conversion, but they are strongly decreasing with increasing alkane conversion due to the fast consecutive olefin combustion.[2,24,58] Despite this extensive scientific effort, it remained, however, unclear, how exactly support material and active site as well as the reactants, alkane and oxygen, are involved in the kinetics of alkane ODH and how many active sites are actually available on the catalyst surface. An especially important motivation for this study was the lack of knowledge about effects controlling the selectivity of such reactions systems. Overall product yields of less than 10% achieved with these catalyst systems motivated us to obtain a better understanding of the reaction mechanism with the aim of increasing the yields of ODH to a degree, which is appropriate for an industrial application.

For this purpose, different supported vanadium oxide catalysts ($V\text{-}CeO_2$, $V\text{-}TiO_2$, $V\text{-}Al_2O_3$, $V\text{-}ZrO_2$ and $V\text{-}SiO_2$) were subject to a basic study of catalyst structure and ODP reaction mechanism. Activity and product selectivity were found to be strongly influenced by the respective support material, expressed as a difference in turn over frequencies, activation energies and rate constants. However, the catalytic performance could not be simply described by invoking the corresponding cationic electronegativities as suggested before by Wachs et al.[56] Because simultaneous propane combustion was found to occur only to a small extent, a simplified reaction network containing only consecutive propene combustion will be appropriate for future kinetic investigations of these catalysts and simplify such investigations to a large extend. A further important finding was the fact that ODP cannot be investigated by separating propane ODH and propene combustion. As a reason for this, the different average oxidation state of the catalyst during the separately studied oxidation of propane and propene, respectively, was specified. This was attributed to propene consuming more lattice oxygen during its combustion than propane during its dehydrogenation. Hence,

for multiple parameter determination, several experimental data sets have to be acquired. Finally, high temperatures were found to favour high product selectivities, independent of the nature of the support material. Besides kinetic aspects the catalyst were investigated by structural means. Using Raman spectroscopy, it was shown that the structure of the vanadium oxide species differs depending on the respective support material. This was indicated by the different shape and position of the Raman bands assigned to the active site. Furthermore, a Raman band was found, emerging after V-ZrO_2 had been exposed to ODP. This was not reported in any previous study, which commonly investigated the fresh catalysts. Even though the band could not be assigned to any known zirconia phase, this was a first hint for an even more complex involvement of the support material in the reaction mechanism.

The important role of the support material was further confirmed by a HF-EPR study. After being exposed to ODP, reduced V^{4+} sites were found in the case of SBA-15 and Al_2O_3 supported catalysts. In addition, signals emerged, which were assigned to partial electron localization on the support lattice (oxoradicals) in the case of Al_2O_3 supported catalysts and surface trapped electrons forming Ti^{3+} centres, generated by the catalytic reaction of TiO_2 supported samples. This clearly indicated the active participation of the support material in the catalytic reaction for Al_2O_3 and TiO_2 supported catalysts. F centres and trapped $O_2^{(-)}$ radicals, additionally found for V-TiO_2 completed the picture of an active support material. Assuming catalytic relevance, the general differences in activity of the investigated catalyst could be explained by the assumption that V-SBA-15, V-Al_2O_3 and V-TiO_2 exhibit different electron sinks which determine the reducibility of the catalyst. Based on this finding the product selectivity could be explained by assuming that the rates of propane oxidative dehydrogenation r_1 and consecutive propene combustion r_2 are affected differently by the reduction mechanism of the respective catalyst. Accordingly, the generally accepted reaction mechanism illustrated in Figure 1-3 should be adjusted to the respective support material. The performed study revealed a more complete description of ODP. It also demonstrates the power of the now available HF-EPR spectroscopy being able to resolve molecular processes more clearly than by previously performed X-band EPR. The application of HF-EPR for the investigation of catalysts was found to be very promising because of the significant improvement of spectral resolution, e.g. enabling separation of spectral components originating from various transition metal ions, carbon centred radicals and oxygen vacancies. A future application of this method is, therefore,

promising. Further information about the details of the catalytic reaction could be obtained, if the present qualitative results are supported by a more quantitative evaluation of the concentration of paramagnetic centres.

For the SBA-15 supported catalyst, V^{4+} was found as the only electron sink for the reduction step. It could, therefore, be assumed that the support material is not participating in the catalytic reaction. Additionally, the SBA-15 supported catalyst used for this study had been characterized in various previous analytical investigations.[17,18,28,87] Vanadium-oxide-silica clusters are also one of the few systems accessible to density functional theory (DFT) calculations. Hence, this catalyst states the only comprehensively studied sample system and was chosen to be subject to a more detailed kinetic investigation of ODP. Reaction orders of one for oxidative dehydrogenation of propane to propene and consecutive combustion of the latter were determined. This indicated similar reaction mechanisms for the activation of propane and propene as both molecules apparently participate in the rate determining step of the respective reaction. On the contrary, the zero reaction order found with respect to oxygen for the oxidative dehydrogenation of propane to propene and its consecutive combustion indicates a fast reoxidation of the catalyst. Summarizing, the applied microkinetic MvK rate law could be simplified to a first order rate law with respect to propane and propene. The experimentally determined reaction orders were subsequently implemented into the kinetic model for the reaction network consisting of first order rate laws with respect to propane dehydrogenation and consecutive propene combustion. The hereby determined lower activation energies of propene combustion as compared to the propane dehydrogenation indicated the participation of the weaker allylic C-H bond of propene in the rate determining step of its combustion. This leads to higher propene selectivities at elevated reaction temperatures in accordance with the results of the kinetic study on different supported vanadium oxide catalysts discussed above. Because vanadium monomers and associated species had been found to be coexisting on the investigated catalyst even at low loadings, future preparative studies are necessary in order to understand the difference between these species. For further kinetic investigations of the reoxidation reaction separate transient experiments with the reduced catalyst need to be performed.

An interesting ambiguity concerning ODH reactions is given by the fact that little is known about quantity and behaviour of the actual active site, the so called “lattice” oxygen. For this purpose fully oxidized, high loaded (~ 7 V nm^{-2}) alumina

supported vanadium oxide catalysts were exposed to both, a stream of H_2 and C_2H_6 without the presence of gas phase oxygen. In both cases, a complete catalyst reduction removed 0.5 oxygen atoms per vanadium atom, thereby reducing the average vanadium oxidation state from V^{5+} to V^{4+}. Thus, not every theoretically available active site can be removed from the catalyst surface or participate in alkane ODH. Another interesting aspect with respect to the role of "lattice" oxygen in ODE is that the removal of one half of the accessible (reducible) oxygen with H_2 does not alter the activity of the catalyst but significantly reduces the secondary combustion of ethene, thus leading to a higher selectivity towards the desired product. The results suggest that the combustion of ethene involves adsorption of the olefin on Lewis acid centers. Since V^{4+} and V^{3+} cations produced by pre-reduction in H_2 are less Lewis acidic than V^{5+} centers, ethene adsorption on these centers should be disfavored with respect to the higher electron density of the allylic double bond. The results of the present study suggest that H_2 reduction may favor formation of V^{3+} versus V^{4+} cations as opposed to a reduction by C_2H_6. Because of the high reoxidation rate, the modification of the catalyst, as done in this study, is reversible under oxidizing atmosphere. Hence, a selectivity increase cannot be achieved under steady state conditions. However, the results illustrate that higher product selectivities can be achieved via catalyst modification. This is an important step towards an implementation of ODH on an industrial scale. Reduced sites should be subject to further investigations under steady state conditions, e.g. by performing reactions in a CSTR type reactor at low oxygen partial pressures.

Overall, the present study provided additional information about ODP and ODE by means of a structure-reactivity relationship. Furthermore product selectivity controlling steps could be identified. Evidence for a correlation between the rate determining reaction step, which was found to be hydrogen abstraction of the alkane and/or alkene and different mechanisms of electron delocalization involving the active site was found. Such mechanisms are apparently influenced by the respective support material and may be an explanation for the different activities and product selectivities found in ODH. Especially the assumption of an inert character of the support material has to be dismissed. It is now necessary to deepen these findings in order to further improve product selectivities of such reactions. A first step towards this goal was achieved by the catalyst reduction in H_2, showing that the selectivity could be increased by altering the topology of reduced vanadium sites.

Literature

(1) **www.petrochemistry.net;** Association of Petrochemicals Producers in Europe: 2008.

(2) Khodakov, A.; Olthof, B.; Bell, A. T.; Iglesia, E. *J. Catal.* **1999**, *181*, 205-216.

(3) Chaar, M. A.; Patel, D.; Kung, H. H. *J. Catal.* **1988**, *109*, 463-467.

(4) Mamedov, E. A.; Corberan, V. C. *Appl. Catal. A* **1995**, *127*, 1-40.

(5) Blasco, T.; Nieto, J. M. L. *Appl. Catal. A* **1997**, *157*, 117-142.

(6) Capannelli, G.; Bottino, A.; Romano, D.; Monticelli, O.; Servida, A.; Cavani, F.; Bartolini, A.; Rossini, S. *Nat. Gas Conv. V* **1998**, *119*, 423-428.

(7) Argyle, M. D.; Chen, K. D.; Bell, A. T.; Iglesia, E. *J. Phys. Chem. B* **2002**, *106*, 5421-5427.

(8) Weckhuysen, B. M.; Keller, D. E. *Catal. Today* **2003**, *78*, 25-46.

(9) Evans, O. R.; Bell, A. T.; Tilley, T. D. *J. Catal.* **2004**, *226*, 292-300.

(10) Grabowski, R. *Catal. Rev. - Sci. Eng.* **2006**, *48*, 199-268.

(11) Shee, D.; Rao, T. V. M.; Deo, G. *Catal. Today* **2006**, *118*, 288-297.

(12) Cavani, F.; Ballarini, N.; Cericola, A. *Catal. Today* **2007**, *127*, 113-131.

(13) Dinse, A.; Frank, B.; Hess, C.; Habel, D.; Schomäcker, R. *J. Mol. Catal. A* **2008**, *289*, 28-37.

(14) Sam, D. S. H.; Soenen, V.; Volta, J. C. *J. Catal.* **1990**, *123*, 417-435.

(15) Gilardoni, F.; Bell, A. T.; Chakraborty, A.; Boulet, P. *J. Phys. Chem. B* **2000**, *104*, 12250-12255.

(16) Rozanska, X.; Fortrie, R.; Sauer, J. *J. Phys. Chem. C* **2007**, *111*, 6041-6050.

(17) Venkov, T. V.; Hess, C.; Jentoft, F. C. *Langmuir* **2007**, *23*, 1768-1777.

(18) Hess, C.; Schlogl, R. *Chem. Phys. Lett.* **2006**, *432*, 139-145.

(19) Hess, C.; Tzolova-Muller, G.; Herbert, R. *J. Phys. Chem. C* **2007**, *111*, 9471-9479.

(20) Wu, Z. L.; Kim, H. S.; Stair, P. C.; Rugmini, S.; Jackson, S. D. *J. Phys. Chem. B* **2005**, *109*, 2793-2800.

(21) Tian, H. J.; Ross, E. I.; Wachs, I. E. *J. Phys. Chem. B* **2006**, *110*, 9593-9600.

(22) Chen, K. D.; Khodakov, A.; Yang, J.; Bell, A. T.; Iglesia, E. *J. Catal.* **1999**, *186*, 325-333.

(23) Chen, K. D.; Bell, A. T.; Iglesia, E. *J. Phys. Chem. B* **2000**, *104*, 1292-1299.

(24) Argyle, M. D.; Chen, K. D.; Bell, A. T.; Iglesia, E. *J. Catal.* **2002**, *208*, 139-149.

(25) Chen, K. D.; Iglesia, E.; Bell, A. T. *J. Phys. Chem. B* **2001**, *105*, 646-653.

(26) Chen, K. D.; Iglesia, E.; Bell, A. T. *J. Catal.* **2000**, *192*, 197-203.

(27) Chen, K. D.; Bell, A. T.; Iglesia, E. *J. Catal.* **2002**, *209*, 35-42.

(28) Hess, C.; Wild, U.; Schlogl, R. *Microporous Mesoporous Mater.* **2006**, *95*, 339-349.

(29) Argyle, M. D.; Chen, K. D.; Iglesia, E.; Bell, A. T. *J. Phys. Chem. B* **2005**, *109*, 2414-2420.

(30) Coker, E. N.; Jia, C. J.; Karge, H. G. *Langmuir* **2000**, *16*, 1205-1210.

(31) Herbert, R.; Hess, C. *unpublished results*.

(32) Cassiers, K.; Linssen, T.; Mathieu, M.; Benjelloun, M.; Schrijnemakers, K.; Van Der Voort, P.; Cool, P.; Vansant, E. F. *Chem. Mat.* **2002**, *14*, 2317-2324.

(33) Hassan, A. K.; Pardi, L. A.; Krzystek, J.; Sienkiewicz, A.; Goy, P.; Rohrer, M.; Brunel, L. C. *J. Magn. Reson.* **2000**, *142*, 300-312.

(34) Frank, B.; Dinse, A.; Ovsitser, O.; Kondratenko, E. V.; Schomäcker, R. *Appl. Catal. A* **2007**, *323*, 66-76.

(35) Lacheen, H. S.; Iglesia, E. *Phys. Chem. Chem. Phys.* **2005**, *7*, 538-547.

(36) Cherian, M.; Rao, M. S.; Deo, G. *Catal. Today* **2003**, *78*, 397-409.

(37) Grabowski, R.; Sloczynski, J.; Grzesik, N. M. *Appl. Catal. A* **2003**, *242*, 297-309.
(38) Grabowski, R.; Pietrzyk, S.; Sloczynski, J.; Genser, F.; Wcislo, K.; Grzybowska-Swierkosz, B. *Appl. Catal. A* **2002**, *232*, 277-288.
(39) Bottino, A.; Capannelli, G.; Comite, A.; Storace, S.; Di Felice, R. *Chem. Eng. J.* **2003**, *94*, 11-18.
(40) Blasco, T.; Galli, A.; Nieto, J. M. L.; Trifiro, F. *J. Catal.* **1997**, *169*, 203-211.
(41) Barsan, M. M.; Thyrion, F. C. *Catal. Today* **2003**, *81*, 159-170.
(42) Martra, G.; Arena, F.; Coluccia, S.; Frusteri, F.; Parmaliana, A. *Catal. Today* **2000**, *63*, 197-207.
(43) Corberan, V. C. *Catal. Today* **2005**, *99*, 33-41.
(44) Kondratenko, E. V.; Steinfeldt, N.; Baerns, M. *Phys. Chem. Chem. Phys.* **2006**, *8*, 1624-1633.
(45) Creaser, D.; Andersson, B.; Hudgins, R. R.; Silveston, P. L. *Appl. Catal. A* **1999**, *187*, 147-160.
(46) Hess, C. *Surf. Sci.* **2006**, *600*, 3695-3701.
(47) Gazzoli, D.; Mattei, G.; Valigi, M. *J. Raman Spectrosc.* **2007**, *38*, 824-831.
(48) Zhao, S.; Gorte, R. J. *Appl. Catal. A* **2004**, *277*, 129-136.
(49) Schwarz, O.; Frank, B.; Hess, C.; Schomacker, R. *Catalysis Communications* **2008**, *9*, 229-233.
(50) Kondratenko, E. V.; Cherian, M.; Baerns, M.; Su, D. S.; Schlögl, R.; Wang, X.; Wachs, I. E. *J. Catal.* **2005**, *234*, 131-142.
(51) Yao, H. C.; Yao, Y. F. Y. *J. Catal.* **1984**, *86*, 254-265.
(52) Sanati, M.; Andersson, A.; Wallenberg, L. R.; Rebenstorf, B. *Appl. Catal. A* **1993**, *106*, 51-72.
(53) Kondratenko, E. V.; Ovsitser, O.; Radnik, J.; Schneider, M.; Kraehnert, R.; Dingerdissen, U. *Appl. Catal. A* **2007**, *319*, 98-110.
(54) Ovsitser, O.; Cherian, M.; Kondratenko, E. V. *J. Phys. Chem. C* **2007**, *111*, 8594-8602.
(55) Xie, S. B.; Iglesia, E.; Bell, A. T. *Langmuir* **2000**, *16*, 7162-7167.
(56) Wachs, I. E. *Catal. Today* **2005**, *100*, 79-94.
(57) Imamura, Y.; Otsuka, T.; Nakai, H. *J. Comput. Chem.* **2007**, *28*, 2067-2074.
(58) Khodakov, A.; Yang, J.; Su, S.; Iglesia, E.; Bell, A. T. *J. Catal.* **1998**, *177*, 343-351.
(59) Bronkema, J. L.; Bell, A. T. *J. Phys. Chem. C* **2007**, *111*, 420-430.
(60) Klose, F.; Wolff, T.; Lorenz, H.; Seidel-Morgenstern, A.; Suchorski, Y.; Piorkowska, M.; Weiss, H. *J. Catal.* **2007**, *247*, 176-193.
(61) Lemonidou, A. A.; Nalbandian, L.; Vasalos, I. A. *Catal. Today* **2000**, *61*, 333-341.
(62) Arena, F.; Frusteri, F.; Parmaliana, A. *Catalysis Letters* **1999**, *60*, 59-63.
(63) Scheurell, K.; Hoppe, E.; Brzezinka, K. W.; Kemnitz, E. *J. Mater. Chem.* **2004**, *14*, 2560-2568.
(64) Martinez-Huerta, M. V.; Gao, X.; Tian, H.; Wachs, I. E.; Fierro, J. L. G.; Banares, M. A. *Catal. Today* **2006**, *118*, 279-287.
(65) Kondratenko, E. V.; Baerns, M. *Appl. Catal. A* **2001**, *222*, 133-143.
(66) Viparelli, P.; Ciambelli, P.; Lisi, L.; Ruoppolo, G.; Russo, G.; Volta, J. C. *Appl. Catal. A* **1999**, *184*, 291-301.
(67) Fogler, H. S. *Reaction Engineering*; 3rd ed.; Prentice-Hall: New Jersey, 1999.
(68) Routray, K.; Reddy, K. R. S. K.; Deo, G. *Appl. Catal. A* **2004**, *265*, 103-113.
(69) Routray, K.; Deo, G. *AIChE J.* **2005**, *51*, 1733-1746.
(70) Vannice, M. A. *Catal. Today* **2007**, *123*, 18-22.

(71) Mestric, H.; Eichel, R. A.; Kloss, T.; Dinse, K. P.; Laubach, S.; Laubach, S.; Schmidt, P. C.; Schönau, K. A.; Knapp, M.; Ehrenberg, H. *Phys. Rev. B* **2005**, *71*, 134109-134119.

(72) Lubitz, W.; Möbius, K.; Dinse, K. P. *Magn. Reson. Chem.* **2005**, *43*, S2-S3.

(73) Krzystek, J.; Fiedler, A. T.; Sokol, J. J.; Ozarowski, A.; Zvyagin, S. A.; Brunold, T. C.; Long, J. R.; Brunel, L. C.; Telser, J. *Inorg. Chem.* **2004**, *43*, 5645-5658.

(74) Chary, K. V. R.; Reddy, B. M.; Nag, N. K.; Subrahmanyam, V. S.; Sunandana, C. S. *J. Phys. Chem.* **1984**, *88*, 2622-2624.

(75) Abragam, A.; Bleaney, B. *EPR of Transition Ions*; Oxford University Press, 1970.

(76) Carrington, A.; McLachlan, A. D. *Introduction to Magnetic Resonance with Applications to Chemistry and Chemical Physics*; Wiley, 1999.

(77) Hurum, D. C.; Agrios, A. G.; Gray, K. A.; Rajh, T.; Thurnauer, M. C. *J. Phys. Chem. B* **2003**, *107*, 4545-4549.

(78) Hurum, D. C.; Gray, K. A.; Rajh, T.; Thurnauer, M. C. *J. Phys. Chem. B* **2005**, *109*, 977-980.

(79) Aboukais, A.; Bogomolova, L. D.; Deshkovskaya, A. A.; Jachkin, V. A.; Krasil'nikova, N. A.; Prushinsky, S. A.; Trul, O. A.; Stefanovsky, S. V.; Zhilinskaya, E. A. *Opt. Mater.* **2002**, *19*, 295-306.

(80) Coronado, J. M.; Maira, A. J.; Conesa, J. C.; Yeung, K. L.; Augugliaro, V.; Soria, J. *Langmuir* **2001**, *17*, 5368-5374.

(81) Sun, Y.; Egawa, T.; Zhang, L. Y.; Yao, X. *J. Mater. Sci. Lett.* **2003**, *22*, 799-802.

(82) Yamashita, H.; Harada, M.; Misaka, J.; Takeuchi, M.; Ikeue, K.; Anpo, M. *J. Photochem. Photobiol. A* **2002**, *148*, 257-261.

(83) Ganduglia-Pirovano, M. V.; Hofmann, A.; Sauer, J. *Surf. Sci. Rep.* **2007**, *62*, 219-270.

(84) Goodrow, A.; Bell, A. T. *J. Phys. Chem. C* **2008**, *112*, 13204-13214.

(85) Sekiya, T.; Yagisawa, T.; Kamiya, N.; Das Mulmi, D.; Kurita, S.; Murakami, Y.; Kodaira, T. *J. Phys. Soc. Jpn.* **2004**, *73*, 703-710.

(86) Eberhardt, M. A.; Proctor, A.; Houalla, M.; Hercules, D. M. *J. Catal.* **1996**, *160*, 27-34.

(87) Hess, C. *J. Catal.* **2007**, *248*, 120-123.

(88) Grabowski, R.; Sloczynski, J. *Chem. Eng. Process.* **2005**, *44*, 1082-1093.

(89) Olthof, B.; Khodakov, A.; Bell, A. T.; Iglesia, E. *J. Phys. Chem. B* **2000**, *104*, 1516-1528.

(90) Argyle, M. D.; Chen, K. D.; Resini, C.; Krebs, C.; Bell, A. T.; Iglesia, E. *Chem. Commun.* **2003**, 2082-2083.

(91) Argyle, M. D.; Chen, K. D.; Resini, C.; Krebs, C.; Bell, A. T.; Iglesia, E. *J. Phys. Chem. B* **2004**, *108*, 2345-2353.

(92) Wu, Z.; Stair, P. C.; Rugmini, S.; Jackson, S. D. *J. Phys. Chem. C* **2007**, *111*, 16460-16469.

(93) Harlin, M. E.; Niemi, V. M.; Krause, A. O. I.; Weckhuysen, B. M. *J. Catal.* **2001**, *203*, 242-252.

(94) Zboray, M. *unpublished results* **2008**.

(95) Che, M.; Canosa, B.; Gonzalezelipe, A. R. *J. Phys. Chem.* **1986**, *90*, 618-621.

(96) Red'kina, A. V.; Belokopytov, Y. V.; Konovalova, N. D.; Khomenko, K. N. *Theor. Exp. Chem.* **2007**, *405*, 43.

(97) Harlin, M. E.; Niemi, V. M.; Krause, A. O. I. *J. Catal.* **2000**, *195*, 67-78.

(98) Ruitenbeek, M.; Van Dillen, A. J.; De Groot, F. M. F.; Wachs, I. E.; Geus, J. W.; Konigsberger, D. C. **2001**, *241*, 10.

Appendix A: Publications

JOURNALS

- **A. Dinse**, B. Frank, C. Hess, D. Habel, R. Schomäcker, Oxidative dehydrogenation of propane over low loaded vanadia catalysts: Impact of the support material on kinetics and selectivity, *Journal of Molecular Catalysis A*, **2008**, *289*, 28
- **A. Dinse**, A. Ozarowski, C. Hess, R. Schomäcker, K.P. Dinse, The potential of high frequency EPR for the investigation of supported vanadium oxide catalysts, *Journal of Physical Chemistry C*, **2008**, *112*, 17664-17671
- **A. Dinse**, B. Frank, C. Hess, R. Herbert, S. Wrabetz, R. Schlögl, R. Schomäcker, Oxidative dehydrogenation of propane over silica SBA-15 supported vanadia catalysts: A kinetic investigation, *submitted to Journal of Molecular Catalysis A*
- **A. Dinse**, R. Schomäcker, A. T. Bell, The role of lattice oxygen on the oxidative dehydrogenation of ethane on alumina supported vanadium oxide, *to be submitted to Physical Chemistry Chemical Physics*
- B. Frank, **A. Dinse**, O. Ovsister, E.V. Kondratenko, R. Schomäcker, Mass and heat transfer effects on the oxidative dehydrogenation of propane (ODP) over a low loaded VO_x/Al_2O_3 catalyst, *Applied Catalysis A*, **323**, 66-76 (2007)
- F. El-Toufaili, F. Ahmadniana, **A. Dinse**, G. Feix, K.H. Reichert, Studies on Hydrotalcite-Catalyzed Synthesis of Poly(ethylene terephthalate), *Macromolecular Materials and Engineering*, **51**, 1136-1143 (2006)

CONFERENCE CONTRIBUTIONS

- **39th Annual Meeting of German Catalyst Researchers,** Synthetic and Mechanistic Aspects of Hydrotalcite Catalysts used for Synthesis of Poly(ethylene terephthalate
- **ISCRE 19**, Kinetic Investigation of Oxidative Dehydrogenation of Propane over Supported V_2O_5 and MoVTe Catalysts

Appendix B: Curriculum Vitae

PERSONAL

Arne Dinse

Ihnestrasse 51

14195 Berlin

adinse@gmx.net

EDUCATION

02/19/2009	**PhD** in Chemical Engineering, Technical University Berlin, Germany, supervisor: Prof. Dr. Reinhard Schomäcker Thesis title: *"New Insights into the Oxidative Dehydrogenation of Propane and Ethane on Supported Vanadium Oxide Catalysts"*
09/2005	**Diploma** (equivalent to MSc) in Chemical Engineering, Technical University Berlin, Germany, Grade 1.9 (Scale 1 (highest) to 4)
03/2005-09/2005	**Diploma Thesis** Technical University Berlin, Germany, supervisor Prof. Dr. Karl-Heinz Reichert, Grade 1.3 (Scale 1 (highest) to 4) Thesis title: *"Influence of Hydrotalcite Catalyst Modification on the Synthesis of Poly(ethylene terephthalate)"*
03/2003	**Pre-Diploma** (equivalent to BSc) in Chemistry, Ruprecht-Karls-University Heidelberg, Germany, Grade 1.9 (Scale 1 (highest) to 4)
06/2000	**Abitur** (required for university entrance), Bunsen Gymnasium, Heidelberg**,** Germany, Grade 1.7 (Scale of 1 (highest) to 6)

INTERNATIONAL

2007	**Visiting Researcher,** University of California, Berkeley, USA, with Prof. Alexis Bell and Enrique Iglesia, 14 months
2004	Industrial Training, Degussa Chemicals, Grasse, France, 4 months
1998	Berkeley High School, Berkeley, USA, 4 months
1992	Telopea High School, Canberra, Australia, 9 months
1986	Bear Creek Elementary School, Boulder, USA, 9 months

SKILLS

- **German** (native), **English** (fluent), **French** (advanced)
- **Microsoft Office** (very good), **Maple** (good), **Athena** (good), **Madonna** (good)